Contents

Chapter 1

Introduction

1.1 Motivation

By the improvement of radioactive nuclear beams facilities, a large door in investigating the nuclear reaction and structure of nuclei far from the stability path is opened, and thus new phenomena arise on. As we go far away toward the drip-line of nuclear existence in the two sides, proton-rich nuclei and neutron rich nuclei, experimental data came with a surprising results, and thus put on a great challengers of the existing models. The main new phenomena appearing far away of stability are the halo structure for light drip lines nuclei and the appearance of new magic numbers for medium and heavy nuclei. In this work we targeted two regions: neutron-rich light nuclei and proton rich nuclei in the vicinity of ^{100}Sn.

Many of light neutron rich nuclei near the drip line have either nucleon or two-nucleon separation energy less than 1MeV. This value is extremely small compared with the common value of 6-8 MeV in stable nuclei. The neutron density distribution in such loosely bound nuclei shows an extremely long tail, called the neutron halo.

The discovery of halo nuclei have opened studies of the weakly bound of nuclear system. Among the current themes of interest related to these nuclei [3] are nuclear interactions in low density, asymmetric nucleus, shells

for high-isospin nuclei, the collective motions of low density nuclear matter and loosely bound three body interactions.

The study of this region of neutron rich nuclei is, also, of great importance in astrophysics. The (r)apid neutron capture process (r-process) which is responsible of the formation of a half of nuclei heavier than iron depends on the light neutron-rich elements reaction rates.

The second targeted region is that of medium masses of proton rich nuclei in the vicinity of ^{100}Sn. It is of great interest in nuclear structure physics and astrophysics because of several reasons. The ^{100}Sn is the heaviest doubly magic Z=N nucleus can be synthesized up to now. It is located at the very limits of nuclear existence giving more possibility to understand the evolution of nuclear shell structure away of stability line.

More study of nuclei in this region can enhance our understanding of other important questions still need more interpretations like as nature of the pairing interaction between proton and neutron, symmetries and charge invariance of the nucleon-nucleon interaction, and collective phenomena.

In addition, the structure of the region has astrophysical consequences since it is predicted that the region 'southwest' of ^{100}Sn lies on the rapid proton capture (rp-process) path, which ends shortly beyond the N=Z=50 shell closure due to fast alpha decays.

1.2 Brief Review

The first landmark in the field of halo nuclei was in 1985 by Tanihata et al [1, 2] with a series of experiments at Lawrence Berkely laboratory's Bevalac, in which they found much larger measured rms matter radii of ^{6}He and ^{11}Li than they would be expected. Since than many hundreds of papers in both experimental and theoretical perspectives have been published.

^{6}He and ^{11}Li are the most studied experimentally and theoretically in Borromean three body model. Along with these two nuclei several others are confirmed to have the same feature: in 2001 by Labiche et al [7] for ^{14}Be, in

2002 by Suzuki et al[7] for ^{17}B, and recently, in 2010,by Tanaka et al [12] for ^{22}C.

The other kind of halo structure is the one neutron halo. Beside the many theoretical studies in two body model, this structure is confirmed experimentally for : ^{11}Be by Kelley et al in 1995 [5], ^{19}C by Bazin et al[8] and Nakamura et al [6] in 1995 and 1999 respectively, and for ^{15}C to have a moderate halo structure, are confirmed to have one neutron halo structure and they are studied in two body model in several reviews. More details about the reviews on the field can be found in the next chapter.

In the other hand, the second region has attracted a growing interest and it has been studied extensively in the two perspectives: experimentally and theoretically. In this introduction we limit ourselves to mention some examples of those works focusing on ^{100}Sn and its nearest neighbours because of their significant role in structure models and they have a relationship of our work.

Experimentally, studies of nuclei in the vicinity of ^{100}Sn are hampered by low cross sections and they require very sensitive and selective experimental apparatus. Despite this, β-decay half life of ^{101}Sn was reported [10] and the first data on its relative single particle states have been measured, recently, by Seweryniak et al [1]. The production cross section for ^{103}Sn is much larger than for ^{101}Sn, so its β-decay properties have been measured with considerable precision [11]. The excited states in this nucleus have been observed using in-beam spectroscopic methods [13]. The $0^+_{gs} \rightarrow 2^+$ transition strengths have been measured in ^{106,108}Sn isotopes by Ekström et al [4].

Theoretically, Coraggio et al [3] have performed shell model calculations for odd-odd nuclei with neutron particles and proton holes around ^{100}Sn using realistic effective interaction derived from the CD-Bonn nucleon-nucleon potential. The even-even Te isotopes with $116 < A < 130$ have been studied in shell model framework to explain shell structure and collectivity in this isotopic chain [5].

1.3 Outline

The work here presented is divided into two parts:

Part A: Halo structure of light neutron-rich nuclei: Study of ^{17}C and ^{18}C in two and three body models. This part is divided into four chapters.

In chapter 2, a brief historical development of the field of halo nuclei is presented, definition and experimental evidences of this new phenomena of light exotic nuclei and their astrophysical interests are expanded.

Chapter 3 is devoted to explain the theoretical framework. The two- and three-body models usually used to study one neutron halo and two neutron halo nuclei are specified. Mainly, the hyperspherical harmonics technique and the anti-symmetrization procedure is discussed.

In chapter 4 definition of the n-^{16}C interaction is made by studying the ^{17}C as two body system. The cost we have pay for this purpose is discussed.

In chapter 5, we studied ^{18}C in three body model using the interaction determined in chapter 3 and GPT potential to describe the interaction between the two neutrons. Bound states are compared to the available experimental data, and the astrophysical interests of resonance states predicted are discussed.

Part B: Structural study of nuclei in the vicinity of ^{100}Sn: $^{96-104}$Cd, $^{104-108}$Sn, ^{106,108}Te and $^{102-108}$Mo nuclei. This part consists to study even even nuclei in the vicinity of the doubly magic nucleus ^{100}Sn and is divided into two chapters:

Chapter 6 is devoted to the description of the theoretical framework needed in the study of the selected isotopic chains. The many body shell model (SM) and the algebraic interacting boson model (IBM) are described.

In chapter 7, we present the results obtained for spectra of even-even $^{96-104}$Cd, $^{104-108}$Sn and ^{106,108}Te isotopes studied within the shell model, and of $^{102-108}$Mo isotopes studied within the IBM model. The obtained results are discussed upon the available experimental data.

Finally, an overall evaluation of this work, conclusions and future perspectives are given in an outlook chapter.

Bibliography

[1] I. Tanihata et al., Measurement of interaction cross sections and radii of He isotopes, Phys. Lett. B 160, 380 (1985)

[2] I. Tanihata et al., Measurements of interactions cross sections and nuclear radii in the light p-shell region, Phys. Rev. Lett. 55, 2676 (1985)

[3] I. Tanihata: The neutron halo nuclei, J. Phys. G: Nucl. Part. Phys. 22, 157 (1996)

[4] D. Bazin et al., One neutron halo of ^{19}C, Phys. Rev. Lett. 74, 3569 (1995)

[5] J. H. Kelley et al.: Parallel momentum distributions as a probe of halo wave functions, Phys. Rev. Letts. 74, 30 (1995)

[6] Nakamura et al: coulomb dissociation of ^{19}C and its halo structure. Phys. Rev. Letts 83, 1112(1999)

[7] Labiche et al.: Halo Structure of 14Be, Phys. Rev. Letts. 86, 600(2001)

[8] T. Suzuki et al.: Momentum distribution of 15B fragments from the breakup of ^{17}B, Phys. Rev. Lett. 89, 012501 (2002)

[9] k. Tanaka et al.: Observation of a large reaction cross section in the drip-line nucleus ^{22}C, Phys. Rev. Lett. 104, 062701 (2010)

[10] O. Kavatsyuk et al., Beta Decay of ^{101}Sn, Eur. Phys. J. A 31, 319 (2007).

[11] O. Kavatsyuk et al., Beta Decay of ^{101}Sn, Eur. Phys. J. A 25, 211 (2005).

[12] D. Seweryniak et al.:Single-Neutron States in ^{101}Sn, Phys. Rev. Lett. 99, 022504 (2007)

[13] C. Fahlander et al., Excited states in ^{103}Sn: Neutron single-particle energies with respect to ^{100}Sn, Phys. Rev. C 63, 021307 (2001).

[14] L. Coraggio, A. Covello, A. Gargano, and N. Itaco :Structure of particle-hole nuclei around 100Sn, Phys. Rev. C 70, 034310 (2004)

[15] A. Ekström et al, $0^+_{gs} \rightarrow 2^+$ Transition Strengths in ^{106}Sn and ^{108}Sn, Phys. Rev. Lett. 101, 012502 (2008)

[16] Somnath Nag, Purnima Singh, S. K. Ghorui, and A. K. Singh: Shell Model Calculation for Te isotopes, proceeding of DAE Symp. on Nucl. Phys. 55, 60 (2010)

Part A

Halo Structure of Neutron Rich Nuclei: Study of ^{17}C and ^{18}C in two- and Three-body models

Chapter 2

Halo Nuclei

2.1 Historical Development of the Field

The field of halo nuclei represents a paradigm shift in the study of nuclear physics, and it is still regarded as a 'hot' topic even after more than two decades of its first discovery. The consensus view is that this field was actually begin in 1985 with a series of experiments by Tanihata and his group at Lawrence Berkely laboratory's Bevalac in which they measured the interaction cross sections of He [1] and Li [2] isotopes and found much larger values for the rms matter radii than would be predicted by the normal $A^{1/3}$ dependence. The next remarkable landmark in this journey would be the two years later pioneering paper, 1987, by Hensen and Jonson [3] in which the term "halo" was first applied to these nuclei, and they proposed that the large size of these nuclei is due to the halo effect. They explained the large matter radius of ^{11}Li by treating it as a binary system of ^{9}Li core plus a dineutron and showed how the weak binding between the pair could form an extended halo density.

Over since then, an important number of review articles, from both experimental and theoretical perspectives, have been written. A number of nuclei have been confirmed to have a halo structure. Some of other halo candidates are still waiting for experimental confirmation and more theoretical studies.

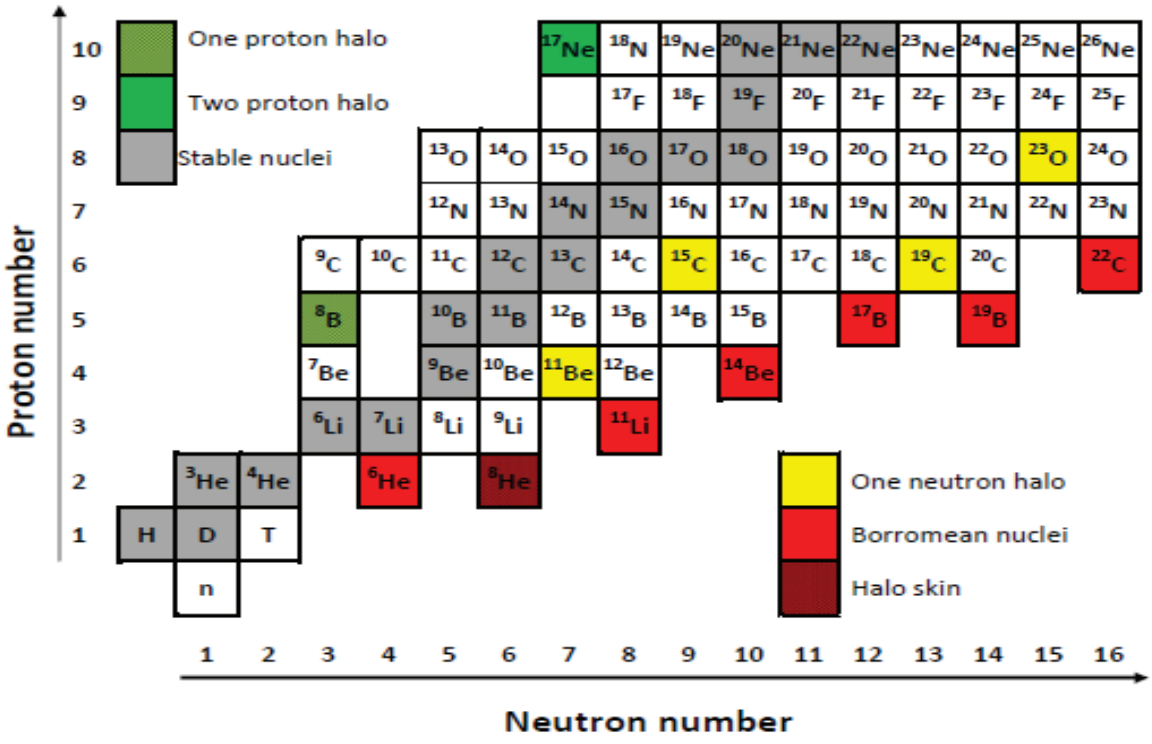

Figure 2.1: A light nuclei part of the Segre chart showing the halo nuclei

Carbon isotopes The isotopic chain of carbon nuclei interestingly shows an abrupt increase in interaction cross-section for two isotopes, namely, ^{15}C and ^{19}C [8]. This feature, together with the relatively narrow momentum distribution [9] for one neutron removal suggested this nucleus(^{19}C) to have a one neuron halo structure. The large Coulomb dissociation cross-section also support the halo nature in this nucleus.

In 1995, and ten years after the first paper published in the field, Bazin et al [8] in simultaneous measurement of the longitudinal moment distribution experiment of ^{18}C, ^{17}C and ^{16}C following the breakup of ^{19}C, ^{18}C and ^{17}C, respectively. In the ^{19}C data, both the observation of a large value for the one neutron removal cross-section and a narrow momentum peak of the ^{18}C fragments compared to those for the lighter carbon isotopes, indicate the presence of one-neutron halo. This result is confirmed in a supplementary

experiment by observing the coulomb breakup of ^{19}C on a Ta target [9]. The observed width is very similar in both breakup processes.

The ^{15}C nucleus is known to have a structure dominated by the s-wave valence neutron coupled to ^{14}C(0^+) with $S_n = 1.218$ MeV. In this sense, ^{15}C may be called a "moderate" halo nucleus [11]

The latest up to date nucleus confirmed to have this particular feature is ^{22}C. The obtained results about it have been published just the early of 2010. Tanaka et al [12] report in their paper the first measurement of reaction cross sections for ^{19,20,22}C + p reactions. The observed reaction cross section for ^{22}C is significantly larger than those for ^{19,20}C. Using a finite-range Glauber calculation under an optical-limit approximation, the rms matter radius of ^{22}C was deduced to be $5.4\pm0.9fm$. It does not follow the systematic behavior of radii in carbon isotopes with $N \leq 14$, suggestive of a two neutron halo nucleus.

Boron isotopes In 2002, Suzuki et al report in their letter [7] the first measurements of the ^{15}B longitudinal momentum distribution and the two neutron removal cross section for ^{17}B. A Glauber-type analysis of the data obtained of the two neutron cross section and the width of the ^{17}B$\rightarrow^{15}$B moment distribution provides clear evidence of a two-neutron halo structure in ^{17}B. This conclusion was the same deduced by ZhengGuo et al [10] where they report, using a Gauss + Harmonic Oscillator tail, a rms radii of the core and halo are extracted to be 2.25 and 5.85 fm, respectively.

Proton halo nuclei Nuclei exhibiting proton halos are not so common due to the confining effects of the Coulomb barrier. Nevertheless, there are a number of candidates along the proton drip-line, such as ^{8}B, ^{13}N, ^{17}Ne and the first excited state of ^{17}F.

The common feature of all nuclei with prominent interaction cross section is that they lie close to the neutron drip-line. We can distinguish two types of these nuclei. Some of theme have a small binding energy of the last nucleon and the nucleus manifests as a two body system. In the others, constituting

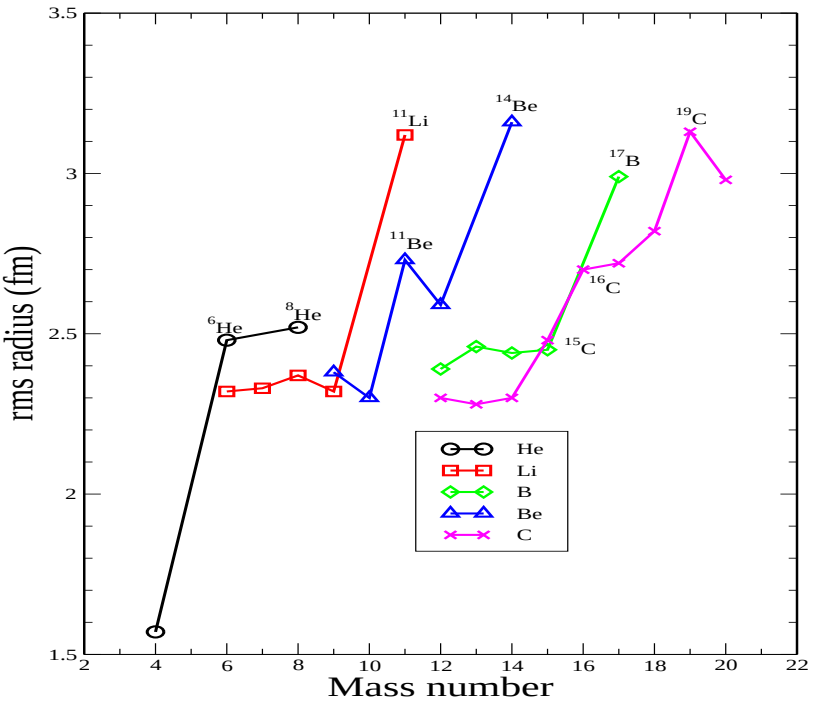

.

Figure 2.2: A plot of the matter radii of isotopes of light nuclei as predicted by reaction cross section measurements and deduced from Glauber-model analysis. The rms radii belonging to the same isotope chain are connected by line. A summary of rms matter radii is given in [6]

the most part of the halo nuclei[8], the last two nucleons are weakly bound to the core, and the nucleus is well looked to a three body system. The same phenomena is observed for the later halo nuclei, when one of their neutron is removed, they become unstable and eject one more neutron. In other words, any binary subsystem of the three body system is unstable. They are called Borromean nuclei.

The binding of the last one or two neutrons in these nuclei is very weak, typically around 1MeV or even less. This should be compared with the average single-nucleon separation energy which is about 8MeV.

The small binding of the last one or two neutrons, and the large nuclear radii Fig.2.2, lead to the idea of halo structure: one or two neutrons orbit, in

extremely extensive orbits, around a compact core of the remaining nucleons of the nucleus, and tied to the core very weakly.

2.2 Definition and Experimental Evidences of Halos

Definition and Necessary Conditions: The halo is a threshold effect arising from the very weak binding of the last one or two nucleons (usually neutrons) to, and hence decoupling from, a well-defined inert "core" containing all the other nucleons. Textbook quantum mechanics states that the combination of weak binding and short range nuclear force (since the core is relatively compact) means that the nucleon(s) can tunnel out into a volume well beyond the nuclear core and into the classically -forbidden region. Due to the small separation energy, the exponential wave-function tail extends far into the classically forbidden region, which enhances the nuclear radius with respect to the $A^{1/3}$ systematic. Quantum mechanically, this means that there is a significant probability of finding the particle outside of the well.

To more emphasize the threshold nature of the halo in nucleus, let us consider this example given in [8]. We consider a single neutron bound in an s-orbit in a spherically symmetric potential well as a simple model for the halo structure. Closest to this model is the nucleus ^{11}Be, whose g.s. is supposed to have a predominantly s-wave one-neutron halo. In the Fig.(2.3) the 1s- and 0p-wave single-neutron radial wave functions are shown in a Woods-Saxon potential, which is also plotted. The shape of the potential is tailored for ^{11}Be, and its depth is adjusted to reproduce the neutron separation energy of the g.s., 0.503 MeV, and then, separately, of the first excited state, 0.187 MeV.

The figure shows that it has a large probability that the neutron stays outside the region that is prohibited in classical mechanics. A one-particle halo is nothing but an orbit with a classically forbidden long tail. The neutron wave function in the classically forbidden region is proportional to $\frac{1}{r}e^{-\kappa r}$where κ

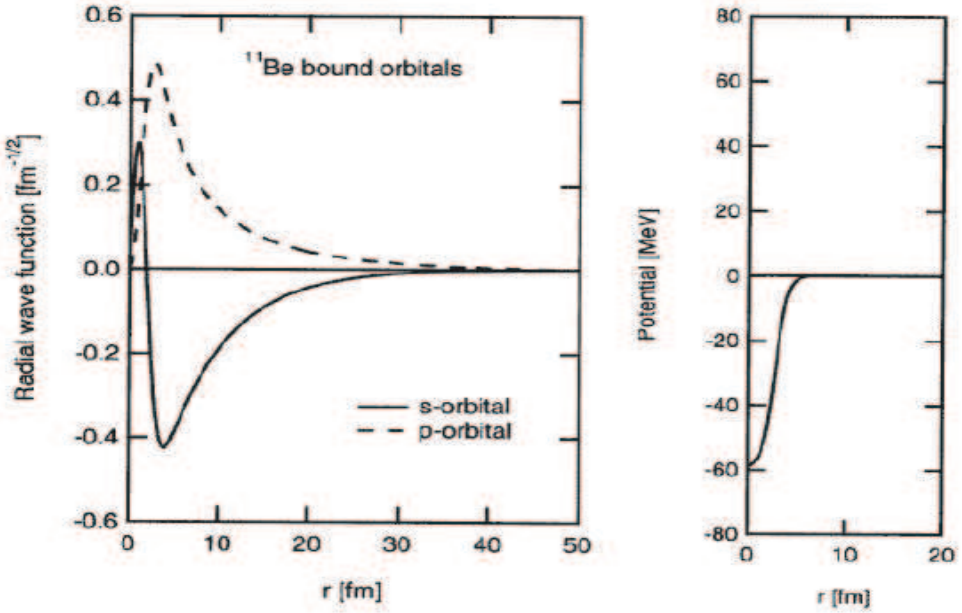

.

Figure 2.3: Radial wave functions of weakly bound single-particle (s.p.) s-wave (solid curve) and p-wave (dashed curve) orbits in a Woods-Saxon potential, imitating the g.s. and first excited state of ^{11}Be in a ^{10}Be+n model, with energies -0.503 MeV and -0.187 MeV, respectively. The potential shape is also shown in a separate panel. The classical turning points are around 6 fm for both partial waves..[8]

is related to the neutron separation energy $|\varepsilon|$ by $|\varepsilon| = \frac{\hbar^2\kappa^2}{2\mu}$, with , being the reduced mass of the neutron and the core. Taking $|\varepsilon| = 0.503$ MeV, we obtain $\kappa^{-1} \simeq 7fm$, which is much larger than the radius of light nuclei, which accounts for the long tail. Since all nuclei with large interaction cross sections are characterized by small neutron separation energies, it is natural to attribute the large interaction cross section to the large spatial extension of their halo.

Therefore, the accepted definition of a halo nucleus is [9, 13] that the halo nucleon(s) is required to have more than 50% of its probability density outside the range of the core potential and thus in the classically forbidden region.

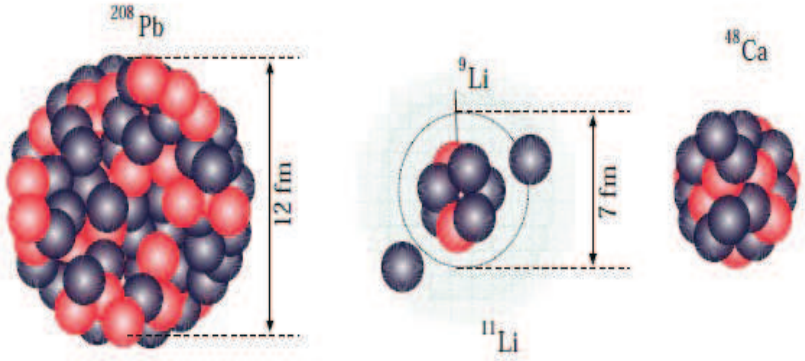

.

Figure 2.4: The size and granularity for the most studied halo nucleus ^{11}Li. The matter distribution extends far out from the nucleus such that the rms matter radius of ^{11}Li is as large as ^{48}Ca, and the radius of the halo neutrons as large as for the outermost neutrons in ^{208}Pb.[13]

The necessary conditions for the formation of a halo are now known that, besides the condition of a small binding energy for the valence particle(s), only states with small relative angular momentum may form halo states. Two-body halos can thus only occur for nucleons in s- or p-states, while three-body halos are restricted to states with $l_x + l_y \leq 1$ (see more for the hypermoment quantum number k in the next chapter)

Narrow Longitudinal Momentum Distribution Additional clear evidence for the halo structure has been observed, late 1980s just three years after the first discovery of the halo phenomena in nuclei at the drip line of neutron existence. Kobayachi el al [14] have observed that the longitudinal momentum distributions of ^{9}Li from the fragmentation of ^{11}Li show two Gaussian components with different widths. The width of the wide compo-

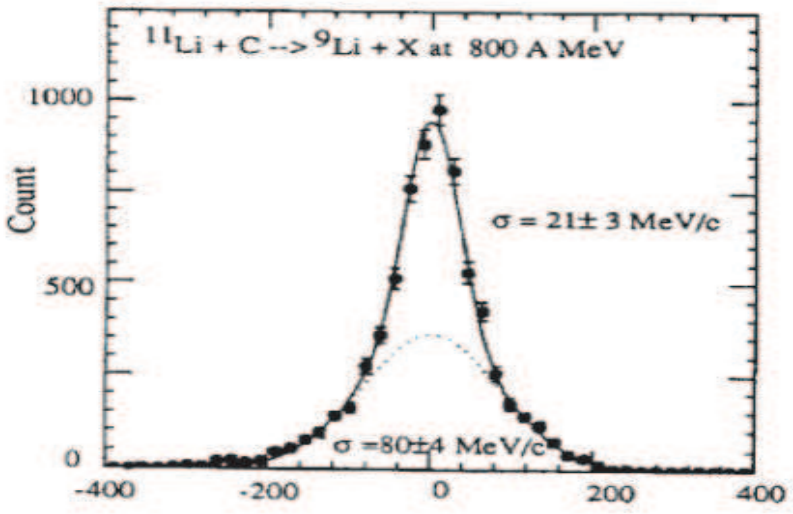

.

Figure 2.5: Transverse momentum distribution of the ^{9}Li fragment removed from ^{11}Li in a collision with ^{12}C at E=800 A MeV. The measured momentum distribution can be fitted by a superposition of two Gaussians. The narrower one has a width of 213 MeV/c, which should be compared with the momentum width of normal nuclei, 50-200 MeV/c. Taken from Ref.[8].

nent is consistent with the values observed in the fragmentation of stable nuclei, whereas the other component shows an extremely narrow width reflecting the week binding of the two outer neutrons in ^{11}Li nucleus.

It is well-known that the momentum of a fragment obtained by removing a nucleon from the projectile in a high-energy collision reflects their relative momentum in the g.s. of the projectile. In systematic measurements of the fragment momenta of unstable nuclei it was found that, for projectiles that are known to have halo structure, the core momentum distribution shows a very narrow peak [14]

The narrow momentum distribution may be intuitively understood by considering the uncertainty principle between the position and momentum [8]. A large spatial spread implies large uncertainty in the position, as we see

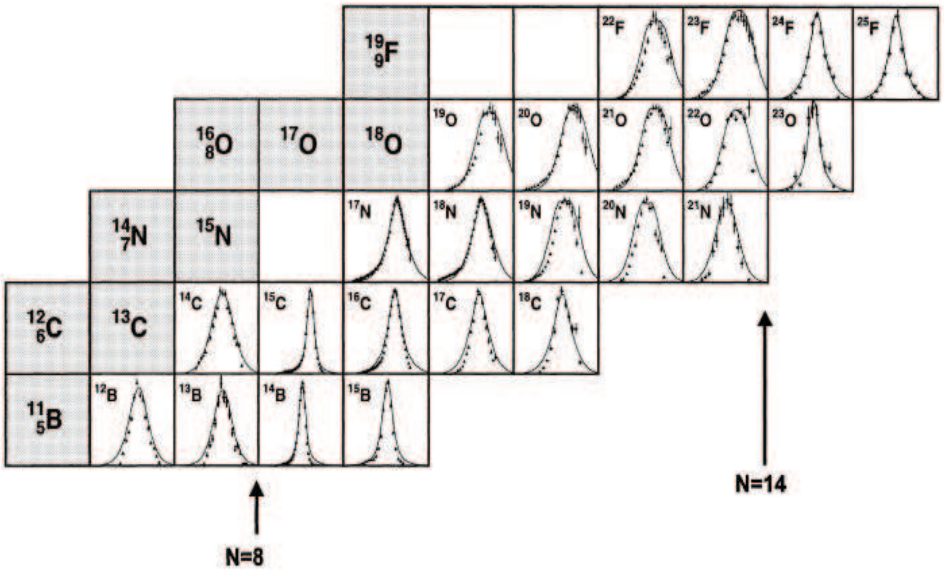

.

Figure 2.6: longitudinal momentum distribution

in Fig. 2.3, which, in turn, corresponds to a narrow momentum distribution.

Large Reaction Cross Section Another observation characteristic of halo nuclei has been found in their reactions with heavy target nuclei. The interaction cross section has been found to be much larger than originally expected based on the nuclear reaction mechanism. This is due to the increase of the neutron-removal cross section and the breakaway of the halo [8]

2.3 Astrophysical Interest of Halo Nuclei Reactions

Almost all the hydrogen and the helium in the cosmos, along with some of the lithium, was created in the first three minutes after the Big Bang. Two more light nuclei, beryllium and boron are synthesized in the interstellar space by collisions between cosmic rays and gas nuclei. All the other elements in nature are formed by nuclear reactions inside stars [16]. Fusion nuclear

reactions are responsible of formation of all elements up to iron-56. These reactions are exothermic. They release energy that powers stars against gravitational contraction.

But binding energy per nucleon increases with nuclear mass only up to iron-56, the most tightly bound nucleus of all nuclei. The production of any heavier nucleus is affected by two impediments: the direct fusion after iron-56 isotope is endothermic, the second is the growth of the coulomb barrier with increasing proton number Z. At sufficiently high Z, the coulomb barrier prevents all nuclear reaction induced by charged particles in stellar temperatures. Therefore, the isotopes of elements heavier than iron are exclusively formed in neutron-capture processes.

The two main n-capture processes were identified in a pioneering work of Burbidge et al in 1957[15]. After a nucleus has captured a neutron to become a heavier nucleus, the time scale τ_n for it to capture an additional neutron is either slow or rapid on competing time scale τ_β for it to undergo beta decay.The former refers to the slow (s-process) neutron capture, whereas the later is associated to rapid (r-process) neutron capture.

It is generally believed that the r-process is associated with supernova (SN) explosions , neutron star mergers, or gamma-ray bursts in which a neutron-rich environment is realized. However, the astronomical site for the r-process has not been unambiguously determined. Clarifying the origin of the r-process and understanding the heavy-element production therein are, currently, important subjects in astrophysics. In this context, light nuclei, as well as heavy nuclei, are expected to play important roles in the production of seed nuclei and r-process elements.

Many works have been published in this subject. As examples of the recent works, Terasawa et al [18] have confirmed that light neutron rich nuclei reaction have a critical role during r-process nucleosynthesis in supernovae. Sasaqui et al [17] have studied the sensitivity of r-process nucleosynthesis to light-element nuclear reactions. Two neutron capture reactions of some light neutron rich nuclei, ^{4}He(2n, γ)^{6}He and ^{6}He(α, n)^{9}Be, and their effects on

r-process nucleosynthesis have been studied by Bartlett et al. [19].

In this part of the work we studied the effect of light neutron rich nuclei reaction, ^{17}C(n,γ)^{18}C, on r-process nucleosynthesis.

Bibliography

[1] I. Tanihata et al.: Measurement of interaction cross sections and radii of He isotopes, Phys. Lett. B 160, 380 (1985)

[2] I. Tanihata et al.: Measurements of interaction cross sections and nuclear radii in the light p-shell region, Phys. Rev. Lett. 55, 2676 (1985)

[3] P.G. Hansen, B. Jonson: The neutron halo of extremely neutron-rich Nuclei, Europhys. Lett. 4, 409 (1987)

[4] D. Bazin et al.: One neutron halo of ^{19}C, Phys. Rev. Lett.74, 3569 (1995)

[5] D. Bazin et al.: Probing the halo structure of ^{19,17,15}C and ^{14}B, Phys. Rev. C.57, 2156 (1998)

[6] A. Ozawa et al.: Nuclear size and related topics, Nucl. Phys. A 693, 32 (2001)

[7] T. Suzuki et al.: Momentum distribution of ^{15}B fragments from the breakup of ^{17}B, Phys. Rev. Lett. 89, 012501 (2002)

[8] Y. Suzuki, R. G. Lavas, K. Yabana and K. Varga,*structure and reactions of light nuclei*, 1st edition, Taylor and Francis, London (2003)

[9] J. Al-khalili: An introduction to halo nuclei, Lect. Notes Phys. 651, 77 (2004)

[10] Hu ZhengGuo et al: The properties of halo structure for ^{17}B, Sci China Ser G-Phys. Mech. Astron. 51, 781 (2008)

[11] T. Nakamura et al.: Coulomb dissociation of halo nuclei, Nucl. Phys. A722, 301 (2003)

[12] k. Tanaka et al.: Observation of a large reaction cross section in the drip-line nucleus ^{22}C, Phys. Rev. Lett. 104, 062701 (2010)

[13] B. Jonson: Light dripline nuclei, Phys. Repts. 389, 1 (2004)

[14] T.Kobayashi, O.Yamakawa, K.Omata, K.Sugimoto, T.Shimoda, N.Takahashi and I.Tanihata: Projectile fragmentation of the extremely neutron rich nucleus ^{11}Li at 0.79 GeV/nucleon, Phys. Rev. Lett. 60, 2599 (1988).

[15] E. M. Burbidge et al.: Synthesis of the elements in stars. Rev. Mod. Phys. 29, 547 (1957).

[16] J. J. Cowan and F. K. Thielemann: R-process nucleosynthesis in supernovae, Phys. Today 57, 47 (2004).

[17] T. Sasaqui, et al.: Sensitivity of r-process nucleosynthesis to light-element nuclear reactions. Astrophys. J 634, 1173 (2005).

[18] M. Terasawa et al.: New nuclear reaction flow during r-process nucleosynthesis in supernovae: critical role of light, neutron-rich nuclei, Astrophys. J 562, 470 (2001).

[19] A. Bartlett et al.:Two-neutron capture reactions and the r process, Phys. Rev. C 74, 015802 (2006)

Chapter 3

The Theoretical Framework: Two Body and Three Body Models

3.1 Two Body Problem

In this section we present the theory of the two body, core+n in our case, systems. The problem of these systems within a Schrödinger formalism is generally well known to physicists.

Using the two body cluster model is for two aims. The first is to study the so called one neutron halo nuclei. The second is to define the core-neutron interaction to use it in the three body model to study the two neutron halo nuclei.

In this model we assume that the core is deformed and allowed to excite into excited states as well as the ground state. This assumption has several consequences. Mainly, it leads to couplings between the various channels deduced for the problem.

The Hamiltonian of the core neutron system is

$$\hat{H} = \hat{T}_r + \hat{h}_{core}(\xi) + \hat{V}_{cn}(\boldsymbol{r}, \xi) \tag{3.1}$$

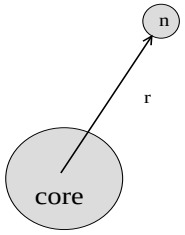

.

Figure 3.1: Two body coordinates

where $\hat{h}_{core}$ is the Hamiltonian of the core which contains the internal dynamics of the core, ξ, and its eigenfunctions are defined by the eigenvalue equation:

$$\hat{h}_{core}(\xi)\phi_i(\xi) = \varepsilon_i\phi_i(\xi) \tag{3.2}$$

As the potential $\hat{V}_{cn}(\boldsymbol{r}, \xi)$ has a spherical symmetry, it is usually to express the Hamiltonian in polar coordinates, and it is sufficient for that to write the Laplace operator in this system. The Schrödinger equation for the two body problem is thus

$$\left[-\frac{\hbar^2}{2\mu}\left(\frac{d^2}{dr^2} + \frac{2}{r}\frac{d}{dr}\right) + \frac{\hat{L}^2}{2\mu r^2} + \hat{h}_{core}(\xi) + \hat{V}_{cn}(\boldsymbol{r}, \xi)\right]\Psi = E\Psi \tag{3.3}$$

The total wavefunction of the system is expanded in a basis with an appropriate coupling of angular momenta: the orbital angular momentum l and the total spin s of the neutron couple to a total angular momentum of the neutron j: $[l \otimes s]^j_{m_j}$, and thereafter the total angular momentum j of the neutron couples with the intrinsic spin I of the core to a total angular momentum of the two body system J: $[j \otimes I]^J_M$. As we are interested in studying a halo type system, it is useful to separate the core internal motion from the relative motion of the neutron. We will therefore express the total wavefunction in terms of the core's eigenfunctions as

$$\Psi = \sum_{i}^{N_{core}} \psi_i(r, \hat{r}, \sigma)\phi_i(\xi) \tag{3.4}$$

and we anticipate that only a few terms $\phi_i(\xi)$ are required for a good description. By substituting this expression of the total wavefunction in the Schrödinger equation we obtain a set of coupled channels equations of the general form:

$$\begin{aligned}(\hat{T}_r + \hat{V}_{ii} + \varepsilon_i - E)\psi_i = -\sum_{j\neq i} V_{ij}\psi_j \quad , \quad i = 1, ..., N_{core};\\ \text{where} \quad V_{ij}(\boldsymbol{r}) = \langle\phi_i(\xi)|\hat{V}_{cn}(\boldsymbol{r}, \xi)|\phi_j(\xi)\rangle\end{aligned} \tag{3.5}$$

The total wavefunction expanded in a basis with the appropriate coupling of the angular momentum, as it is mentioned above, allow us to write it as

$$\begin{aligned}\Psi^{JM} = \sum_{\lambda} \frac{\chi^J_\lambda(r)}{r}\mathcal{Y}^{JM}_\lambda(\hat{r}, \sigma, \xi)\\ \text{with} \quad \mathcal{Y}^{JM}_\lambda(\hat{r}, \sigma, \xi) = \{[Y_l \otimes X_s]^j \otimes \phi_I\}^{JM}\\ \text{and} \quad \lambda = \{l, j, I\}\end{aligned} \tag{3.6}$$

One can substitute this expression in eq.(3.5) to obtain the radial set of two-body coupled channels equations:

$$\begin{aligned}\left(-\frac{\hbar^2}{2\mu}\left[\frac{d^2}{dr^2} - \frac{l(l+1)}{r^2}\right] + V^J_{\lambda\lambda}(r) - E + \varepsilon_I\right)\chi^J_\lambda(r) = -\sum_{\lambda'\neq\lambda} V^J_{\lambda\lambda'}(r)\chi^J_{\lambda'}(r),\\ V^J_{\lambda\lambda'}(r) = \left\langle\mathcal{Y}^{JM}_\lambda(\hat{r}, \sigma, \xi)|V_{cn}(r, \hat{r}, \xi)|\mathcal{Y}^{JM}_{\lambda'}(\hat{r}, \sigma, \xi)\right\rangle,\\ \text{where } \lambda = \{l, j, I\} \text{ and } \lambda' = \{l', j', I'\}.\end{aligned} \tag{3.7}$$

where the boundary conditions are:

$$\chi^J_\lambda(r) \xrightarrow{r\to 0} 0 \quad \text{and} \quad \chi^J_\lambda(r) \xrightarrow{r\to\infty} 0, \quad \forall\lambda. \tag{3.8}$$

Next we define the interaction between the neutron and the core. Based on the idea of rotating objects generating a deformed field, we use a deformed Woods-Saxon nuclear potential in the core's rest frame,

$$V_{core-n}(r,\theta,\phi) = \frac{V}{1+e^{\left(\frac{r-R(\theta,\phi)}{a}\right)}}, \quad R(\theta,\phi) = R(1+\beta\, Y_{20}(\theta,\phi)) \tag{3.9}$$

where $R = r_0 A^{1/3}$ and a are the radius and the diffuseness of the interaction, respectively. The core exhibits a quadrupole deformation parametrized by the fractional parameter β.

We also include a standard undeformed spin-orbit term, where the form factor is proportional to the derivative of the undeformed Woods-Saxon potential:

$$V_{ls}(r) = -\left(\frac{\hbar^2}{m_\pi c}\right)^2 (2\vec{l}.\vec{s})\frac{V_{so}}{r}\frac{d}{dr}\left[1+e^{\left(\frac{r-R}{a}\right)}\right]^{-1} \tag{3.10}$$

As it has been shown that the level shifts due to deformation of the spin-orbit potential are negligible for nuclei lighter than the rare earths [9]. The undeformed spin-orbit potential has been successfully used in three body calculations of ^{12}Be [7]. The parameters V, r_0, a and β are chosen to reproduce the experimental spectrum of the $(core+n)$ nuclei. More details of this point will be discussed in the results chapters.

3.2 Three Body Problem

Cluster models of light nuclei allow us to approximate the many-nucleon problem by few-body one, by enclosing the inner nucleons in a so called core and the remaining nucleons are called the valence nucleons. For the treatment of the latter problem a number of methods have been developed.

Faddeev [1] and Schrödinger few-body formulations have been successfully solved with the help of momentum space[1], variational technique [4] and

Hyperspherical Harmonic [2, 3] procedures. Faddeev equations have also been solved with the adiabatic hyperspherical method [5].

In the case where there are two valence nucleons we have a three body system, two neutrons in our case, interacting with the core and with each other. Here, in order to solve the three-body problem, we will work within the Schrodinger formalism combining it with the Hyperspherical method. Despite this method was used for a long time in atomic, molecular and nuclear reaction physics, it was only for the two last decades that this method was applied to exotic nuclei, spontaneously with the discovery and the abundance studies of the halo nuclei. We refer to Refs. [2, 3, 14, 8] which contain more details of the method.

In the following sections we develop the formalism needed to handle the bound state properties of core+n+n systems where the core is deformed and allowed to excite. In this development we will not include the isospin dependence since the interactions assume a fixed isospin. The full Hamiltonian of the system, after extracting the center of mass motion, contains the intrinsic Hamiltonian of the core, the relative energy and the two body interactions between the three bodies:

$$\hat{H} = \hat{T}_r + \hat{T}_R + \hat{h}_{core}(\xi) + \hat{V} \tag{3.11}$$

where

$$\hat{V} = \hat{V}_{cn}(\boldsymbol{r}_{31}, \xi) + \hat{V}_{cn}(\boldsymbol{r}_{32}, \xi) + \hat{V}_{nn}(\boldsymbol{r}, s_{nn}, l_{nn}) \tag{3.12}$$

The distances between each neutron and the core (labeled 1,2 and 3 respectively): $\vec{r}_{31}$ and $\vec{r}_{32}$, can be easily expressed in terms of Jacobi coordinates ($\vec{r}$,$\vec{R}$), where $\vec{r} = \vec{r}_{12}$ is the distance between the two neutrons and $\vec{R}$ is the distance between the core and the two neutron's centre of mass:

$$\vec{r}_{31} = \vec{r}_1 - \vec{r}_3 = -\vec{R} - \frac{1}{2}\vec{r} \quad \text{and} \quad \vec{r}_{32} = \vec{r}_2 - \vec{r}_3 = -\vec{R} + \frac{1}{2}\vec{r} \tag{3.13}$$

The intrinsic Hamiltonian of the core determines a set of eigenstates ϕ_I

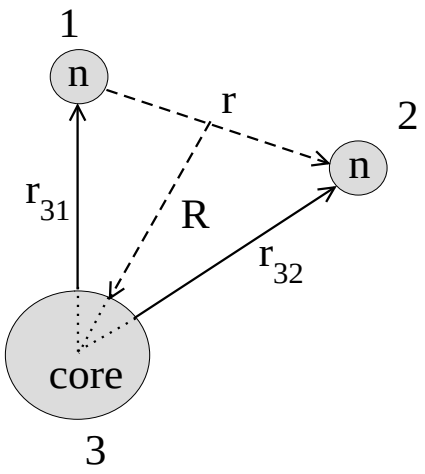

.

Figure 3.2: Two body interactions in three body system

and eigenvalues ϵ_I given by the eigenvalue equation:

$$\hat{h}_{core}(\xi)\phi_I(\xi) = \epsilon_I\phi_I(\xi) \tag{3.14}$$

where ξ represents the degree of freedom of the core.

The procedure consists of expanding the total wavefunction of the system in terms of these ϕ_I states and separating the degree of freedom of the core from the neutron's:

$$\Psi^{JM} = \sum_I \phi_I\psi_I \tag{3.15}$$

Here, ψ_I contains the radial, angular and spin dependence for the valence neutrons. This process is advantageous if only a small number of core states ϕ_I is needed to describe the system accurately and this is the case for halo systems.

Thus, the Schrodinger equation of the system we have to solve is:

$$\hat{H}\Psi^{JM} = E\Psi^{JM} \tag{3.16}$$

The useful method to solve the problem is to transform the Schrodinger equation into the Hyperspherical coupled channels equations. For that a Hyperspherical coordinates and explicit Hyperspherical expansions of the wave function are needed.

3.2.1 The Hyperspherical Coordinates

The Hyperspherical method for solving the three body problem makes use of the Hyperspherical coordinates (hyper-radius ρ and hyper-angle θ). The latter are defined on the bases of general Jacobi coordinates.

It is convenient to introduce translation-invariant sets of normalized Jacobi coordinates:

$$\boldsymbol{x}_k = \sqrt{A_{ij}}\boldsymbol{r}_{ij} \;\; and \;\; \boldsymbol{y}_k = \sqrt{A_{(ij)k}}\boldsymbol{r}_{(ij)k} \tag{3.17}$$

where A_{ij} and $A_{(ij)k}$ are respectively the reduced mass of the subsystem (i+j) and the reduced mass of the cluster (ij) with respect to the particle k, given in unit of nucleon mass by:

$$A_{ij} = \frac{A_i A_j}{A_i + A_j} \;\; and \;\; A_{(ij)k} = \frac{(A_i + A_j)A_k}{A_i + A_j + A_k} \tag{3.18}$$

The figure (3.3) illustrates the scaled Jacobi coordinates for the particular case we are interesting in: that is of two valence neutrons interacting with a core. It is easy to deduce the following relations between these and the standard Jacobi coordinates, pointing out that the two sets (x_1, y_1) and (x_2, y_2) are defined in equivalent manner due to the mass symmetry between the particles 1 and 2.

$$\boldsymbol{x_3} = \frac{\boldsymbol{r}}{\sqrt{2}} \qquad \boldsymbol{y_3} = \sqrt{\frac{2A_3}{A_3+2}}\boldsymbol{R} \tag{3.19}$$

$$\boldsymbol{x_1} = \sqrt{\frac{A_3}{A_3+1}}\boldsymbol{r}_{23} \qquad \boldsymbol{y_1} = \sqrt{\frac{(A_3+1)}{A_3+2}}\boldsymbol{r}_{\mathbf{(23)1}} \tag{3.20}$$

For obvious graphic reasons, (x_3, y_3) is often called the T basis set, and both (x_1, y_1) and (x_2, y_2) are called the Y basis set.

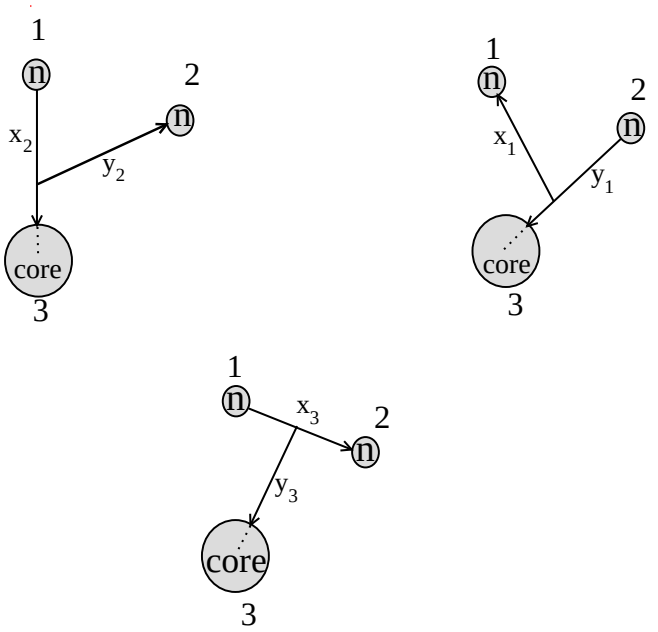

.

Figure 3.3: Jacobi coordinates for the cor+n+n system

As we mention before, to solve the three body problem we need to make transformation from the Jacobi coordinate system to the Hyperspherical coordinate system. This transformation does not affect the angular and spin variables of the two neutrons, nor the degree of freedom of the core.

The Hyperspherical coordinates are explicitly defined as:

$$\rho^2 = (x_i^2 + y_i^2) = \Sigma_i^3 A_i r_i^2 \quad \theta_i = \arctan(\frac{x_i}{y_i}) \tag{3.21}$$

We mention that the hyperradius, $x_i^2 + y_i^2$, is the same for all $i = 1, 2, 3$. This aspect is a basic advantage offered by the hyperspherical coordinate system. It is an invariant variable under translations, rotations and (1,2) permutations. An other important physical feature is, although the absolute value of x and y no longer coincide with the relative physical distances between the bodies of the system, the hyperradius is directly related to the overall size of the nucleus.

On the other hand, the hyperangle,$\theta_i = \arctan\frac{x_i}{y_i}$, is different for the

T and the **Y** basis. It contains radial correlations and it is related to the relative magnitude of the two Jacobi coordinates. As an example in the **T** basis, $\theta = 0$ means that the two neutrons are much closer to each other than to the core. The opposite case is obtained for $\theta = \frac{\pi}{2}$ which consists of two neutrons far from each other and the core is sitting in between.

In the following, the development of the formalism will assume that the Jacobi coordinates are taken in the **T** basis. The use of this choice will ease for us the construction of the anti-symmetrization of the wave function of the two neutrons. When constructing the channels for the **T** basis we have to account the anti-symmetrization of the total wave function and of the two neutron wave function. For the latter the antisymmetrisation can be accounted for just by imposing $\{l_x + S + T = odd\}$, where l_x is the relative orbital angular momentum between the two neutrons, S and T are the total spin and the total isospin of the two neutrons subsystem. As the isospin of the two neutron subsystem is one, the condition is equivalent to $\{l_x + S = even\}$. The discussion of the antisymmetrisation between the valence neutrons and the neutrons of the core will be later.

3.2.2 The Schrodinger Equation in the Hyperspherical Coordinates: General Treatment

According to Danilin et al [3], the kinetic energy operator in the hyperspherical variables has the separable form

$$-\frac{\hbar^2}{2m}(\frac{1}{A_{12}}\nabla_x^2 + \frac{1}{A_{(12)3}}\nabla_y^2) = -\frac{\hbar^2}{2m}(\frac{\partial^2}{\partial\rho^2} + \frac{5}{\rho}\frac{\partial}{\partial\rho} - \frac{1}{\rho^2}\hat{K^2}(\Omega_5)) \qquad (3.22)$$

where the generator of rotations in the hyperangular coordinate is the hypermomentum operator $\hat{K}$

$$\hat{K^2}(\Omega_5) = -\frac{\partial^2}{\partial\alpha^2} - 4\cot(2\alpha)\frac{\partial}{\partial\alpha} + \frac{1}{\cos^2\alpha}l^2(\hat{x}) + \frac{1}{\sin^2\alpha}l^2(\hat{y}) \qquad (3.23)$$

with eigenvalues $K(K+4)$, where $K = 2n + l_x + l_y$ for integer n. The quantum number K is called the hypermomentum, and does not depend on

the particular choice of the system coordinates.
The Schrodinger equation in the hyperspherical coordinates is

$$-\frac{\hbar^2}{2m}\left(\frac{\partial^2}{\partial\rho^2}+\frac{5}{\rho}\frac{\partial}{\partial\rho}-\frac{1}{\rho^2}\hat{K}^2(\Omega_5)\right)\Psi=(E-V)\Psi \tag{3.24}$$

we seek to find the total wavefunction Ψ as

$$\Psi(\rho,\Omega)=R(\rho)\mathcal{Y}(\Omega_5) \tag{3.25}$$

where $R(\rho)$ are functions of the hyperradius ρ only, and $\mathcal{Y}(\Omega_5)$ are the hyperspherical harmonic basis functions containing all angular dependence $(\Omega_5=\alpha,\hat{x},\hat{y})$of the three body system, and thus are eigenfunctions of $\hat{K}^2$ with the eigenvalues $K(K+4)$. The Schrodinger equation becomes

$$-\frac{\hbar^2}{2m}\left(\frac{\partial^2}{\partial\rho^2}+\frac{5}{\rho}\frac{\partial}{\partial\rho}-\frac{K(K+4)}{\rho^2}\right)R(\rho)=(E-V)R(\rho) \tag{3.26}$$

Now to eliminate the second term we define $R(\rho)$ as

$$R(\rho)=\frac{\chi(\rho)}{\rho^{5/2}} \tag{3.27}$$

making this substitution we get

$$-\frac{\hbar^2}{2m}\left(\frac{\partial^2}{\partial\rho^2}-\frac{15}{4\rho^2}-\frac{K(K+4)}{\rho^2}\right)\chi(\rho)=(E-V)\chi(\rho) \tag{3.28}$$

By puting $\mathcal{L}=K+3/2$, the Schrodinger equation becomes

$$-\frac{\hbar^2}{2m}\left(\frac{\partial^2}{\partial\rho^2}-\frac{\mathcal{L}(\mathcal{L}+1)}{\rho^2}\right)\chi(\rho)=(E-V)\chi(\rho) \tag{3.29}$$

3.2.3 The Hyperspherical Expansion of the Three Body Wavefunction

In the previous section we obtained the Schrodinger equation in the general case without paying any attention to the details parameters. A small modification will be taken into account in this section where we will introduce

all the parameters of the core, and we assume that the core is deformed and allowed to excite, which is the fact of the nuclei targeted in this study.

Given the orbital angular momenta (l_x, l_y), relative to the coordinates (x, y), the spin of the core I, and the spin of the two neutrons (σ_1, σ_2), and by including all the couplings, the total wavefunction can be written in the T basis as:

$$\Psi^T_{JM} = \sum_{l_x,l_y,L,I,\sigma_1,\sigma_2,S,j} \psi^{LSIJj}_{l_x,l_y}(r,R)\{([Y_{l_x} \otimes Y_{l_y}]_L \otimes [X_{\sigma_1} \otimes X_{\sigma_2}]_S)_j \otimes \phi_I\}_{JM} \tag{3.30}$$

The radial wavefunction $\psi(r, R)$ can be expanded in the hyperspherical variables. The separation between hyperangle and hyperradial dependence of the wavefunction can be performed. Taking into account the expressions (3.27) we can write:

$$\psi^{LSIjJ}_{l_x l_y}(r,R) = \rho^{-\frac{5}{2}} \sum_K \chi^{LSIjJ}_{K l_x l_y} \varphi^{l_x l_y}_K(\theta) \tag{3.31}$$

where $\varphi^{l_x l_y}_K(\theta)$ is the hyperangle function, eigensolution of the hyperangle equation, are explicitly defined in terms of the Jacobi polynomials as:

$$\varphi^{l_x l_y}_K(\theta) = N^{l_x l_y}_K (\sin\theta)^{l_x} (\cos\theta)^{l_y} P^{l_x+1/2, l_y+1/2}_n(\cos 2\theta) \tag{3.32}$$

where $P^{l_x+1/2,l_y+1/2}_n(\cos 2\theta)$ is the Jacobi polynomial and $N^{l_x l_y}_K$ is the normalisation coefficient. This expansion introduces the hyper-angle-momentum quantum number directly related to the order of the corresponding Jacobi polynomial $K = l_x + l_y + 2n (n = 0, 1, 2...)$

Comparing the expressions of the total wave function(3.25 and 3.30), we can define the hyperspherical harmonics, sometimes called hyperharmonics, including all but hyperradial dependence $(\Omega_5, \sigma_1, \sigma_2, \xi)$

$$\mathcal{Y}^{LSIjJM}_{K l_x l_y}(\Omega_5, \sigma_1, \sigma_2, \xi) = \varphi^{l_x l_y}_K(\theta)\{([Y_{l_x} \otimes Y_{l_y}]_L \otimes [X_{\sigma_1} \otimes X_{\sigma_2}]_S)_j \otimes \phi_I\}_{JM} \tag{3.33}$$

such that the total wavefunction can be written as:

$$\Psi^{T}_{JM} = \rho^{-5/2} \sum_{l_x,l_y,L,I,\sigma_1,\sigma_2,S,j,K} \chi^{LSIjJ}_{Kl_xl_y}(\rho)\mathcal{Y}^{LSIjJM}_{Kl_xl_y}(\Omega_5,\sigma_1,\sigma_2,\xi) \qquad (3.34)$$

When the previous expansions of the wavefunctions are substituted in the three body Schrodinger equation(3.24), one is left with a set of coupled equations, equivalent to those obtained for a single particle with scale mass m moving in deformed mean field. The hyperspherical coupled channels equation is thus

$$\left(-\frac{\hbar^2}{2m}\left[\frac{\partial^2}{\partial\rho^2} - \frac{\mathcal{L}(\mathcal{L}+1)}{\rho^2}\right] + V_{\gamma\gamma}(\rho) - E + \epsilon_I\right)\chi_\gamma(\rho) = -\sum_{\gamma'\neq\gamma} V_{\gamma,\gamma'}\chi_{\gamma'}(\rho)$$

$$V_{\gamma,\gamma'}\chi_{\gamma'}(\rho) = \langle\mathcal{Y}_{\gamma'}(\Omega_5,\sigma_1,\sigma 2,\xi)|\sum_{j\neq i=1}^{3} V_{ij}(\rho,\Omega_5,\xi)|\mathcal{Y}_{\gamma}(\Omega_5,\sigma_1,\sigma 2,\xi)\rangle$$

$$\gamma = \{l_x,l_y,L,S,I,j,K\}\,;\mathcal{L} = K+3/2 \quad (3.35)$$

In this hyperspherical coupled channels equation, the hypermomentum K generates a three body effective centrifugal barrier $\frac{\mathcal{L}(\mathcal{L}+1)}{\rho^2}$, which does not vanish even if the angular momenta l_x and l_y of the subsystems are equal to zero [3]. This centrifugal barrier contains not only the single particle centrifugal barriers associated with each variable, but an added repulsion term reflecting the difficulty of finding both neutrons close to the core simultaneously.

The Asymptotic Behavior of the Wavefunction and the Interaction
In the formalism for the three-body bound states in Borromean systems and finite range two-body interactions, the three-body asymptotic are easily specified by an exponential decay

$$\chi(\rho) \xrightarrow{\rho\to\infty} exp(-\kappa\rho), \;\; where \;\; \kappa = \sqrt{\frac{2m(\epsilon_I - E)}{\hbar^2}} \qquad (3.36)$$

However, if any two-body subsystems is bound when the third is removed, the three-body asymptotic in one part of configuration space will be ruled

by the two-body asymptotic and no simple representation for the boundary conditions can be found in this coordinate system.

It is of relevance for the numerical treatment of the problem, to know the asymptotic behaviour of the three body couplings. It has been proved [12] that, for short range two body interactions, the three body potential behaves as:

$$V_{KK'}(\rho \to \infty) \sim \rho^{-n}, \ \ with\ n \geq 3 \ \ (n = 3 \text{ for the diagonal terms}) \quad (3.37)$$

The slow rate decay reflects the peculiar feature of three body systems, where two particles can still interact when at large distances from the third. The long tail for the mean field has numerical implications, namely that a large radial range will be needed for the calculations.

3.3 Hyperspherical Sturmians

3.3.1 The Sturmians

The usual procedure to reduce a set of coupled differential equations to an algebraic one is either to expand the wave function of the system using a complete set of known eigenfunctions or to use some other set of trial functions in variational way [8]. However there are three requirements that should primarily be satisfied: a) the complete set should be discrete (otherwise the problem would become impossible to solve); b) the method should give good convergence; c) the expansion should provide simple boundary conditions. Choosing a set of known eigenfunctions that satisfy b) and c) may be difficult and one often finds himself with complex boundary conditions. On the other hand, an expansion using trial functions involves fitting many parameters and often offers very slow convergence.

The Sturmian eigenfunctions were introduced by Rotenberg [10] as a basis set for solving 2^{nd} order differential equations. Subsequently, this method is successfully applied to several problems in atomic and nuclear physics

[11]. The Sturmians are generated by an equation that much resembles the Schrodinger equation,

$$\left\{-\frac{\hbar^2}{2\mu}\frac{d^2}{dr^2}+\frac{\hbar^2 l(l+1)}{2\mu r^2}+\alpha_{n\lambda}V^{\lambda}_{sturm}(r)+\varepsilon_I\right\}S_{n\lambda}(r)=E_0 S_{n\lambda}(r)$$
$$n=1,2,...,N_{sturm} \quad and \quad \lambda=\{l,j,I\} \tag{3.38}$$

The boundary conditions for the Sturmian functions at large distances are given by:

$$S_{n,\lambda}(0)=0$$
$$S_{n,\lambda}(r)\xrightarrow{r\to\infty} Aexp(-\kappa_0 r), \text{ where } \kappa_0^2=\frac{2\mu(\varepsilon_I-E_0)}{\hbar^2} \tag{3.39}$$

Note that if $S_{n\lambda}(r)$ is to be square integrable, then $\varepsilon_I - E_0 > 0$.

The Sturmians $S_{n,\lambda}(r)$ form a complete set in the regions where the potential is either positive or negative ($V_{sturm}(r) \neq 0$), whichever its shape.

In this equation the core properties are accounted by introducing the core energy term ε_I. By this way, the Sturmian eigenfunction will depend on the spin of the core I along with the l, j quantum numbers

The orthogonality condition for the Sturmians differs from the standard definition for wave functions, since it is weighted by the Sturmian potential as:

$$\int_0^\infty S_{n\lambda}(r)V^{\lambda}_{sturm}S_{n'\lambda}(r)dr=-\delta_{nn'} \tag{3.40}$$

The sign on the right hand side of the equation (3.40) already assumes that the Sturmian interaction is attractive

The set of the Sturmian states generated by the equation (3.38) satisfy both requirements a) and c) presented above. Whether or not these functions satisfy the second requirement depends on the choice of E_0 and $V^{\lambda}_{sturm}(r)$.

These two ingredients, E_0 and $V^{\lambda}_{sturm}(r)$, present a useful feature of this basis if they can be chosen in accordance with the physics of the system under study. Specifically, the parameter E_0 should be chosen to match the known asymptotic for of the eigenfunctions of the Hamiltonian. An other feature of the Sturmian functions is that they behave very much like the ordinary bound state Schrodinger wavefunctions.[8].

3.3.2 The Sturmian Coupled Channels Equations for Two Body Problem

In order to solve the equation (3.7) we expand the two body radial wave function in terms of the Sturmian basis functions:

$$\chi_\lambda(r) = \sum_{\mu=1}^{N_{sturm}} C_{\mu\lambda} S_{\mu\lambda}(r) \tag{3.41}$$

where $S_{\mu\lambda}(r)$ are the Sturmians functions generated by the equation (3.38) and satisfy the boundary conditions of the equation (3.39) Due to the asymptotic properties of the Sturmians, and because of the coefficients $C_{\mu\lambda}$ do not diverge, the radial wavefuction χ_λ is limited and stisfies the boundary conditions of the equation (3.8).
Substituting this expansion in equation (3.7) we get:

$$\sum_\mu \left(-\frac{\hbar^2}{2\mu}\left[\frac{d^2}{dr^2} - \frac{l(l+1}{r^2}\right] + V^J_{\lambda\lambda}(r) - E + \varepsilon_I \right) C_{\mu\lambda} S_{\mu\lambda}(r) = \\ - \sum_{\mu,\lambda'\neq\lambda} V_{\lambda\lambda'}(r) C_{\mu\lambda'} S_{\mu\lambda'}(r). \tag{3.42}$$

Multiplying the equattion (3.38) by $C_{\mu\lambda}$ and make summation over the lable μ we get:

$$\sum_\mu \left\{ -\frac{\hbar^2}{2\mu}\frac{d^2}{dr^2} + \frac{\hbar^2 l(l+1)}{2\mu r^2} + \alpha_{\mu\lambda} V^\lambda_{sturm}(r) + \varepsilon_I \right\} C_{\mu\lambda} S_{\mu\lambda}(r) = \\ \sum_\mu E_0 C_{\mu\lambda} S_{\mu\lambda}(r) \tag{3.43}$$

By subtracting the latter equation from the former, one can eliminate the kinetic energy terms and we get:

$$\sum_\mu \{V_{\lambda\lambda}(r) - \alpha_{\mu\lambda} V^\lambda_{sturm}(r) + (E_0 - E)\} C_{\mu\lambda} S_{\mu\lambda}(r) + \sum_{\mu,\lambda'\neq\lambda} V_{\lambda\lambda'}(r) C_{\mu\lambda'} S_{\mu\lambda'}(r) = 0 \\ \text{where} \quad \mu = 1, 2, ..., N_{sturm}, \lambda = \{l, j, I\}, \lambda' = \{l', j', I'\} \tag{3.44}$$

A further simplification can be obtained if we take $V^\lambda_{sturm}(r) = V_{\lambda\lambda}(r)$

The next step consists of obtaining a set of algebraic equations such that the problem is reduced to a matrix equation. Multiplying equation (3.44) on the left by $S^*_{\nu\lambda}(r)$ and integrating over the radial coordinate from zero to infinity, we get:

$$\sum_{\mu}\left\{\int S^*_{\nu\lambda}(r)V_{\lambda\lambda}(r)S_{\mu\lambda}(r)dr+\alpha_{\mu\lambda}\delta_{\mu\nu}+E_0\int S^*_{\nu\lambda}(r)S_{\mu\lambda}(r)dr\right\}C_{\mu\lambda}+$$
$$\sum_{\mu}\sum_{\lambda'\neq\lambda}\int S^*_{\nu\lambda}(r)V_{\lambda\lambda'}(r)S_{\mu\lambda'}(r)drC_{\mu\lambda'}=E\sum_{\mu}\int S^*_{\nu\lambda}(r)V_{\lambda\lambda'}(r)S_{\mu\lambda}(r)drC_{\mu\lambda},$$
$$\text{where}\quad \mu,\nu=1,2,....,N_{sturm},\lambda=\{l,j,I\}\ \text{ and }\ \lambda'=\{l',j',I'\}\quad(3.45)$$

If one defines N_{chan} as the total number of channels $\lambda=\{l,j,I\}$ then the equation (3.45) contains $(N_{chan}\times N_{sturm})$ coupled equations for the same unknown number $C_{\mu\lambda}$. This means that the problem is completely determined.

This matrix equation describes a generalized eigenvalue problem and is of the form $(Hc=E_iMc)$ where H and M are real symmetric matrices. There are library subroutines available to solve the generalized eigenvalue problem and the eigenvalues obtained are always real.

The most important advantage of the application of the Sturmian expansion to physical problems is the good and rapid convergence of the energy curves. A wise choice for E_0 present the fundamental criteria for this purpose[8].

3.3.3 The Sturmian Coupled Channels Equation for Three Body Problem

The motivation of the correct use of the Sturmians method in three body problem is what exist of structural similarities between the two body Schrodinger equation and the three body hyperspherical Schrodinger equation, and thus between the two body coupled channels equations (3.7) and the hyperspherical coupled channels equations (3.35). The hyperspherical Sturmians are the direct generalization of the standard Sturmians to the three body hyper-

spherical problem. They satisfy an equation exactly analogous to eq.(3.38):

$$\left\{-\frac{\hbar^2}{2m}\frac{\partial^2}{\partial\rho^2}+\frac{\hbar^2\mathcal{L}(\mathcal{L}+1)}{2m\rho^2}+\alpha_n^{KLSI}V_{sturm}(\rho)+\varepsilon_I\right\}S_n^{KLSI}(\rho)=E_0S_n^{KLSI}(\rho)$$
$$n=1,2,...\text{ and }\mathcal{L}=K+3/2 \quad (3.46)$$

and have boundary conditions similar to those which constrain the standard Sturmians:

$$S_n^{KLSI}(0)=0$$
$$S_n^{KLSI}(\rho)\xrightarrow{\rho\to\infty}Ae^{-k_I\rho} \qquad k_I^2=\frac{2m(\varepsilon-E_0)}{\hbar^2} \quad (3.47)$$

When applying Sturmians to hyperspherical three body problem we have to be careful do not make all the traditional associations. The hyper-radius ρ is directly related to the size of the three body system rather than any two body distance. The term resembling the centrifugal barrier has no obvious physical meaning, as in the two body case, and it arises in the three body problem simply from the hyperspherical expansion that generates a new quantum number $K(\mathcal{L}=K+3/2)$. The simple form of the boundary conditions expressions offers an enormous advantage of the Sturmians method compared to others (the Gaussian expansion,..). In general and specially for three body systems, convergence is always harder to be obtained for loosely bound systems. The Sturmian method overcomes this problem by choosing the appropriate tail for the basis states (i.e. by choosing E_0)

Due to the asymptotic behaviour of the diagonal terms of the three body mean field given in the equation(3.37) the use of the coulomb field for the Sturmian potential may be a better choice than the monopole part of any particular two body short-range interactions.

In order to solve the hyperspherical coupled channels equation (3.35) we follow an identical procedure to that used for the two body problem: expanding the radial wave function χ_ρ on the Sturmian basis , obtaining the hyperspherical Sturmian coupled channels equation, and obtaining a set of algebraic equation and reducing the problem to a matrix equation.

The three body radial wave function can be expanded in terms of the hyperspherical Sturmian basis functions, generated by the equation (3.46), as:

$$\chi_\gamma(\rho) = \sum_{\mu=1}^{N_{sturm}} C_{\mu\gamma} S_{\mu\gamma}(\rho) \tag{3.48}$$

where $\gamma = \{KLSJIj\}$ and $\chi(\rho)$ hyperradial wave fuction given by the expression (3.34)

Substituting this expression in the three body hyperspherical coupled channels equations (3.35) we get:

$$\sum_{\mu=1}^{N_{sturm}} \left(-\frac{\hbar^2}{2m}\left[\frac{\partial^2}{\partial\rho^2} - \frac{\mathcal{L}(\mathcal{L}+1)}{\rho^2}\right] + V_{\gamma\gamma}(\rho) - E + \epsilon_I \right) C_{\mu\gamma} S_{\mu\gamma}(\rho) = - \sum_{\mu,\gamma'\neq\gamma}^{N_{sturm}} V_{\gamma,\gamma'} C_{\mu\gamma} S_{\mu\gamma}(\rho) \tag{3.49}$$

By multiplying the equation (3.46) by $C_{\mu\gamma}$ and make summation over the lable μ we get:

$$\sum_\mu \left\{ -\frac{\hbar^2}{2m}\frac{\partial^2}{\partial\rho^2} + \frac{\hbar^2\mathcal{L}(\mathcal{L}+1)}{2m\rho^2} + \alpha_\mu^\gamma V_{sturm}(\rho) + \varepsilon_I \right\} C_\mu^\gamma S_\mu^\gamma(\rho) = \sum_\mu E_0 C_\mu^\gamma S_\mu^\gamma(\rho) \tag{3.50}$$

By subtracting the latter equation from the former, one can eliminate the kinetic energy term and the to the centrifugal barrier similar term, and we get:

$$\sum_\mu \{V_{\gamma\gamma}(\rho) - \alpha_{\mu\gamma} V_{sturm}^\gamma(\rho) + (E_0 - E)\} C_{\mu\gamma} S_{\mu\gamma}(\rho) + \sum_{\mu,\gamma\neq\gamma'} V_{\gamma\gamma'}(\rho) C_{\mu\gamma} S_{\mu\gamma}(\rho) = 0$$
$$\text{where} \quad \mu = 1, 2, ..., N_{sturm}, \gamma = \{KLSJIj\}, \gamma' = \{K'L'S'J'I'j'\} \tag{3.51}$$

As in the previous section, the next step consists of reducing the problem to a matrix equation by doing the same thing of multiplying the equation

(3.51)on the left by $S^*_{\nu\gamma}(\rho)$ and integrating over the hyperradial coordinate ρ from zero to infinity.

$$\sum_{\mu}\left\{\int S^*_{\nu\gamma}(\rho)V_{\gamma\gamma}(\rho)S_{\mu\gamma}(r)dr+\alpha_{\mu\gamma}\delta_{\mu\nu}+E_0\int S^*_{\nu\gamma}(\rho)S_{\mu\gamma}(\rho)dr\right\}C_{\mu\gamma}+$$
$$\sum_{\mu}\sum_{\gamma'\neq\gamma}\int S^*_{\nu\gamma}(\rho)V_{\gamma\gamma'}(\rho)S_{\mu\gamma'}(\rho)drC_{\mu\gamma'}=E\sum_{\mu}\int S^*_{\nu\gamma}(r)V_{\gamma\gamma'}(\rho)S_{\mu\gamma}(r)drC_{\mu\gamma}, \tag{3.52}$$

As identical to the Sturmian coupled channels equation for the two body problem, we can define N_{chan} as the total number of channels $\gamma=\{KLSJIj\}$, then the problem is totally determined because the equation (3.52) contains $(N_{chan}\times N_{sturm})$ coupled equations for the same unknown number $C_{\mu\gamma}$. This matrix equation is of the form ($\mathbf{H}c=E_i\mathbf{M}c$), where $\mathbf{H}$ and $\mathbf{M}$ are real symmetric matrices, and there are software tools to solve this generalized eigenvalue problem.

3.4 Treatment of the Pauli Principle

The model developed, till now, requires some treatment of antisymmetrisation of the system's wavefunction. In few body models the alternative to the full microscopic antisymmetrisation of (A+2) nucleon system is the use of Pauli principle inter-clusters subsystems. For the system we are concerned with $(core+n+n)$, the total wavefunction would,firstly, be antisymmetric under the two neutrons permutation and, secondly, we would consider the restrictions introduced by the neutrons of the core.

Concerning the first point, introducing antisymmetrisation under neutron permutation within the $\mathbf{T}$ basis consists simply of requiring that $\{l_x+S+T=odd\}$, where l_x is the relative angular moment between the two neutrons, $S=\{0,1\}$ and $T=1$ are the total spin and the total isospin of the two neutron system, respectively.

It is useful to mention again that the T basis is chosen to do the calculations of the Schrödinger equation to simplify the obtaining of the two neutrons wavefunction antisymmetrisation by imposing this simple constraint.

As for the second point, and of special interest is the question of Pauli blocking, arising because the neutron-core interactions have deeply bound eigenstates which must be regarded as already occupied by core nucleus, and blocked to the halo neutrons. Pauli blocking is needed to remove components of the halo wave function that would disappear under full antisymmetrisation [14].

The effect of Pauli blocking in three body models has been addressed in detail by Thompson *al.* [14], who investigate different techniques to remove two-body forbidden states. These techniques can be classified in three main methods:

1. The full projection operator method.

2. Method using repulsive potentials in those neutron-core partial waves with bound states.

3. Hyperspherical adiabatic approximation in which the lowest-energy eigensurface is removed.

It appeared from the results obtained that the projection operator method gives results nearer to experiment than those using local $l-$dependent potentials. This is what makes it the favoured method used in treating the wavefunction antisymmetrisation problem in three body model.

The method consists of two main steps. Firstly, we construct the three body forbidden states. Secondly, we have to guarantee that the total wave function for the system is orthogonal to these forbidden states. This is done by projecting them out of the Hamiltonian model space. More details about the technique procedure are developed in Appendix A.

Bibliography

[1] D. R. Lehman and W. C. Parke, Phys. Rev. C 28, 364 (1983); 29, 2319(1984); 39, 1685(1989).

[2] M. V. Zhukov, B. V. Danilin, D. V. Fedorov, J. M. Bang, I. J. Thompson, J.S. Vaagen, Phys. Rep. 231, 151(1993) .

[3] B. V. Danilin, I. J. Thompson, J. S. Vaagen and M.V. Zhukov, Nucl. Phys. A 632, 383(1998)

[4] V. I. Kukulin, V. N. Pomerantsev, K.D. Razikov, V.T. Voronchev and G.G. Ryzhikh, Nucl. Physics. A586, 151 (1995)

[5] D.V. Fedorov, A.S. Jensen, and K. Riisager, Phys. Rev. C 50, 2372 (1994) .

[6] F. M. Nunes, I. J. Thompson, R. C. Johnson, Nucl. Phys. A 596, 171 (1996)

[7] F. M. Nunes, J. A. Christley, I. J. Thompson, R. C. Johnson, V. D. Efros, Nucl. Phys. A609, 43(1996)

[8] F. M. Nunes: Core excitation in few body systems: Application to light exotic nuclei, PHD thesis, university of surrey (uk) (1996).

[9] W. I. Van Rij and C.T. Hess, Nucl. Phys. A 142, 72 (1970)

[10] M. Rotenberg, Ann. Phys. 19 (1962) 262

[11] J. M. Bang, F. G. Gareev, W. J. Pinkston and J. S. Vaagen, Phys. Rep. 125, 253(1985)

[12] V. M. Efimove, Comments Nucl. Part. Phys. 19, 271(1990).

[13] J. Raynal and J. Revai, Nouvo Cimento A68, 612(1970).

[14] I. J. Thompson, B. V. Danilin, V. D. Efros, J. S. Vaagen, J. M. Bang and M. V.Zhukov, Phys. Rev C 61, 024318(2000)

Chapter 4

Application of the Two Body Model to ^{17}C

4.1 Overview of the Studies on Neutron Rich Carbon Isotopes

Bazin et al [8], in 1995, have measured the longitudinal momentum distribution of ^{18}C, ^{17}C and ^{16}C of the one-neutron breakup of ^{19}C, ^{18}C and ^{17}C respectively. The observed narrow width for the ^{18}C fragments indicates that ^{19}C is a new example of one-neutron halo.

To complete and to perfect the results obtained in this experiment, three years later in 1998, Bazin et al [9] have measured the parallel momentum distributions of outcome fragments in the one-neutron breakup of the odd-mass carbon isotopes ^{19,17,15}C. Results indicates that ^{17}C halo appears hindered by the d-wave neutron ground state configuration. The data on the halo nucleus ^{19}C suggests a structure of s-wave neutron around the 2^+ excited state of ^{18}C

Just the next year, the neutron-rich nucleus ^{19}C was the objective of coulomb dissociation experiment by Nakamura et al [6]. The study resulted to a large E1 strength of 0.71 $\pm$0.07 e^2fm^2, small separation energy of 530 $\pm$130 KeV, and the ground state structure is dominated by an s-wave valence neutron. These results provide a consistent picture of the neutron halo

structure of this nucleus.

Using one neutron knockout reactions, Maddalena et al [7] have studied the structure of neutron-rich carbon isotopes ^{16,17,19}C. The study leaded to the ground state spins of ^{17,19}C of $3/2^+$ and $1/2^+$ respectively.

In 2004 the ^{16}C properties were a target of an experiment by Imai et al[5] where they have studied the electric quadrupole transition from 2^+ to the ground state 0^+ in ^{16}C. The measured mean life is found to be 77$\pm$ 14 (stat) $\pm$ 19(syst) which coresponds to a B(E2: $2_1^+ \rightarrow 0^+$) value of 0.63 e^2fm^4. This value is anomalously small compared to the empirically predicted value.

Theoretically, several papers have been published on the isotopes of this chain. In this brief overview we mention the most recent ones.

In 2004, Suzuki et al [2] have applied the three body model of ^{14}C+n+n to study the E2 transition in ^{16}C. The n-^{14}C potential is chosen to reproduce the single particle energies of ^{15}C. It turns out that the model is reasonable to account for the hindered transition strength as well as the longitudinal moment distribution of ^{15}C fragments from ^{16}C breakup.

In the same year another paper had been published in which Sagawa et al [3] have studied the deformation and electromagnetic moments of neutron rich carbon isotopes. They have shown that the quadrupole moments Q, and the magnetic moments μ of odd C isotopes depend clearly on assigned configurations, and their experimental data will be useful to determine the deformation of nuclei near the neutron drip-line. The electric quadrupole (E2) transitions in even carbon isotopes are also studied, and the observed isotope dependence of the E2 transition strength is properly reproduced, even its abnormal observed value in ^{16}C.

Two years later and motivated by its general properties, Horiuchi et al [1] have studied the drip-line nucleus ^{22}C in a Borromean three body model of ^{20}C + n+ n. The valence neutrons, interacting via a realistic potential, are constrained to be orthogonal to the occupied orbits in ^{20}C. In this work, Horiuchi and Suzuki obtained results which support that ^{22}C is an ideal s-wave two neutron halo nucleus.

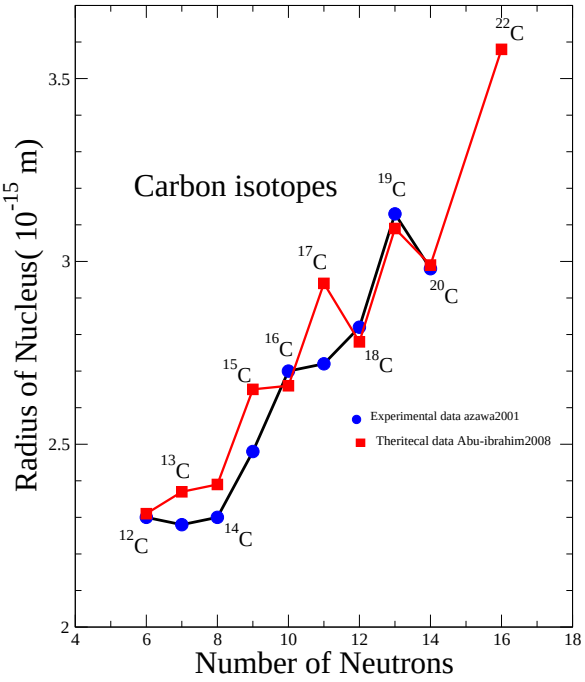

.

Figure 4.1: rms matter radius of neutron rich carbon isotopes .

In This work a systematic study of the total reaction cross sections of carbon isotopes with N=6-16 on a proton target has been made. Abu-Ibbrahim et al [4] used two types of dynamical models: one is a core + n for odd neutron nuclei, and the other is a core+n +n model for ^{16}C and ^{22}C. The study results to empirical formulas which are useful in predicting unknown cross sections.

4.2 Understanding the ^{17}C Spectrum on the Basis of Nilsson Model

The three experimental low-lying levels of ^{17}C are shown in Fig.4.2. The ground state is $3/2^+$ with a neutron separation energy of 0.728 MeV. The other two bound excited states are $1/2^+$ and $5/2^+$, located at 0.210 MeV

and 0.330 MeV respectively. The spin-parity assignments for these states have been established by analysing the γ-ray spectrum observed in p+^{17}C inelastic scattering [10], and by studying the one neutron removal reaction from ^{18}C [11].

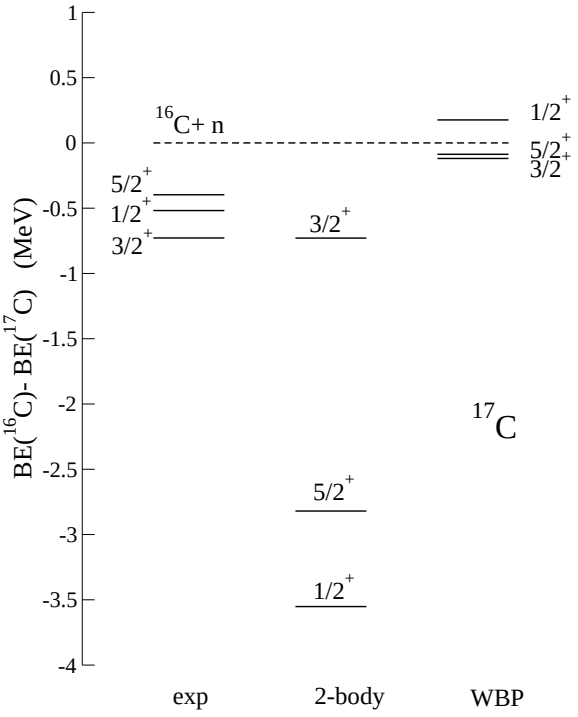

.

Figure 4.2: Low lying experimental spectrum of ^{17}C plotted relatively to the ^{16}C+n threshold and compared to the shell model with WBP interaction from [10] and the two-body model calculations with a ^{16}C-n potential from Ridikas *et al* [14].

The shell model calculations using the WBP interaction predict the ^{17}C ground state to be $J^\pi = 3/2^+$ [10], consistent with experiment. However, the shell model predicts the first excited state to be $5/2^+$ at $E_x = 0.032$ MeV while the second excited state should be $1/2^+$ at 0.295 MeV. Experimentally, $1/2^+$ is below $5/2^+$, as can be seen in Fig.4.2.

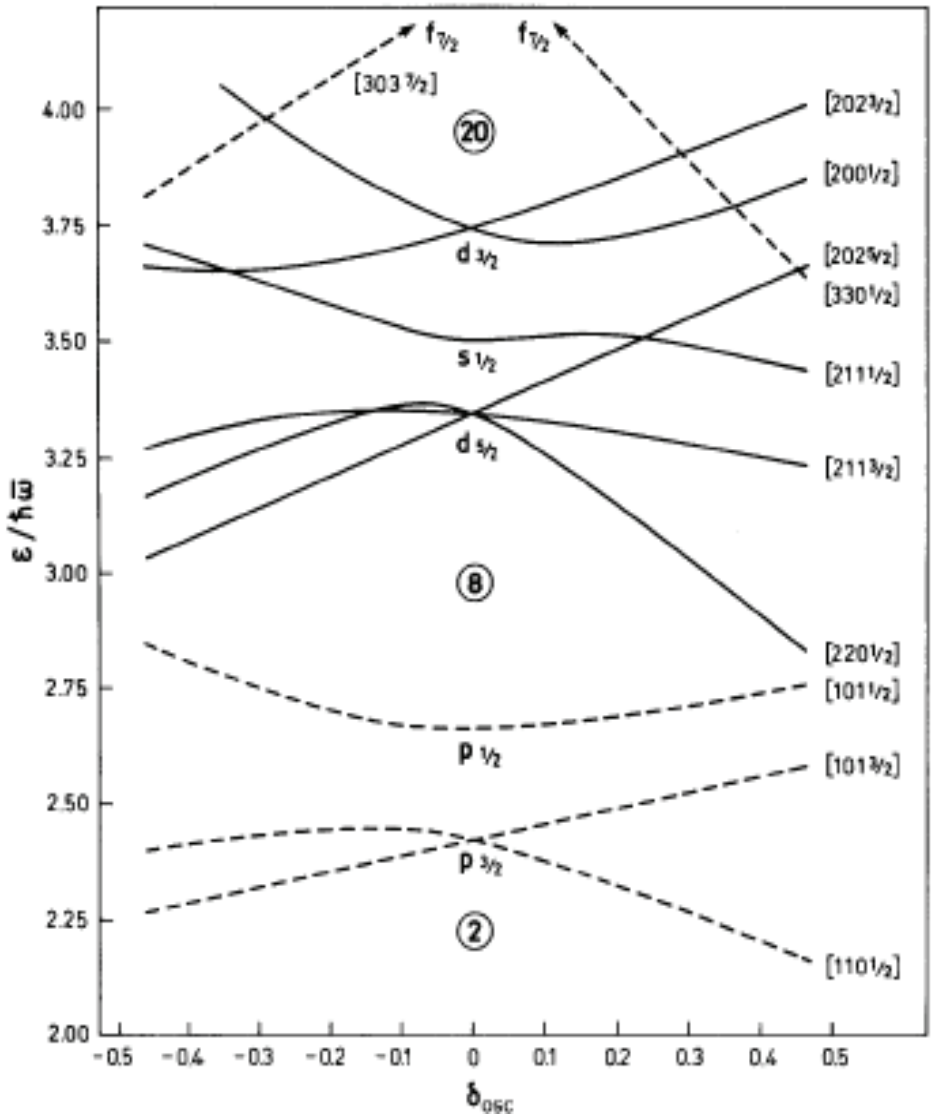

.

Figure 4.3: Spectrum of single particle orbits in spherical potential (N and Z < 20). The figure is taken from Bohr and Mottelson texbook [12]. The orbits are labled by the asymtotic quantum numbers $[Nn_3\Lambda\Omega]$ refering to large prolate deformation. Levels with even and odd parity are drawn with solide and dashed lines, respectively.

The level ordering in ^{17}C can be understood on the basis of a simple Nilsson model. According to this model, in light nuclei the $0d_{5/2}$ level splits into three levels, $[220\frac{1}{2}]$, $[211\frac{3}{2}]$ and $[202\frac{5}{2}]$ [12]. For $\beta > 0$, typical for the carbon isotopes, the lowest level is $[220\frac{1}{2}]$ followed by $[211\frac{3}{2}]$ and for $\beta > 0.25$ the $[202\frac{5}{2}]$ level rises above $[211\frac{1}{2}]$. The first eight neutrons from ^{17}C fill $0s$ and $0p$ shells. The two out of three remaining neutrons fill the $[220\frac{1}{2}]$ shell. Therefore, the low-lying spectrum of ^{17}C is determined by the single-particle spectrum of the Nilsson model above this shell, which, for typical values of $\beta \sim 0.5$, is $3/2^+$, $1/2^+$ and $5/2^+$.

The successful interpretation of the ^{17}C spectrum on the basis of the Nilsson model, combined with its small separation energy, suggests that ^{17}C could be described by a deformed two-body model. However, the Coulomb breakup [13] and the single-neutron knockout [7] experiments imply that ^{17}C is built mostly on the ^{16}C(2^+) state. Therefore, to understand ^{17}C, the 2^+ excitation of the ^{16}C core should be taken into account.

^{17}C has already been studied in a two-body deformed model with core excitations by Ridikas *et al* [14]. At that time, the spin-parity of the ^{17}C ground state was unknown. Therefore, Ridikas *et al* have found different sets of the ^{16}C-n interaction, that binds ^{17}C by 0.728 MeV, for each J^π, $1/2^+$, $3/2^+$ and $5/2^+$, separately. In particular, for the $3/2^+$ state to be bound by the experimental value of 0.728 MeV, the set of parameters V=−54.101 MeV, V_{so} = 6.5 MeV, r_0 = 1.083 fm, a=0.65 fm and β = 0.55 should be used. However, our calculations of ^{17}C performed with this set of parameters give $1/2^+$ as a ground state at a much lower energy (see Fig.4.2). Therefore, we cannot use this potential in three-body ^{16}C+n+n calculations because we would get a strongly overbound ^{18}C.

4.3 Determination of the n-^{16}C Interaction

In this work, we find the ^{16}C-n interaction that exactly reproduces the ^{17}C spectrum. We use the same model as in Ridikas *et al*, which is a coupled channel problem with a deformed ^{16}C-n potential and non-diagonal interaction described by the rotational model. We use the deformed Wood-Saxon potential and the non-deformed spin-orbit potential given by Eqs. (3.9) and (3.10). For r_0 we use the standard value of 1.25 fm, which is widely accepted by various two-body models and which is larger than the value of 1.083 fm used by Ridikas *et al*, and we use the same diffuseness $a = 0.65$ fm. Both r_0 and a are fixed in these calculations.

In our calculations we have used two values for the deformation parameter β. The first one, $\beta = 0.55$, calculated by Ridikas *et al* from the experimental transition probability $B(E2 : 0^+_{gs} \rightarrow 2^+_1)$, available at the time, and used in Ref. [15] to study effects of dynamical core deformation on single nucleon knockout reactions. The second one, $\beta = 0.48$ has been calculated by us from the experimental matter deformation lenth $\delta_m = \beta_m R_m = 1.3$ fm obtained in Ref. [16] from the Coulomb-nuclear interference in the ^{208}Pb+^{16}C inelastic scattering. To get this value, we used the ^{16}C matter radius R_m equal to 2.82 fm. This value was used in Ref. [8] to deduce the r.m.s. radii of the carbon isotopes.

To reproduce the ^{17}C spectrum, we vary the depths of the Woods-Saxon and the spin-orbit potentials. There are two important features of the potential we have found. To make the $3/2^+$ state lower than $5/2^+$ we had to inverse the sign of the spin-orbit potential, and to reproduce the narrow splitting between all three states we had to use an l-dependent ^{16}C-n potential, which is stronger in d-wave than in s-wave. We have found one set of parameters for each β: the set A for $\beta = 0.55$ and the set B for β=0.48, both presented in Table I. These potentials are similar to each other, so we use only one of them (namely, the set B) in calculations of the ^{18}C spectrum.

Although our two-body model reproduced very well the ^{17}C spectrum, it cannot explain the probability of the core excitations observed in the

Coulomb breakup [13] and one-neutron knockout experiments [7]. In our model, 69% of the ^{17}C wave function is built on the ground state of the ^{16}C core, while only 31% is built on the 2^+ excitation of ^{16}C. Experimentally, the probabilities of $^{16}\mathrm{C}(0^+)$ and $^{16}\mathrm{C}(2^+)$ are 19 ± 9 % and 58 ± 8 % respectively. Nevertheless, we have to use potentials A or B in three-body calculations since they give correct binding for the ^{16}C+n two-body subsystem.

The decomposition of the ^{17}C wave function for each bound state into the $^{16}\mathrm{C}(J^\pi) \otimes nlj$ configurations is shown in Table II in more details. One can see that the $3/2^+$ and $5/2^+$ states have similar probabilities of the core excitations while the $1/2^+$ state is very different. The r.m.s. radius of the $^{16}\mathrm{C}(0^+) \otimes s_{1/2}$, shown in Table II as well, is typical for halo states. However, the probability of this configuration in ^{17}C is only 44%.

Table 4.1: The parameter sets A and B for the $n-^{16}$C potential that fits the ^{17}C spectrum in a deformed two-body model with core excitations, corresponding to two deformations β, and the binding (B.E.) and excitation (E_x) energies of the 0^+_1, $2^+_{1,2}$ and 4^+_1 states in ^{18}C obtained with these sets. The $V_{l=0}$ and $V^{even}_{l\neq 0}$ are the depths of the central potentials in $l = 0$ and $l \neq 0$ even partial waves, V_{ls} is the depth of l-independent spin-orbit potential. Two values of the central potentials in odd partial waves, V_{odd}, has been used in three-body calculations for each set A and B. The radius and diffuseness for all potentials are fixed as r_0=1.25 fm and a=0.65 fm. All potential depths and binding energies are in MeV.

		β	$V_{l=0}$	$V^{even}_{l\neq 0}$	V_{ls}	V_{odd}	B.E.(0^+_1)	$E_x(2^+_1)$	$E_x(2^+_2)$	$E_x(4^+_1)$
A	A1	0.55	−30.95	−44.05	−0.58	−44.05	−5.18	3.07	4.23	1.75
	A2	0.55	−30.95	−44.05	−0.58	0.0	−5.22	1.12	3.89	2.23
B	B1	0.48	−32.15	−44.72	−0.56	−32.00	−4.92	1.77	3.92	1.62
	B2	0.48	−32.15	−44.72	−0.56	0.0	−5.26	1.11	4.07	2.18

Table 4.2: The probabilities P (in per cents) of the $^{16}\mathrm{C}(J^\pi) \otimes nlj$ configuration and their r.m.s. radii $\langle r^2 \rangle^{1/2}$ (in fm) for bound states in ^{17}C.

	$^{16}\mathrm{C}(0^+) \otimes s_{1/2}$		$^{16}\mathrm{C}(0^+) \otimes d_{3/2}$		$^{16}\mathrm{C}(0^+) \otimes d_{5/2}$		$^{16}\mathrm{C}(2^+) \otimes s_{1/2}$		$^{16}\mathrm{C}(2^+) \otimes d_{3/2}$		$^{16}\mathrm{C}(2^+) \otimes d_{5/2}$	
	P	$\langle r^2 \rangle^{1/2}$	P	$\langle r^2 \rangle^{1/2}$	P	$\langle r^2 \rangle^{1/2}$	P	$\langle r^2 \rangle^{1/2}$	P	$\langle r^2 \rangle^{1/2}$	P	$\langle r^2 \rangle^{1/2}$
$^{17}\mathrm{C}(\frac{3}{2}^+)$			69	4.34			8	3.28	16	4.00	5	3.99
$^{17}\mathrm{C}(\frac{1}{2}^+)$	44	6.37							28	4.10	28	4.14
$^{17}\mathrm{C}(\frac{5}{2}^+)$					68	4.53	9	3.57	5	4.05	17	4.07

Chapter 5

Study of ^{18}C in Three Body System

5.1 ^{18}C Bound States

The ^{16}C-n interaction found in previous section is, strictly speaking, defined only for even partial waves as all the bound state of ^{17}C have positive parity. However, in the three-body system ^{16}C+n+n, odd partial waves will be present in the ^{16}C+n subsystem too. There are no experimental data which would allow us to fix the V_{odd} interaction in such subsystems. There are three strategies to deal with such a situation: (i) to use V_{odd} =0. This makes sense as the odd parity states in known neutron-rich carbon isotopes lie relatively high; (ii) To put V_{odd} equal to the V_{even} interaction in one of even partial waves and (iii) to find V_{odd} by fitting the ground state binding energy of ^{18}C. In this work, we try all three options.

For $V_{odd} \neq 0$, bound states may be present in the $0p$-wave. Such states should be forbidden as the $0p$ neutron shell is occupied. Therefore, we eliminate these states, as well as the $0s$ states, using the Pauli projection technique when $V_{odd} \neq 0$ is used. We reference the potential sets A and B for $V_{odd} \neq 0$ as $A1$ and $B1$, while for $V_{odd} = 0$ we use notations $A2$ and $B2$.

We have investigated convergence of the three-body solutions for the ^{18}C

binding energy. For 0^+ states, we were able to go up to $K_{\max} = 28$, for which the ground state energy is practically converged. The other two excites 0^+ states are above the ^{17}C+n threshold. The convergence in their energy is similar to that in ground state, however, one should keep in mind that no convergence could be achieved for states above the two-body threshold since such states are resonances whose energies are defined within their widths. For non-zero spins, computer memory limitations allowed us to go only up to $K_{\max} = 14$ for 4^+ state, $K_{\max} = 16$ for 1^+ and 2^+, and $K_{\max} = 18$ for 1^-. Although for these $K_{\max}$ the eigenenergies have not completely converged, their excitation energies are more stable with respect to increase of $K_{\max}$. Therefore, the all the excitation energies shown below are calculated with respect to the ground state energy at $K_{\max} = 14$.

The ^{18}C ground state binding energy calculated with $V_{odd} = 0$ is practically the same (see Table 4.1) for potentials $A2$ and $B2$. Including V_{odd} does not change it too much. Thus, for potential $A1$, where V_{odd} is the same as the V_{even} interaction in $l \neq 0$ it changes only by 33 keV. Such a small change in binding energy despite a huge change in odd potential results from a small probability of the odd partial waves in ^{18}C. This probability is approximately equal to 4 and 2 % for the A1 and A2 potentials respectively. Similar contributions from odd partial waves are obtained for the B1 and B2 potentials.

The energy of the first excited state 2^+ is more sensitive to the choice of the odd interactions. When V_{odd} is fitted to reproduce the ^{18}C ground state binding energy (potential set B1), the excitation energy of the 2^+ is above the experimental one by only 100 keV. This looks like a very good result but for the same potential the first 4^+ level unexpectedly decreases just below 2^+ (see Table 4.1), which contradicts our knowledge about nuclear structure. It is very difficult to know whether this is a consequence of the two-body potential model chosen, or is a result from unnoticed numerical problems arising in large scale three-body calculations. For $V_{odd} \neq 0$, the model space is much larger than that for $V_{odd} = 0$ because it includes also the model space

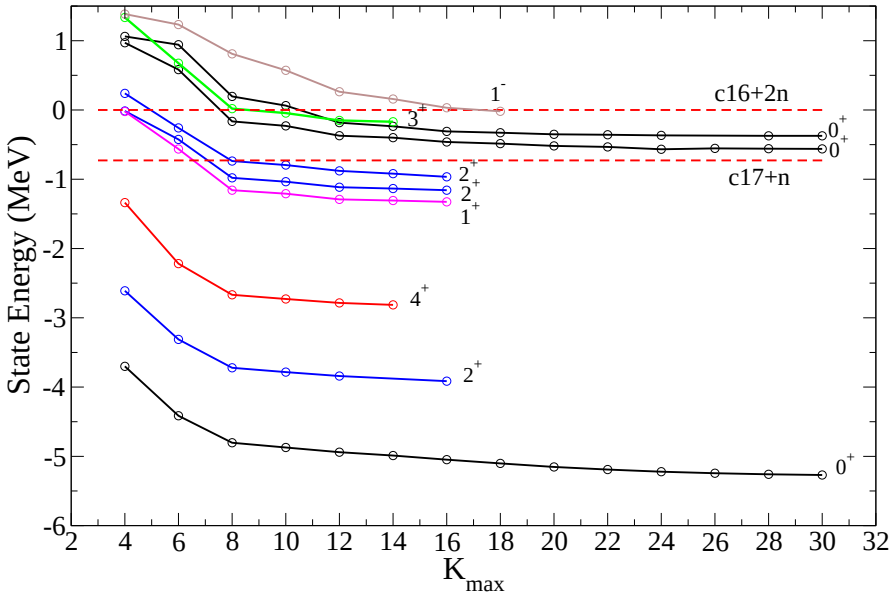

Figure 5.1: Convergence of the three body energies of ^{18}C states as a function of K_{max} obtained for the B2 potential.

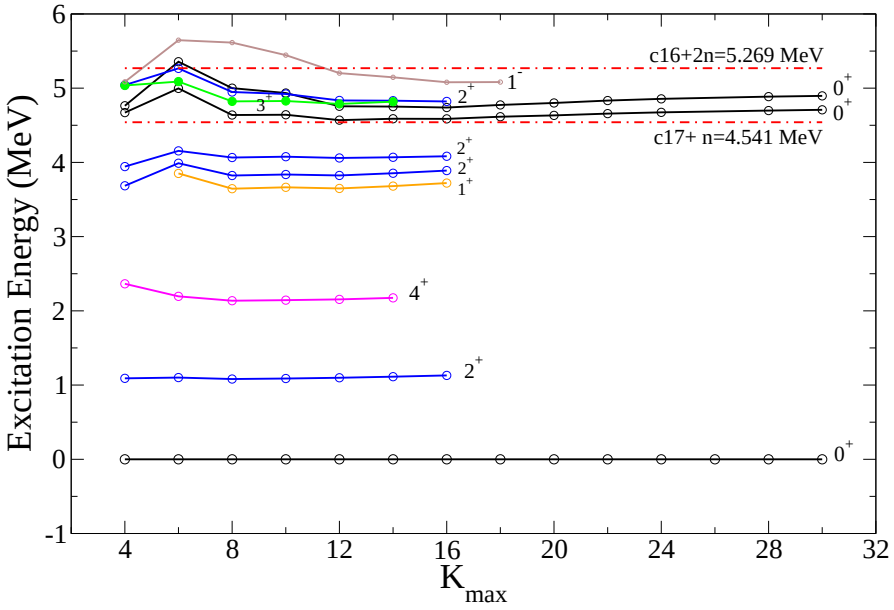

Figure 5.2: Convergence of the excitation energies of ^{18}C states, studied in three body model, as a function of K_{max} and obtained for the B2 potential.

of $0p$ forbidden states to which the total three-body wave function should be orthogonal. For 4^+, the number of channels becomes so large that it becomes physically impossible to verify the sensitivity of the three-body solutions to all the parameters that control their quality. We use the same sets of such control parameters both for $V_{odd} \neq 0$ and $V_{odd} = 0$, where no problems were encountered. However, this may not guarantee us from numerical problems in larger model spaces. On the other hand, there may be also a physical reason for abnormally low 4^+ state with the interaction chosen. At least, we have found out that the reason for low position of the 4^+ state obtained with the B2 potential was the l-dependence of the ^{16}C-n potential. When this l-dependence is removed, the split between the 0^+, 2^+ and 4^+ states looks more traditional but the ^{18}C three-body ground state becomes over-bound. Therefore, below we mainly discuss the results obtained with B2 potential for which the ordering of 2^+ and 4^+ states is correct.

For B2, the calculated ^{18}C binding energy of the ground state, $E = -5.26$ MeV is only about 350 keV larger than the experimental value of -4.92 MeV. The r.m.s. radius has converged to 2.932 fm. The distance between the two valence neutrons is $R_{nn} = 4.64$ fm and ^{16}C-n distance is $R_{n-^{16}C} = 3.85$ fm. The ^{18}C wave function is built on the ground state of the ^{16}C core rather than on its first excited state, with P(^{16}C(0^+))=62% and P(^{16}C(0^+))=28%. The composition of the ground state in terms of the $^{17}\mathrm{C}(J^\pi) \otimes nlj$ configurations is shown in Table 5.1.

The three-body 2^+_1 state is lower that the experimental one by 472 keV. The life time of this state has been recently measured and the $B(E2; 2^+ \rightarrow 0^+)$ transition probability has been determined in a lifetime measurement experiment [17] to be $4.3 \pm 0.2 \pm 1.0\ e^2fm^4$. The calculated three-body value of $B(E2 : 2^+ \rightarrow 0^+)$ for ^{18}C is 9.47 e^2 fm^4. This value has been calculated at $K_{\max} = 12$ and it differs from that obtained at $K_{\max} = 10$ by $\sim 1\%$. The three-body $B(E2)$ probability is about twice as large as the experimental value. Such an overestimation can result from neglecting interactions in odd partial waves. Indeed, using the potential set B1 instead of B2 we get 7.79

Table 5.1: The probabilities P (in per cents) of the $^{17}\mathrm{C}(J^\pi)\otimes nlj$ configuration for bound states in ^{18}C calculated with B2 potential

^{18}C	$^{17}C(3/2^+)\otimes$			$^{17}C(1/2^+)\otimes$			$^{17}C(5/2^+)\otimes$		
	$s_{1/2}$	$d_{3/2}$	$d_{5/2}$	$s_{1/2}$	$d_{3/2}$	$d_{5/2}$	$s_{1/2}$	$d_{3/2}$	$d_{5/2}$
0^+_1		38		11					42
2^+_1	6	12	5		10	16	9	5	14
2^+_2	0	3	22		0	0	0	45	21
4^+_1		32						32	12
1^+	0	0	42	0	0			41	0

e^2 fm^4, which is closer to experiment.

Apart from the 2^+_1 and 4^+ states discussed above, the B2 potential predicts another three states below the ^{17}C+n threshold, which are 1^+, 2^+_2 and 2^+_3. The 1^+ state, predicted at 3.68 MeV, is reasonably close the state at 4 MeV observed in Refs. [11, 18]. The 1^+ state could not be seen in the recent neutron knockout experiment with the ^{19}C beam because the cross section for population of this state should be very small [11]. On the other hand, the shell model calculations from [19] do not predict any 1^+ states below the ^{16}C+2n threshold, so that the low position of the three-body 1^+ state could have the same origin as the abnormal decrease of the 4^+ state, namely, the l-dependence of the ^{16}C+n interaction. As well as the 4^+ state, the 1^+ state is built on the d^2 configuration (see Table II), where the interaction is stronger. Including non-zero V_{odd} (using potential B1) pushes 1^+ into the region between the ^{17}C+n and ^{16}C+2n thresholds. Interestingly, the modification of the shell model interaction made in Ref. [18] brings the shell model 1^+ state into the vicinity of the ^{17}C+n threshold too.

The last two bound states, predicted with B2, are the two 2^+ states at 3.85 and 4.07 MeV. Both of them are close to the observed 4 MeV state with the tentative (2^+,3^+) parity assignment. For B1, the 2^+_2 state almost does not change its position, slightly shifting to 3.92 MeV, while the 2^+_3 state becomes

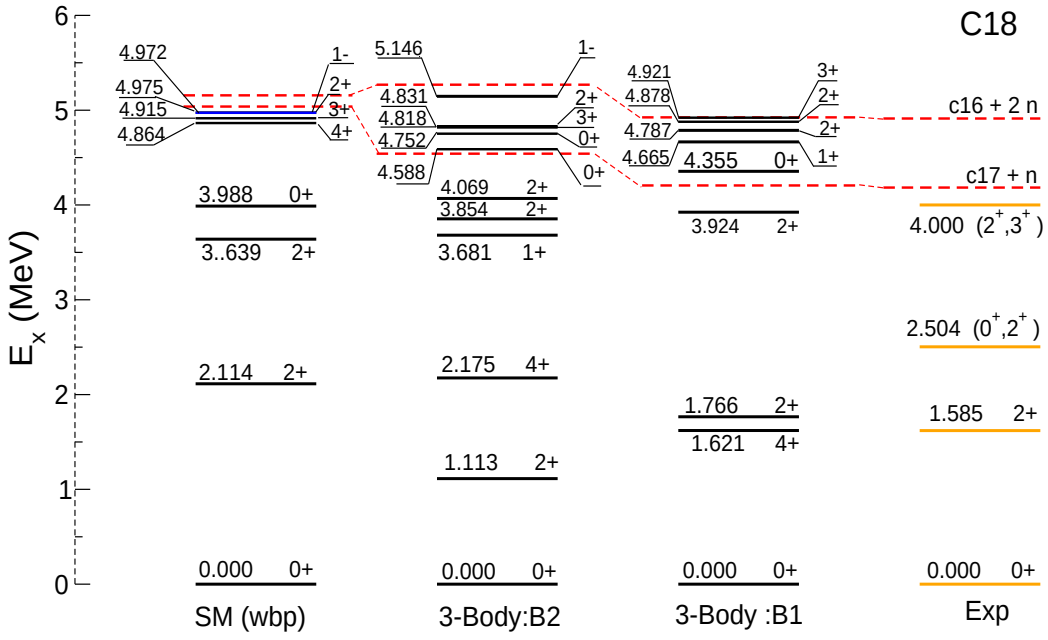

Figure 5.3: The three-body ^{18}C spectrum obtained with potential B2 and B1 in comparison to shell model spectrum from Ref. [10] and the latest experimental spectrum from Ref. [11].

unbound. Although the energy of the 2^+_3 is not converged, its decrease with $K_{\max}$ suggests that 2^+_3 becomes a two-body ^{17}C+n resonance. Both calculations support the 2^+ interpretation of the observed 4 MeV state. Such an interpretation is also consistent with the modified shell model calculations from Ref. [18]. However, this interpretation is not consistent with large cross sections for the neutron removal reaction of ^{19}C [11]. This contradiction could be resolved if two states, 2^+ and 3^+, existed in ^{18}C very close to each other near $E_x = 4$ MeV.

Finally, the three-body model cannot offer an explanation for the observed state at 2.5 MeV. Although it predicts a 4^+ state at 2.18 MeV, our current knowledge about the split between the first 0^+, 2^+ and 4^+ levels suggest that the lowering of the 4^+ state is more likely a by-product of the chosen two-body interaction. On the other hand, if a 4^+ excited state existed very close to 2.5 MeV next to either a hypothetical 0^+ or 2^+ state, then its de-excitation

by γ-ray emission would be almost indistinguishable from that from the 0^+ or 2^+ states. A hypothetical 4^+ state near 2.5 MeV would not have been seen in neutron knockout from ^{19}C either as it would require an $l = 4$ momentum transfer, which should be suppressed for dynamical reasons.

5.2]Unbound States Above the ^{17}C+n Threshold and their Contribution to the ^{17}C$(n,\gamma)^{18}$C Reaction Rate

The three-body model predicts five states above the ^{17}C+n but below the ^{16}C+2n threshold: two 0^+ sates along with a 2^+, 3^+, and 1^-. They should be seen a resonances in the ^{17}C+n two-body continuum. However, we predicted these states by solving a bound state problem and therefore do not know their widths. We estimate these widths in a single channel two-body ^{17}C+n model with a standard spherical Woods-Saxon potential (r_0 = 1.25 fm, a = 0.65 fm) whose depths is fitted to reproduce the calculated positions of theoretical resonances. The single-particle widths obtained in this way were multiplied then by the probabilities of the corresponding $^{17}\mathrm{C}(3/2^+) \otimes nlj$ configurations. The 0^+_2, 0^+_3 and 3^+ states are pure d-wave resonances, and their estimated widths are 0.04, 0.4 and 2 keV respectively. The p-wave resonance 1^- has an estimated width of 150 keV. The 2^+_4 state has s-wave and d-wave components built on $^{17}\mathrm{C}(3/2^+)$, the probability of the d-wave channel being about three times larger than that in the s-wave channel. The partial width in the d-wave channel is easily estimated in a similar way to be $\sim$4 keV. However, since there is no centrifugal barrier in the s-wave channel, we cannot provide any estimate for its width. It is questionable whether such a state could exist at all as the absence of any barriers could spread it over all the continuum. It is possible that it can exist as a virtual state, similar to ^{10}Li or ^{9}He, however, at present we cannot make any predictions for its scattering length.

Table 5.2: Reduced transition probabilities $B(J_i \rightarrow J_f;\sigma\lambda)$ (in $e^2fm^{2\lambda}$ for $\sigma\lambda = E\lambda$ and in μ_N^2 for $\sigma\lambda =$ M1), the corresponding partial widths Γ_γ and resonance strendth $\omega\gamma$ (both in eV). The resonance energies E_{res} and the γ-ray energies E_γ are in MeV. Transitions with very small contributions are not included in the table.

J_i^π	E_{res}	J_f^π	E_γ	$\sigma\lambda$	$B(\sigma\lambda)$	Γ_γ	$\omega\gamma$
0_2^+	0.047	2_1^+	3.46	E2	0.30	1.24×10^{-4}	1.55×10^{-5}
0_3^+	0.21	2_1^+	3.63	E2	0.54	2.82×10^{-4}	3.53×10^{-5}
		1^+	1.07	M1	3.51	4.99×10^{-2}	6.23×10^{-3}
3_1^+	0.28	2_1^+	3.71	E2	0.18	1.01×10^{-4}	8.84×10^{-5}
				M1	0.012	9.80×10^{-3}	8.58×10^{-3}
		2_2^+	0.96	E2	2.50	1.69×10^{-6}	1.48×10^{-6}
		2_3^+	0.75	M1	0.023	1.10×10^{-4}	9.68×10^{-5}
		1_1^+	1.14	E2	6.11	9.44×10^{-6}	8.26×10^{-6}
		4_1^+	2.64	E2	0.24	2.56×10^{-5}	2.24×10^{-5}
				M1	0.055	1.2×10^{-2}	1.05×10^{-2}
2_4^+	0.29	2_1^+	3.72	E2	0.30	1.71×10^{-4}	1.07×10^{-4}
				M1	2.2×10^{-4}	1.31×10^{-4}	8.19×10^{-5}
		2_2^+	0.98	E2	2.33	1.69×10^{-6}	1.06×10^{-6}
		1_1^+	1.15	E2	2.28	3.73×10^{-6}	2.33×10^{-6}
		0_1^+	4.83	E2	0.033	7.14×10^{-5}	4.46×10^{-5}
		4_1^+	2.66	E2	0.46	4.93×10^{-5}	3.08×10^{-5}
1_1^-	0.61	2_1^+	4.03	E1	0.21	14.45	5.42
		0_1^+	5.15	E1	0.018	2.53	0.95

The resonance energies of 0_3^+, 3^+ and 2_4^+ states, 0.211, 0.277 and 0.290 MeV respectively, are very close to those that corresponding to supernovae temperatures. We have calculated the contribution from these states to the resonant ^{17}C(n,γ)^{18}C reaction rate $N_A\langle\sigma\nu\rangle_R$. For an isolated narrow resonance i this rate is [19]

$$N_A\langle\sigma\nu\rangle_R = 1.54\times10^5\mu^{-3/2}T^{-3/2}\sum_i(\omega\gamma)_i \times\exp(-11.605E_i/T_9)\ \ \mathrm{cm^3mole^{-1}s^{-1}}, \tag{5.1}$$

where E_i is the resonance energy in MeV, T_9 is the temperature in 10^9 K, μ is the reduced mass $m_n m_{^{17}C}/(m_n+m_{^{17}C})$, where m_n is the neutron mass and $m_{^{17}C}$ is the mass of ^{17}C, and $\omega\gamma$ is the resonance strength (in eV) given by:

$$\omega\gamma = \frac{2J+1}{2(2j_t+1)}\frac{\Gamma_n\Gamma_\gamma}{\Gamma_{tot}}. \tag{5.2}$$

Here J and j_t are the spins of resonance and the target nucleus ^{17}C respectively, Γ_n and Γ_γ are the partial widths of the entrance and the exit channels respectively, and the total width Γ_{tot} is the sum over the partial widths of all channels. The partial widths Γ_γ are calculated from the electromagnetic reduced transition probabilities $B(J_i\rightarrow J_f;L)$ which is calculated in the same three-body model. Two types of electromagnetic transitionsn are possible for the 0_3^+, 3^+ and 2_4^+ resonances, E2 and M1, for which the Γ_γ partial widths are given by expressions [19]

$$\Gamma_{E2}[\mathrm{eV}] = 8.13\times10^{-7}E_\gamma^5[\mathrm{MeV}]\,B(E2)[\mathrm{e^2fm^4}], \tag{5.3}$$

$$\Gamma_{M1}[eV] = 1.16\times10^{-2}E_\gamma^3[\mathrm{MeV}]\,B(M1)[\mu_N^2]. \tag{5.4}$$

To calculate the electromagnetic transitions E2 and M1 in the three-body model, two terms in the transition operator are required: one that acts on the two valence neutrons and the other treating the collective excitation of the ^{16}C core. No effective charges were applied for neutrons in this work. Effective charges arise normally when the electromagnetic transitions have strong

contributions from the model spaces absent in the model Hamiltonians. This is the case in conventional shell model which does not account for clustering and correct asymptotic behaviour outside the range of the nucleon-nucleus interaction. Microscopic cluster models include them explicitly and do not use effective charges. Whether effective charges are needed in few-body models is still unclear. The three-body calculations of ^{16}C have shown that effective charges that reproduce the B(E2) value for ^{15}C lead to overestimated B(E2; $2^+ \rightarrow 0^+$) value for ^{16}C [1]. In the case of ^{18}C, the model space is much larger than was used for ^{16}C in [1], so the introduction of effective charges appears to be less necessary. The contributions that come from effective charges can be compensated by various other effects like, for example, two-body potentials in odd partial waves or contribution from other excited states of the core.

The E2 transition involves two matrix elements $\langle^{16}\mathrm{C}(0^+)|E2|^{16}\mathrm{C}(2^+)\rangle$, responsible for the core excitation, and $\langle^{16}\mathrm{C}(2^+)|E2|^{16}\mathrm{C}(2^+)\rangle$, which induces reorientation and is related to the quadrupole moment of ^{16}C. Both of these terms were taken to be consistent with the experimental deformation length of $\delta_m = \beta_m R_m = 1.3fm$ used to calculate the three-body ^{18}C wave functions. As for the M1 transition, we require the matrix element $\langle^{16}\mathrm{C}(2^+)|M1|^{16}\mathrm{C}(2^+)\rangle$. We calculate it in the spsdpf shell model with the WBP interaction [20] using the code NuShell@MSU [5].

The calculated Γ_{E2} are presented in Table 5.2. All of them are much smaller than neutron widths, which means that the resonance strength $\omega\gamma$ depends only on Γ_γ:

$$\omega\gamma \approx \frac{2J+1}{2(2j_t+1)}\Gamma_\gamma. \tag{5.5}$$

The resonant $E2$ reaction rates for 0_3^+, 3^+ and 2_4^+ are presented in Fig. 5.4, where they are compared to the non-resonant reaction rate,

$$N_A\langle\sigma\nu\rangle_{NR} = 3417.69\,T_9 - 358.029\,T_9^{1.66}\,\mathrm{cm^3 mole^{-1} s^{-1}}, \tag{5.6}$$

obtained by Herndl *et al* earlier in Ref. [19]. The resonant rates are about three order of magnitude smaller. This happens because the non-resonant

$E1$ capture proceeds via the p-wave entrance channel where the centrifugal barrier is smaller.

In calculating B(M1), we encountered two types of situations. For some transitions, this value is large for small $K_{\max}$ but decreases with increasing model space, and this decrease becomes faster with increasing $K_{\max}$. The B(M1) in such situations is not converged so we cannot estimate the corresponding M1 reaction rate. For only five transitions, $2^+_4 \rightarrow 2^+_1$, $0^+_3 \rightarrow 1^+$, $3^+ \rightarrow 2^+_1$, $3^+ \rightarrow 2^+_3$ and $3^+ \rightarrow 4^+$, have we obtained converged B(M1) values, which are shown in Table 5.2. The corresponding M1 contributions to the resonant reaction rate, arising from 0^+_3 and 3^+ resonances, are shown in Fig.5.4. They are two orders of magnitude larger than the corresponding E2 reaction rates, but still smaller than the non-resonant rate from Ref. [19]. The M1 contribution from 2^+_4 is about an order of magnitude smaller than the E2 one for the same state and it is not shown.

The three-body model predicts existence of the 1^- state around 600 keV, which is close to the energies relevant for supernovae explosions. We have calculated the resonant E1 contribution to the ^{17}C(n,γ)^{18}C reaction rate due to this state. The width Γ_γ for this case is [19]

$$\Gamma_{E1}[eV] = 1.06 E^3_\gamma[\mathrm{MeV}]\, B(E1)[\mathrm{e}^2\mathrm{fm}^2]. \tag{5.7}$$

The $B(E1)$ transition probabilities and Γ_{E1} are given in Table 5.2. The resonant E1 capture rate, shown in Fig.5.4, dominates the non-resonant capture calculated by Herndl *et al* at $T_9 \geq 1.2$.We have to mention, however, that the $\omega\gamma \sim 10$ eV obtained in our three-body calculations is much larger than the shell model value of 0.022 eV from Ref. [19]. If the shell model value is used in our calculations, the resonant reaction rate would still be lower than the non-resonant rate.

The resonant rates discussed above were obtained using the B2 potential set where interaction in odd partial waves is absent. Including V_{odd} (by using potential B1) pushes the 1^-, 3^+, 0^+_3 and 2^+_4 states above the ^{16}C+2n threshold. The 0^+_2 state will take place of the 0^+_3 state and the 1^+ state becomes unbound with respect to neutron emission. The 2^+_3 state will be just

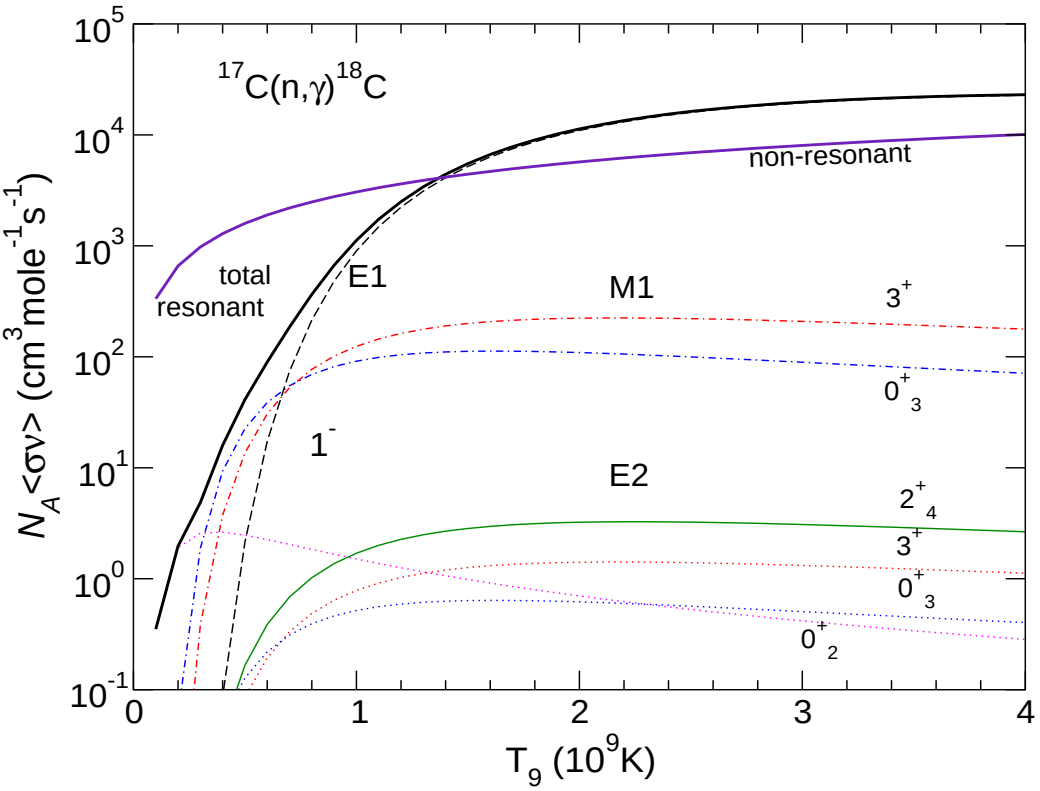

Figure 5.4: The resonant E2 (dot curves), M1 (dot-dashed curves) and E1 (dashed curves), contributions to the ^{17}C(n,γ) ^{18}C reaction rate, obtained in this work for individual resonant states J^π, in comparison with non-resonant reaction rate from [19] (violet solid line). The total resonant neutron capture is shown by a black solid line.

under the ^{16}C+2n, which is a bit far from the astrophysical relevant energies. In this case, the only important contribution to the resonant reaction rate may come from the M1 transitions from 1^+. However, we do not calculate it here.

5.3 Summary and Conclusions

We have studied the ^{18}C spectrum within a three-body deformed ^{16}C+n+n model with 2^+ excitation of the ^{16}C core. This study reveals that the bound state energy of ^{18}C is compatible with the three-body structure of this nucleus. Our model gives the energy of the first excited 2^+ state within 0.4 MeV of the experimentally observed one and suggest that there should exist another 2^+ state around 4 MeV, which is compatible with recent experimental studies. However, our model gives low positions of the first 4^+ and 1^+ levels, which could be a drawback of the ^{17}C+n interaction used. Although this interaction reproduces exactly the observed spectrum of ^{17}C, its composition in terms of probabilities of the core states is not reproduced. Including more excitation, for example, by adding the ^{16}C(4^+) into the coupled channel problem, could improve this situation, however it would increase the number of channels in the three-body problem to such extent that it would make such calculations impossible.

Our calculations suggest that there may be resonances in the region between the ^{17}C+n and ^{16}C+2n thresholds, the most important of which is 1^-. Interestingly, the recent analysis of the two-neutron knockout from ^{19}C [22] suggests that the important part of the removal cross section comes from population of the intermediate 1^- state in ^{18}C. If this resonance has a three-body structure and a large E1 strength associated with it, then it will give a large contribution to the ^{17}C(n,γ)^{18}C capture rate. The increased reaction rate may significantly influence the abundances of actinides synthesized in the r-process and, therefore, a search for this resonance is an important and timely task.

The three-body calculations suggest that a 2^+ state may be present in the astrophysical relevant region between the ^{16}C+2n and ^{17}C+n. This state should have a significant s-wave component in which the valence neutron does not see any centrifugal barrier. Such a state may manifest itself as a virtual state in the ^{17}C+n continuum. To calculate the contribution from this state correctly, a scattering three-body problem includes a binary channel

should be solved. This problem should also include core excitations and Pauli projection of forbidden states, which is too complicated at the moment. However, it is very important to perform such calculations properly because the presence of a virtual s-wave states could lead to an enhanced neutron M1 capture rate. Predictions for strong M1 enhancement have been recently made for a similar reaction, ^{17}F(p,γ)^{18}Ne, in the Gamow shell model [23].

Bibliography

[1] Horiuchi W. and Suzuki Y.: ^{22}C:An s-wave two-neutron halo nucleus. Phys. Rev.C 74, 034311(2006)

[2] Suzuki Y., Matsumura H. and Abu-Ibrahim B.: Structure of ^{15,16}C and phenomenology of the hindered E2 transition in ^{16}C. Phys. Rev.C 70, 051302(2004)

[3] Sagawa H., Zhou X. R., Zhang X. Z. and Suzuki T.: Deformation and electromagnetic moments in carbon and neon isotopes.Phys. Rev.C 70, 054316(2004)

[4] Abu-Ibrahim B., Horiuchi W., Kohama A. and Suzuki Y.: Reaction cross sections of carbon isotopes incident on a proton. Phys. Rev.C 77, 0346007(2004)

[5] Imai N. et al: Anomalously hindred E2 strenght B(E2: $2_1^+ \rightarrow 0^+$) in ^{16}C. Phys. Rev. Letts 92, 062501(2004)

[6] Nakamura et al: coulomb dissociation of ^{19}C and its halo structure. Phys. Rev. Letts 83, 1112(1999)

[7] Maddalena et al: Single neutron knockout reactions: Application to the spectroscopy of ^{16,17,19}C. Phys. Rev.C 63, 024613(2001)

[8] Bazin D. et al: One neutron halo of ^{19}C, Phys. Rev. Letts 74, 3569(1995)

[9] Bazin D. et al: Probing the halo structure of ^{19,17,15}C and ^{14}B. Phys. Rev.C 57, 2156(1998)

[10] Elekes, Z. et al.: Low-lying excited states in 17,19C. Phys. Lett. B 614, 174 (2005)

[11] Kondo, Y. et al.: One-neutron removal reactions of 18C and 19C on a proton target. Phys. Rev. C 79, 014602 (2009)

[12] Bohr, A., Mottelson, B.R.: Nuclear Structure, vol. II: Nuclear Deformation. Benjamin, New York (1975)

[13] Datta, U. et al.: Coulomb breakup of the neutron-rich isotopes 15C and 17C. Phys. Lett. B 551, 63 (2003)

[14] Ridikas, D. et al.: Exploratory coupled channels calculations for loosely bound carbon isotopes. Nucl. Phys.A628, 363 (1998)

[15] Batham, P., Thompson, I.J., Tostevin, J.A.: Dynamical core deformation effects on single-nucleon knockout reactions at fragmentation beam energies. Phys. Rev. C 71, 064608 (2005).

[16] Elekes, Z. et al.: Decoupling of valence neutrons from the core in 16C. Phys. Lett. B 586, 34 (2004)

[17] Ong, H.J. et al.: Lifetime measurements of first excited states in 16,18C. Phys. Rev. C 78, 014308 (2008)

[18] Stanoiu, M. et al.: Disappearance of the N = 14 shell gap in the carbon isotopic chain. Phys. Rev. C 78, 034315 (2008)

[19] Herndl H. et al.: Reaction rates for neutron capture reactions to C, N, andOisotopes to the neutron rich side of stability. Phys. Rev. C 60, 064614 (1999)

[20] Warburton E.K., Brown B.A.: Effective interactions for the 0p1s0d nuclear shell-model space. Phys. Rev. C 46, 923 (1992)

[21] Brown B.A., Rae W.D.M.: NUSHELL@MSU, MSU-NSCL Report, 2007 (unpublished).

[22] E.C.Simpson and J.A.Tostevin: One- and two-neutron removal from the neutron-rich carbon isotopes, Phys. Rev. C 79, 024616 (2009)

[23] R.Chatterjee, J.Okolowicz, M.Ploszajczak: Description of the ^{17}F(p,γ)^{18}Ne radiative capture reaction in the continuum shell model Nucl.Phys. A 764, 528 (2006)

Part B

Structural Study of Nuclei in the Vicinity of ^{100}Sn: $^{96-104}$Cd, ^{104,108}Sn, ^{106,108}Te and $^{102-108}$Mo Nuclei

Chapter 6

Study of Nuclei in the Vicinity of ^{100}Sn:Theoretical Framework

6.1 Introduction

In this second part of the work we chose to study an other mass region of nuclei far from stability. It is located at the other side of nuclear chart including proton-rich nuclei in the vicinity of ^{100}Sn. The importance of this region is due to its interest in nuclear structure and nuclear astrophysics.

The region, especially its cornerstone ^{100}Sn nucleus, is located at the very limits of nuclear stability giving more possibility in understanding the evolution of nuclear structure away from the stability line. The interest in the structure of nuclei located in the direct vicinity of the ^{100}Sn nucleus comes in part from the fact that this nucleus is the heaviest doubly-magic N=Z nucleus which can be synthesized. Hence, it offers a possibility to test the validity of the shell model in a many-body system where protons and neutrons occupy the same orbitals, also for relativistic mean field and Hartree-Fock calculations. This fact might also lead to interesting information about the interaction between the protons and neutrons, collective phenomena, and symmetries and charge invariance of the nucleon-nucleon forces.

In addition, the structure of the region has astrophysical consequences

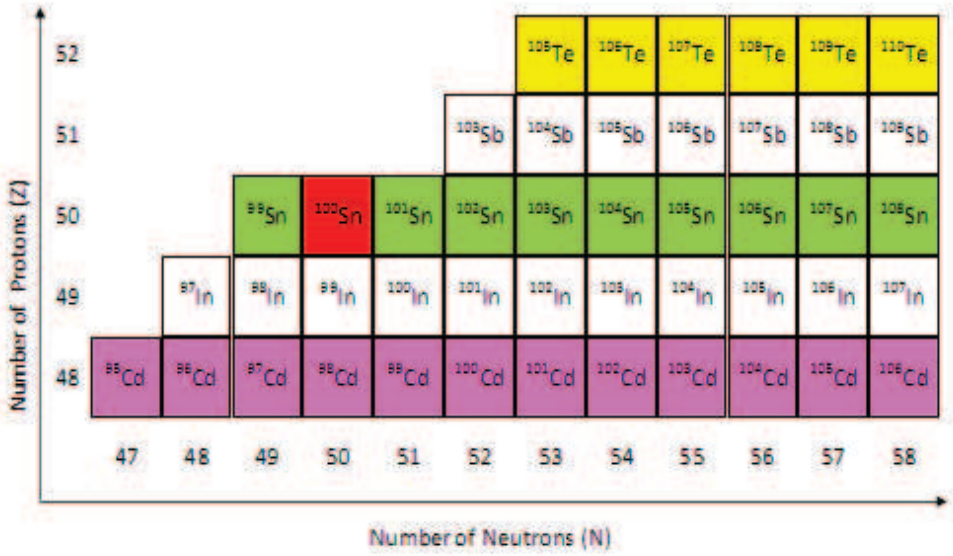

Figure 6.1: Segre nuclei chart part in the vicinity of the doubly magic nucleus ^{100}Sn

since it is predicted that the region 'southwest' of ^{100}Sn lies on the rapid proton capture (rp-process) path, which ends shortly beyond the N=Z=50 shell closure due to fast alpha decays.

For these reasons, this region is attracting growing interests in theoretically and experimentally perspectives. In this brief introduction we can mention, as examples, those works focusing on the nearest neighbors of ^{100}Sn because of its significant role in structure models and which have relationship with our work. In 2007 , Seweryniak et al [1] have measured the first two neutron states in ^{101}Sn, and the energy splitting between the single neutron $g_{7/2}$ and $d_{5/2}$ orbitals is evaluated to be 171.7(6) KeV. This work was a subject of a perfection two years later by the author and his collaborators [2]. The $0^+_{gs} \rightarrow 2^+$ transition strengths have been measured in ^{106,108}Sn

isotopes by Ekström et al [4]. The obtained results, $B(E2 : 0^+_{gs} \rightarrow 2^+) = 0.222(19)e^2b^2$ for ^{108}Sn and $B(E2 : 0^+_{gs} \rightarrow 2^+) = 0.195(39)e^2b^2$ for ^{106}Sn, are $\sim 30\%$ larger than shell model predictions and deviate from the generalized seniority model, which may be an indication of a weak N=Z=50 shell closure. Theoretically, Coraggio et al [3] have performed shell model calculations for odd-odd nuclei with neutron particles and proton holes around ^{100}Sn using realistic effective interaction derived from the CD-Bonn nucleon-nucleon potential. The even-even Te isotopes with $116 < A < 130$ have been studied in shell model framework to explain shell structure and collectivity in this isotopic chain [5].

In this work we aim to add a theoretical contribution in studying nuclei in the vicinity of the doubly magic nucleus ^{100}Sn, using two different models:shell model and and interacting boson model. The objective is to test the validity of these two models in region far from the stability. The many body shell model, is applied on even even isotopes of three chains with different model spaces: Cd, Sn and Te. Whereas the algebraic interacting boson model is applied on the lightest even-even molybdenum isotopes, $^{102-108}$Mo, which have the ratio $E4^+/E2^+$ higher than 2, an indicator of the existence of collective excitations.

6.2 Nuclear Shell Model

6.2.1 Prologue:The Nuclear Magic Numbers

The starting point of the nuclear shell model was, without any doubt, the nuclear properties of the magic nuclei and their neighbors. In nuclear physics nuclei with nucleons number, protons or neutrons or both of them, equal to 2, 8, 20, 28, 50, 82 and 126 are called magic nuclei because of their impressive properties compared to their neighbors. The accumulated experimental data for decades show the similarities of nuclear properties of these nuclei pointing out to closed shell structure corresponding to numbers of nucleons equal to magic numbers. Briefly, we can enumerate the most important of them.

More details can be reviewed in [6, 7]

- Nuclei with a magic number of protons or neutrons, or both of them, are found to be particularly stable. They are more tightly bound nuclei; and the separation energy of the last nucleon in nuclei with one more nucleons than the magic numbers is particularly low.
- Nuclei with magic numbers have an abundance of stable nuclides particularly large. Systematic study of stable isotones shows that nuclides with neutron numbers 20, 28, 50, and 82 are more abundant by 5 to 7 times than those with non-magic neutron numbers.
- The first excited states of even-even nuclei have higher than usual energies at the magic numbers, indicating that the magic nuclei are more tightly bound.
- The neutron capture cross sections for magic nuclei are small, indicating a wider spacing of the energy levels just beyond a closed shell

6.2.2 Basic Nuclear Nhell Model: The Mean Field

The Nucleus is a system of A nucleons, N neutrons and Z protons, interaction with each other by strong nuclear interactions. In addition, protons also feel the coulomb force. At first the nucleons are assumed to be point particles without any internal structure, the nuclear forces are described without attention to the basic mechanisms underlying them, and the two nucleon interaction is described by two body interaction matrix elements.

The aim of the targeted nuclear shell model is to reproduce the shell structure of nuclei where the closed shells correspond to the magic numbers of nucleons: protons or neutrons.

As the number of the nucleons, A, grows, the Schrodinger equation becomes impossible to be solved exactly. And to overtake this problem, one has to convert the strongly interacting system of A nucleons into a system of A particles freely moving in an average potential: the mean field potential.

This potential is assumed to resume all the mutual interactions between the nucleon and all the remaining A-1 nucleons of the system.

The Hamilton H of the many-body nucleus system consisting of kinetic energy T and potential energy V is

$$H = T + V = \sum_{i=1}^{A} t(r_i) + \sum_{i,j=1,j>i}^{A} v(r_i, r_j) = \sum_{i=1}^{A} \frac{-\hbar^2}{2m_0} \nabla_i^2 + \sum_{i,j=1,j>i}^{A} v(r_i, r_j) \tag{6.1}$$

where m_0 is the mass of a nucleon, and r_i denotes the nucleon coordinates of the nucleon i. By adding and subtracting a sum of single particle potential energy, $v(r_i)$, we get

$$H = \left[T + \sum_{i=1}^{A} v(r_i) \right] + \left[V - \sum_{i=1}^{A} v(r_i) \right] = H_{MF} + V_{RES} \tag{6.2}$$

where the nuclear mean field Hamiltonian is

$$H_{MF} = T + \sum_{i=1}^{A} v(r_i) = T + V_{MF} = \sum_{i=1}^{A} [t(i) + v(i)] = \sum_{i=1}^{A} h(i) \tag{6.3}$$

and

$$V_{RES} = V - \sum_{i=1}^{A} v(r_i) = \sum_{i,j=1,j>i}^{A} v(r_i, r_j) - \sum_{i=1}^{A} v(r_i) \tag{6.4}$$

is the residual interaction presumed to be much smaller in strength from the potential energy V.

In the mean field approximation we convert the strongly interacting A fermions system to a system of A non-interacting fermions where each nucleon can be viewed as moving in an external potential $v(r)$ created by the remaining A-1 neighbors.

The corresponding Schrodinger equation of the A non-interacting fermions system is:

$$H_{MF}\Psi_0(r_1, r_2, ..., r_A) = E\Psi_0(r_1, r_2, ..., r_A) \tag{6.4}$$

where the total wave function can be written, a priori, as the product of all the one-nucleon wave functions

$$\Psi_0(r_1, r_2, ..., r_A) = \phi_{\alpha_1}(r_1)\phi_{\alpha_2}(r_2)...\phi_{\alpha_A}(r_A). \tag{6.5}$$

Substituting this wave functions product into the Schrödinger equation (6.4) yields A identical one-nucleon Schrödinger equations for an external potential well

$$h(r)\phi_\alpha(r) = \epsilon_\alpha\phi_\alpha(r), \quad h(r) = t(r) + v(r) = \frac{-\hbar^2}{2m_0}\nabla^2 + v(r) \tag{6.6}$$

with the partial eigenvalues ϵ_{α_i} satisfying the condition

$$E = \sum_{i=1}^{A} \epsilon_{\alpha_i} \tag{6.6}$$

By the concept of the mean field we succeed to simplify the complicated many nucleon problem to a simple one-nucleon one. But the problem remains how to determine the mean field that minimizes the residual interaction between the non-interacting valence particles.

Hartree-Fock self consistency potential There are two point of view how to deal with the mean field potential V_{MF}: the microscopic method (Hartree-Fock) and the phenomenological method. Since our aim is not to enter into all the details of the field, and just to follow the procedure how to

solve the many body system problem at the nucleus scale, we refer for more details about the microscopic mean field method to [7, 10].

The Hartree-Fock is a method to solve the non-linear Hartree-Fock equation obtained from the Schrödinger equation by the variational method. The solution can be only carried out by *iteration*. A set of guessed single particle wave functions $\{\phi_i^{(0)}\}_{i=1}^{A}$ are used to calculate the initial potential term $V_{HF}^{(0)}$. As the following step we solve the equation for a complete set of new wave functions $\{\phi_\alpha^{(1)}\}_{\alpha=1}^{\infty}$ and eigenenergies $\epsilon_\alpha^{(1)}$. With this new set of eigenfunctions we generate the next potential $V_{HF}^{(1)}$ and solve again the Hartree-fock equation for the next set of eigenfunctions and eigenvalues. In schematic way, this process can be represented as

$$\phi_i^{(0)} \longrightarrow V_{HF}^{(0)} \longrightarrow \phi_\alpha^{(1)}, \epsilon_\alpha^{(1)} \longrightarrow V_{HF}^{(1)} \longrightarrow ... \longrightarrow \phi_\alpha^{(n)}, \epsilon_\alpha^{(n)} \tag{6.7}$$

This process is repeated until self consistency is achieved.

6.2.3 Phenomenological Potentials

The other method to determine the mean field, that is very often used and represents a practical shortcut, is just one selects a particular type of mean field potential. The more realistic choise is the Woods-Saxon potential

$$v_{WS}(r) = \frac{-V_0}{1 + e^{(r-R)/a}} \tag{6.8}$$

Its usual parameters are: The nuclear radius $R = r_0 A^{1/3} = 1.27 A^{1/3} fm$, the surface diffuseness $a = 0.67 fm$ and the depth of the well V_0. The later one has different values for neutrons and protons because of the addition of the coulomb interaction effect for the protons. A suitable average value of $V_0 = 57 MeV$ is usually taken when not making distinction between nucleons.

The problem in the Woods-Saxon central potential, in general, is that there is no analytical solutions of the Schrödinger equation. The simplest frequently used potential is the three dimensional harmonic oscillator potential

$$v_{HO}(r) = -V_1 + kr^2 = -V_1 + \frac{1}{2}m_0\omega^2 r^2 \tag{6.9}$$

where V_1 and k are two parameters to be fitted for best result.

This potential is a good approximation of the 2^{nd} order for the Woods-Saxon potential expansion. The central potential succeeds to reproduce the qualitative behavior of the single particle energies. However for the higher values of angular momentum, clear differences between the two potentials appear, especially the asymptotic behavior. Higher order of the expansion are necessary to restore the equivalence (edge term $\sim \overrightarrow{l}^2$). The observed energies bunch into groups, or shells. Only three of the major shells, corresponding to magic numbers: 2, 8 and 20, are reproduced by the central potential .

To reproduce theoretically all the observed numbers experimentally, Goepert-Mayer [8] and Axel, Jensen and Suess proposed [9] the addition of an other term to the mean field called *spin-orbit interaction*.

In fact, this Spin-Orbit interaction, or coupling or force, splits the states of the same orbital angular momentum quantum number l into two, with total single particle angular momenta $j = l + \frac{1}{2}$ and $j = l - \frac{1}{2}$.

The main features of the spin-orbit term are : the splitting energy scale is of the same scale of the single-particle differences which affected the global shell structure, and the splitting has an opposite order so that the the state $j = l + \frac{1}{2}$ is always lower in energy compared to the state $j = l - \frac{1}{2}$.

Thus, the Hamiltonian of single nucleon is written as:

$$h(r) = t(r) + \frac{1}{2}m_0\omega^2 r^2 + D\,\overrightarrow{l}^2 + f(r)\,\overrightarrow{l}\,\overrightarrow{s} \tag{6.9}$$

The term $D\,\overrightarrow{l}^2$, called the edge term, is for adjusting the Harmonic Oscillator to Woods-Saxon potential at the limits of the well. The eigen-wavefunctions of the Hamiltonian $h(r)$ are of the form

$$\phi_{nljm} = R_{nl} \sum_{m_l, m_s} \langle l m_l \frac{1}{2} m_s | jm \rangle Y_l^{m_l}(\theta, \varphi) \chi_s^{m_s}(\sigma) \tag{6.10}$$

where $Y_l^{m_l}(\theta, \varphi)$and $\chi_s^{m_s}(\sigma)$ are the Spherical Harmonics and spin functions respectively. The corresponding eigenenergies are given by:

$$E_{nlj} = (N + 3/2)\hbar\omega + Dl(l+1)\hbar^2 + \frac{\hbar^2}{2}\langle f(r)\rangle_{nl} \begin{cases} -l(l+1) & \text{if} \quad j = l - \frac{1}{2} \\ l & \text{if} \quad j = l + \frac{1}{2} \end{cases} \tag{6.11}$$

The total wave functions Φ_0, solutions of the equation (6.4), are the products of the single nucleon wave function given by eq(6.10) with the eigenenergies given by eq(6.11).

As the nucleons are fermions, the total wave functions have to be antisymmetric according to the exclusive Pauli principle. The representation of the wave functions as Slater determinants can verify this condition. Thus, the total wave function is thus written as the following Slater determinant

$$\Phi_0 = \mathcal{A} \prod_{i=1}^{Z} \phi_{\pi_i} \mathcal{A} \prod_{j=1}^{N} \phi_{\nu_j} \tag{6.12}$$

Here, $\mathcal{A}$ is an antisymmetrization operator that performs the sign-accompanied permutations of the single-particle orbitals in the product wave function; $\mathcal{A}$ also carries a normalization factor. For example, for three particles in single particle states labeled 1,2,3 the normalized antisymmetric state, or Slater determinant, is

$$\Phi_0(r_1, r_2, r_3) = \frac{1}{\sqrt{6}} \begin{vmatrix} \phi_1(r_1) & \phi_1(r_2) & \phi_1(r_3) \\ \phi_2(r_1) & \phi_2(r_2) & \phi_2(r_3) \\ \phi_3(r_1) & \phi_3(r_2) & \phi_3(r_3) \end{vmatrix} \tag{6.12}$$

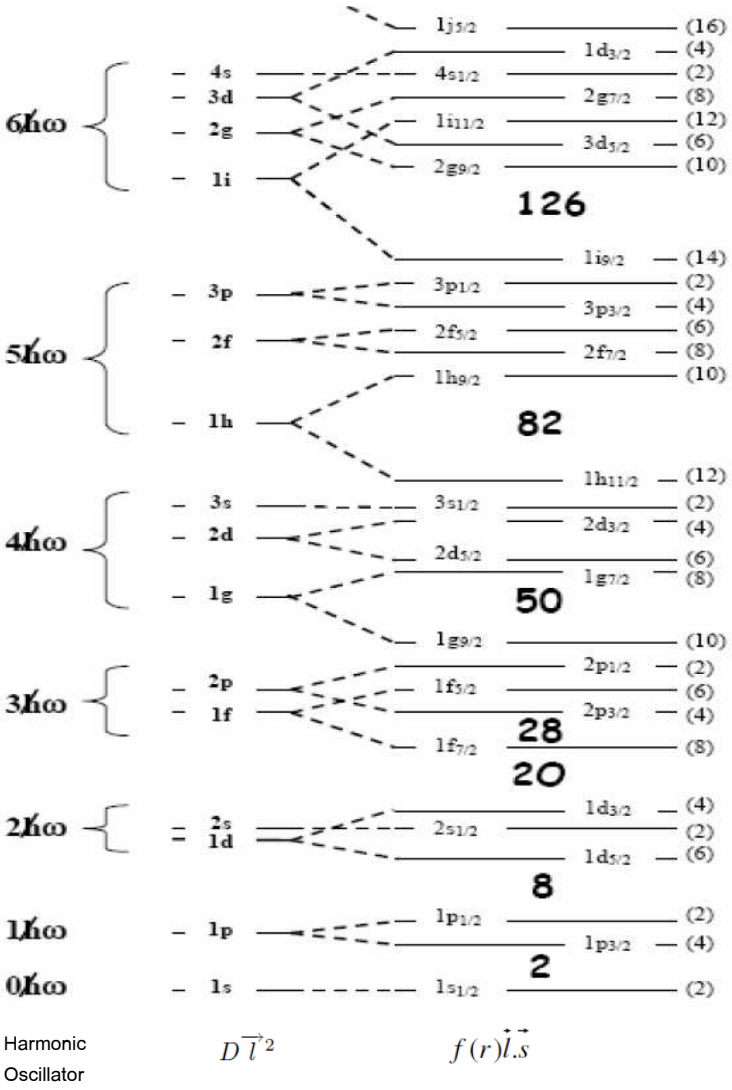

Figure 6.2: Nuclear levels scheme of the mean field with Spin-Orbit term

6.2.4 The Ingredients of Shell Model Calculation

Each Shell Model calculation requires the definition of the following ingredients:

- Definition of a valence (or model) space,
- Derivation of the effective interaction consistent with the chosen model space,
- Calculation code to construct and diagonalize the Hamiltonian of the system.

i) The Model Space

We mean by "model space", also called "valence space", the set of orbitals and the truncation within that set of orbitals assumed in generating a calculation in a many-body model. Generally, the larger is the model space, the best and most complete the results are. However the computation time increases exponentially with the size of the model space.

A typical model spaces are those constitute of the complete LS major shells. There are regions of nuclei in which the valence protons an neutrons go into the same major shell like as:

- *The p shell:* Two orbitals are included in the model space: $0p_{1/2}$ and $0p_{3/2}$ in which nuclei properties of $2 < N, Z < 8$ may be described and the core is the ^{4}He.
- *The sd shell:* This model space is composed of three orbitals: $0d_{3/2}$, $1s_{1/2}$ and $0d_{5/2}$. In this model space we can describe the positive states of nuclei with $8 < N, Z < 20$. The inert core is ^{16}O.
- *The pf shell:* The orbitals included in this valence space are $0f_{7/2}$, $1p_{3/2}$, $0f_{5/2}$ and $1p_{1/2}$. Nuclei with $20 < N, Z < 40$ can be treated within this model space. The core used is ^{40}Ca.

- *The r_3g shell* formed of $r_3 \equiv 1p_{3/2}$, $0f_{5/2}$ and $1p_{1/2}$, and $g \equiv 0g_{9/2}$. Within this model space nuclei with $28 < N, Z < 50$ are described; the inert core is ^{56}Ni.

- *r_4g shell* composed of subsells $0g_{7/2}$, $1d_{5/2}$, $1d_{3/2}$, $2s_{1/2}$ and $0h_{11/2}$ is the most adequate model space to study nuclei with $50 < N, Z < 80$; the inert core is ^{50}Sn.

There are other regions in which the model space involves protons in one major shell and neutrons in another, such as the $p - sd$ region for light neutron-rich nuclei with $2 < Z < 8$ and $8 < N < 20$, and the $sd - pf$ region for medium neutron-rich nuclei with $8 < Z < 20$ and $20 < N < 40$.

In this work in studying nuclei in the A=100 mass region in the vicinity of ^{100}Sn, we used the r_4g model space for Sn isotopes and Te isotopes. Lightest Cd isotopes are studied within the r_3g model space, and a mixing configuration involving r_3g and r_4g model spaces for protons and neutrons, respectively, is used for the heavier isotopes of Cd.

ii) The Effective Interaction

The main problem in nuclear shell model has long been the determination of the effective interactions V_{eff}. The intuitive starting point in the derivation of these interactions is the free nucleon-nucleon potentials.

Any realistic free nucleon-nucleon interaction (N-N) exhibits a strong short range repulsion for small distances, this is the so called hard core potential. At such short distances, carrying nuclear structure and matter calculations, within many body model, faces the problem that the energy between nucleons for such interaction $\langle\psi|V|\psi\rangle$ evaluated for uncorrelated wave function $\psi(r)$ diverges, since the uncorrelated wave function is different from zero, also for relative distances r smaller than the hard core radius. Similarly, even one uses interactions with soft cores, the matrix elements become very large at short distances[4].

For the last 60 years, there were two points of view how to see the solution in order to overcome this problem giving rise for two main approaches of the nuclear effective interaction.

Realistic effective interaction:
This method aims to construct an apropriate effective interaction starting from the bare nucleon-nucleon (N-N) interaction. The traditional way to overcome the divergence difficulty is The Brueckner G-matrix method, elternatively called the renormalized G matrix. Its is used to obtain a set of two body matrix elements (TBME) for the model space. This takes into account the short repulsive behavior of the interaction via the ladder diagrams. The G-matrix can then be renormalized to include the effects of mixing with configurations outside the model space- the core-polarization diagrams. In this method, the renormalized G matrix, one usually takes the experimental single particle energies (SPE), when available, together with the renormalized G matrix (TBME). Calculations with this method for a few valence particles or holes are very successful, which is not the case when the number of valence particles or holes is increasing [19, 4].

To minimase the disadvantages encountered with shell model calculations over a wide mass region using a purely realistic interaction based on the renormalised G matrix, an empirical approaches to the realistic effective interaction are made. In these approaches, the Hamiltonians start from the G matrix but they are empirically renormalised to account the divergence encountered with the G matrix. The remarkable success known of method is based upon the fact that the shell model spectra and excitation energies are related to only a relatively few TBME or linear combinations of TBME [19].

Phenomenological approach of the effective interaction:
Because of the difficulties encountered in using the microscopic approach to nuclear structure and matter density calculations, some studies have been performed at the end of 60's which aimed at building an approach to nuclear structure starting directly from a parametrized form of the effective interaction. This parametrization is chosen to be simple enough in order to be

used in complex calculations such as the fission and matter density. Similarities with the G-Matrix are also accounted in building these interactions, especially those related to the correlations associated with the repulsive core of the bare N-N interaction (short rang correlations), and can thus be employed to describe independant particle states. In the last decades, different phenomenological effective interactions have been proposed. Two of them are the most employed: Skyrme interaction [20] and Gogny interaction [21].

iii) Shell Model Code

There are several methods for carrying out the many body calculation. One of these involves defining the configurations within the model space in terms of an M-scheme basis. Diagonalization of the Hamiltonian in the M-scheme basis results in eigenfunctions with good J

Another method involves configurations defined in terms of definite J_i coupling of the intermediate states to a total value J . The dimension of the M-scheme is much larger than the J-scheme basis. For example, for 12 particles in the sd model space (^{28}Si) the $M = 0$ dimension is 93710 and the $J = 0$ dimension is 839. Although the matrix is much larger in the Mscheme, the computation of the elements of the matrix is much easier. M-scheme and J-scheme codes are competitive, but there are situations where one is preferred over the other.

A third type of code [12] starts with an M-scheme basis and generates a basis of good J states with an angular momentum projection operator.

Modern versions of the M-scheme code are ANTOINE [13], VECSSE [14] and MSHELL [15]. Versions of the J-scheme code are RITSSCHIL [16]and and NATHAN [17]. OXBASH [12] is the only version of the projection method. The OXBASH computer package comes with a library of Hamiltonians. When the OXBASH Hamiltonians are used they should be referenced to original articles in the literature.

In our work we used the NuShell@MUS code. It is a nushell core program with input and output formats in the OXBASH style. It is a set of programs

for carrying out shell model calculations with dimensions up to about 100 000 in the $J-T$ scheme and about 2 000 000 in the M-scheme. As like as OXBASH, NuShell@MSU code comes with library of model spaces and interactions. Carrying out NuShell@MSU calculation needs specification of the model space and the Hamiltonian references in the code library [11].

6.3 The interacting Boson Model (IBM)

The interacting boson model (IBM) is an algebraic model which has been introduced in 1974 by Arima and Iachello. In this approach the collective low lying states of even-even nuclei are described by a system of N interacting bosons: s(L=0) and d(L=2) [22]. The 36 belinear operators $s^{\dagger}s$, $s^{\dagger}\tilde{d}_{\mu}$, $(d^{\dagger}\tilde{d})^{(l)}_{\mu}$, $l=0,1,2,3,4$ and $-l\leq\mu\leq l$ are the generator of the $U(6)$ algebra. Three subalgebra chains can be derived:

$$
\begin{aligned}
&(I) \quad U(6)\supset U(5)\supset SO(5)\supset SO(3)\\
&(II) \quad U(6)\supset SU(3)\supset SO(3)\\
&(III) \quad U(6)\supset SO(6)\supset SO(5)\supset SO(3)
\end{aligned}
$$

The general Hamiltonian can be written as [23]

$$
H=\varepsilon\hat{n}_d+a_0P^{\dagger}P+a_1\ddot{L}\ddot{L}+a_2QQ+a_3T_3T_3+a_4T_4T_4 \tag{6.12}
$$

Where

$$
\begin{aligned}
&P=\frac{1}{2}(\tilde{d}\tilde{d}-ss)\\
&T_l=(d^{\dagger}\tilde{d})^{(l)} \quad , \quad l=0,1,2,3,4\\
&Q=(s^{\dagger}\tilde{d}+d^{\dagger}\tilde{s})^{(2)}-\frac{\sqrt{7}}{2}(s^{\dagger}\tilde{d})^{(2)}=(s^{\dagger}\tilde{d}+d^{\dagger}\tilde{s})^{(2)}-\frac{\sqrt{7}}{2}T_2\\
&\hat{n}_d=\sqrt{5}T_0 \quad , \quad \hat{L}=\sqrt{10}T_1
\end{aligned}
$$

This model has been successfully applied to describe the structure of medium and heavy nuclei either vibrational ($U(5)$ limit (I)), rotational ($SU(3)$ limit (II)) or gamma-unstable ($SO(6)$ limit (III)).

6.4 The Consistent Q Formalism

For deformed nuclei, a simpler version of IBM has been introduced: the consistent Q formalism (CQF) [23]. In the CQF Hamiltonian the effect of the pairing term ($P^\dagger P$) is taken into account through a free value of the T_2 factor in the quadupole operator. This leads to the reduced form:

$$H = a_2 Q^\chi Q^\chi + a_1 \hat{L}\hat{L} \tag{6.10}$$

where

$$Q^\chi = (s^\dagger d + d^\dagger s)^{(2)} + \chi (d^\dagger d)^{(2)} \tag{6.11}$$

Bibliography

[1] D. Seweryniak et al.:Single-Neutron States in ^{101}Sn, Phys. Revi. Lett. 99, 022504 (2007)

[2] D. Seweryniak et al.:New Results Near ^{100}Sn: Observation of Single-Neutron States in 1^{101}Sn, Acta Physica Polonica B, 40, 621 (2009)

[3] L. Coraggio, A. Covello, A. Gargano, and N. Itaco :Structure of particle-hole nuclei around 100Sn, Phys. Rev. C 70, 034310 (2004)

[4] A. Ekström et al, $0^+_{gs} \rightarrow 2^+$ Transition Strenghts in ^{106}Sn and ^{108}Sn, Phys. Revi. Lett. 101, 012502 (2008)

[5] Somnath Nag, Purnima Singh, S. K. Ghorui, and A. K. Singh: Shell Model Calculation for Te isotopes, proceeding of DAE Symp. on Nucl. Phys. 55, 60 (2010)

[6] W. E. Meyerhof, Elements of Nuclear Physics, McGraw-Hill, New York (1967).

[7] Kris L. G. Heyde, The nuclear Shell Model, 2nd edition, Springer-Verlag, Berlin Heidelberg (1994)

[8] M. Mayer: On Closed Shells in Nuclei. II, Phys. Rev. 75, 1969 (1949).

[9] O. Axel, J.H.D. Jensen, H.E.Suess:On the "Magic Numbers" in Nuclear Structure, Phys. Rev. 75, 1766 (1949).

[10] J. Suhonen: From nucleon to nucleus, Springer-Verlag Berlin Heidelberg, New york 2007

[11] B. A. Brown and W. D. M. Rae: NuShell@MSU, MSU-NSCL report (2007) (unpublished).

[12] B. A. Brown, A. Etchegoyen, W. D. M. Rae, N. S. Godwin, W. A. Richter, C. H. Zimmerman, W. E. Ormand and J. S. Winfield, MSU-NSCL Report No. 524, 1985.

[13] E. Caurier et al.: shell-model code ANTOINE, CRN, Strasbourg, 1989; E. Caurier, F. Nowacki, Acta Phys. Pol. B 30, 705 (1999).

[14] A. Schmidt et al.: Low spin structure of the N=Z odd-odd nucleus $^{50}_{25}Mn_{25}$, Phys. Rev. C 62, 044319 (2000).

[15] T. Mizusaki, RIKEN Accel. Prog. Rep. 33, 14 (2000).

[16] D. Zwarts, Comp, Phys, Comm. 38, 365 (1985).

[17] E. Caurier et al.: shell-model code NATHAN, unpublished.

[18] M. Hjorth-Jensen T. T. S. Kuo and E. Osnes: Realistic effective interactions for the nuclear shell model, Phys. Rep. 261, 125 (1995).

[19] B. Alex Brown: The Nuclear Shell Model Towards the Drip Lines, Prog. Part. Nucl. Phys. 47, 517 (2001)

[20] M. Beiner, H. Flocard, Nguyen Van Giai, P. Quentin: Nuclear ground state properties and self-consistent calculations with the Skyrme interaction(I): Spherical description, Nucl. Phys. A238, 29 (1975)

[21] J. Decharge, D. Gogny: Hartree-Fock-Bogolyubov calculations with the D 1 effective interaction on spherical nuclei, Phys. Rev. C 21, 1568 (1980)

[22] F. Iachello and Arima, The Interacting Boson Model, Cambridge University Press 1987

[23] R.F. Casten, D.D. Warner: The interacting boson approximation, Rev. Mod. Phys. 60, 389(1988)

Chapter 7

SM and IBM calculation Results

7.1 Shell model study of ^{100}Sn mass region nuclei

The doubly magic nuclei are the cornerstones of the nuclear landscape. The properties of stable nuclei of them such as ^{16}O, ^{40}Ca and ^{208}Pb are quite well known. Nuclear structure models have achieved a remarkable successes in describing properties of these nuclei and their nieghbours.

In the other hand, the surface of exotic nuclei on the nuclear chart is enlarging abundantly in the two directions: proton-rich and neutron-rich nuclei. New structural phenomena and data about the residual interaction are becoming now available for many nuclei in these regions which provide a challenging testing ground for current models. Much attention is currently focused on nuclei in the regions of shell closures. In this context, data on the exotic doubly magic nuclei ^{48}Ca, ^{78}Ni, ^{100}Sn, and ^{132}Sn are invaluable. In this part of the work, we interest only in studying, within the shell model, nuclei in the vicinity of ^{100}Sn.

The shell model is the basic framework for nuclear structure calculations in terms of nucleons. Since its development early 1950s to now, hundreds of

calculations within this model have been carried out, many of them being very successful in describing a variety of structure phenomena.

One of the challenges of this model, as well as all the other current nuclear models, is to explore the extent to which it can describe nuclei situated far from the line of stability and to develop extrapolations to nuclei which cannot be readily synthesized in a laboratory but play an important role in astrophysics.

In this part, we performed calculations within shell model for even-even nuclei of three isotopic chains in the vicinity of the doubly magic nucleus ^{100}Sn: $^{96-104}$Cd, $^{104-108}$Sn an ^{106,108}Te. The calculations have been carried out using the windows version of NuShell@MSU [5]. The two main ingredients needed are the single particle energies (SPE) of the model space orbitals, and two body matrix elements (TBME) of the effective interaction between valence nucleons. For the former, we will discuss the determination of the SPEs corresponding to orbitals of each chosen model space. What concerns the latter, calculations have been performed using the renormalised two body effective interaction based on G-matrix derived from the CD-Bonn free nucleon-nucleon potential [6]

7.1.1 Cd isotopes chain

For this isotopic chain, we can distinct between two groups of isotopes seeing the model space we have to use in studing them in many body shell model.

For the $^{96}_{48}$Cd$_{48}$ and $^{98}_{48}$Cd$_{50}$ the model space contains the same orbits. The number of protons and neutrons are $28 \leq$ Z,N ≤ 50, and thus they fill the same sub-shells. The wave functions are obtained in the model space ($1p_{3/2}$,$0f_{5/2}$,$1p_{1/2}$,$0g_{9/2}$) for both protons and neutrons.

The single particle energies (SPEs) for protons are obtained from the $^{79}_{29}$Cu$_{50}$ spectrum levels. The relative values of these energies corresponding to the core $^{78}_{28}$Ni$_{50}$ are: -14.938, -13.437, -12.044 and -8.905 MeV for the orbitals : $0f_{5/2}, 1p_{3/2}, 1p_{1/2}$, and $0g_{9/2}$, respectively.

The SPEs for neutrons are obtained from the excitation energies of neu-

.

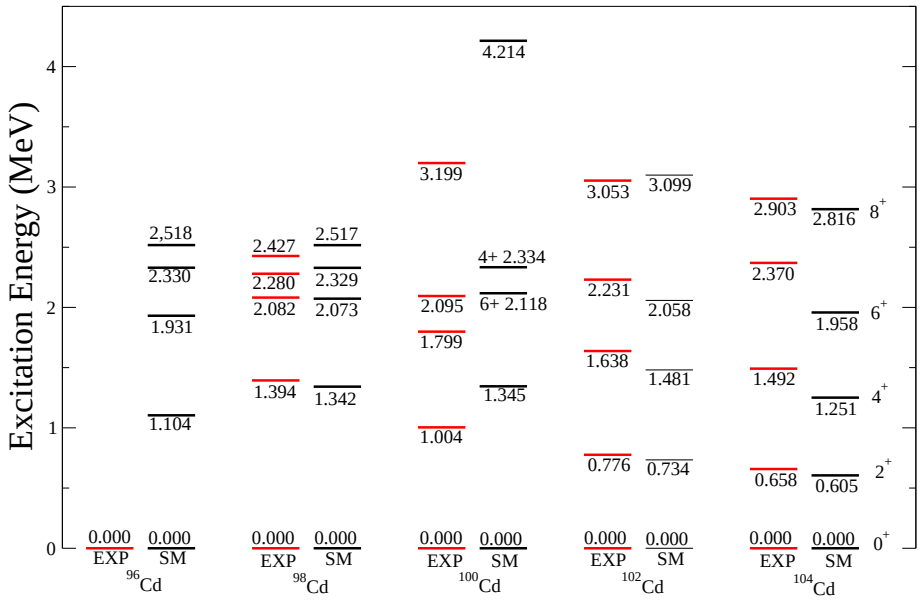

Figure 7.1: NuShell shell model calculations of Cd isotopes chain spectrum compared with the available experimental data. Spectrums of $^{96}_{48}Cd_{48}$ and $^{98}_{48}Cd_{50}$ are obtained using jj44pna interaction [2], whereas the jj45pna interaction is used for the others

tron in $^{57}_{28}Ni_{29}$, and their relative values to the corresponding core $^{56}_{28}Ni_{28}$ are: -9.988, -9.153, -8.361 and -5.255 MeV for levels $1p_{3/2}, 0f_{5/2}, 1p_{1/2}, 0g_{9/2}$, respectively. The interaction used here is the same used by Lisetskiy et al [2] to study nuclei in the vicinity of $^{78}_{28}Ni_{50}$ labeled in the NuShell code by jj44pna.

The results obtained for $^{98}_{48}Cd_{50}$ are in good agreement compared to the existing experimental data, even we did not change the single particle energies (SPEs) of the model space orbitals to adjust them with the region and we saved the same ones used by Lisetskiy et al [2] for nuclei in the vicinity of the doubly magic exotic nucleus $^{78}_{28}Ni_{50}$. In the vicinity of $^{100}_{50}Sn_{50}$ and for these two isotopes of Cd chain, protons and neutrons SPEs should be the orbitals excitation energies of proton hole in $^{99}_{49}In_{50}$ and neutron hole in $^{99}_{50}Sn_{49}$ respectively. More experimental data about the $^{96}_{48}Cd_{48}$ might confirm the predictions of our calculations 7.1, or push to more perfections of the

used interaction.

For the isotopes $^{100}_{48}Cd_{52}$, $^{102}_{48}Cd_{54}$ and $^{104}_{48}Cd_{56}$, the wave functions were obtained in the model space ($0g_{7/2}, 1d_{5/2}, 1d_{3/2}, 2s_{1/2} and 1h_{11/2}$) of neutron particle orbitals, and ($1p_{3/2}, 0f_{5/2}, 1p_{1/2}, 0g_{9/2}$) of proton hole orbitals. We used the interaction in NuShell@MSU library labeled by jj45pna. This interaction is based on the renormalized G-matrix and the single particle energies are adjusted to the ^{132}Sn mass region.

Although we did not make changes on the interaction initially made for nuclei in the vicinity of neutron-rich doubly magic nucleus,^{132}Sn, results for ^{102}Cd and ^{104}Cd are more or less acceptable compared to the experimental data. But significant discrepancies are obvious for the ^{100}Cd spectrum. The states sequence is disordred and the energy differences are significant.

7.1.2 Sn isotopes chain

In this subsection we present results for the even ^{104,106,108}Sn isotopes using the doubly magic nucleus ^{100}Sn as core and distributing the valence neutrons over the model space constituted of the single-particle orbits in the N = 4 oscillator shell ($1d_{5/2}, 0g_{7/2}, 1d_{3/2}, 2s_{1/2}$) and the orbital $0h_{11/2}$ from the N = 5 oscillator shell. Because of the zero valence protons in this isotope chain, there is no effect of the protons on their spectra, and thus we delay the discussion of the model space and the definition of the corresponding single proton energy to the next section where we present the study of the Te isotopic chain.

Because of the poor experimental data available for the system with one valence neutron,^{101}Sn, we used the ^{107}Sn spectrum to establish the single particle energies of the neutron model space orbitals. This method has been used in previous works to overtake the lack of information about the nucleus just next the core [4, 3]. ^{107}Sn is the lightest odd isotope which figures four of the five of the model space orbitals : $1d_{5/2}, 0g_{7/2}, 1d_{3/2}$ and $0h_{11/2}$ with excitation energies 0.0 MeV, 0.152 MeV, 0.703 MeV and 1.667 MeV respectively. The excitation energy of the fifth level, $2s_{1/2}$, is not defined

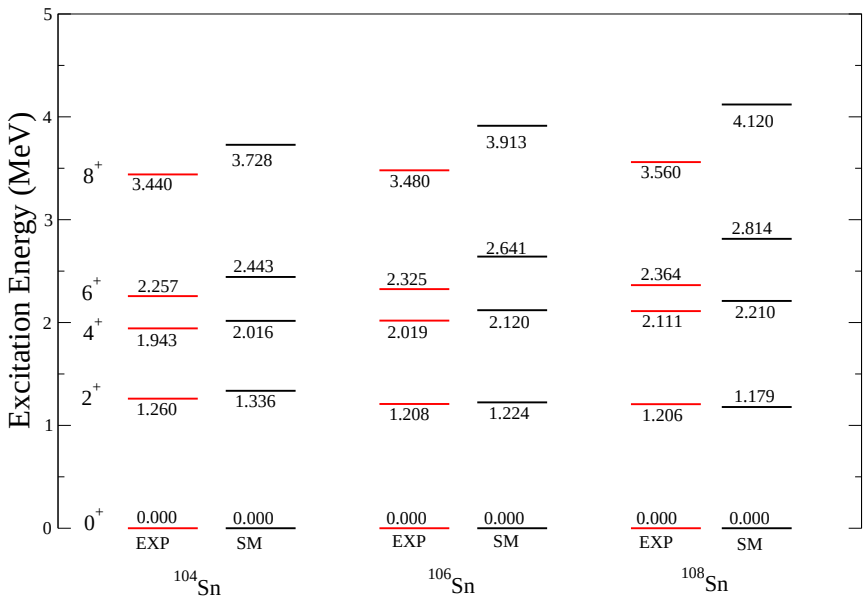

Figure 7.2: NuShell shell model calculations of Sn isotopes chain spectrums compared with the corresponding available experimental data.

yet, we adopt an excitation energy of 0.810 MeV. This value is estimated regarding its excitation energy in ^{109}Sn and the amount of increase of $\sim$ 0.300 Mev of this level compared to ^{111}Sn. Thus, the adopted single particle energies are:-11.567 MeV, -11.415 MeV, -10.864 MeV, -10.767 MeV and -9.900 MeV for $1d_{5/2}, 0g_{7/2}, 1d_{3/2}, 2s_{1/2}$ and $0h_{11/2}$ respectively.

It is clear from the results obtained of the calculations using NuShell code [5] represented on figure 7.2 that there are some agreements and some disagreements compared to the experimental data. The model with the restrictions of the model space and the single particle energies mentioned above can reproduce clearly the order sequences of the states below 4 MeV. The state 2^+ is reproduced with a good agreement of $\sim$ 30 KeV for ^{106}Sn and ^{108}Sn, whereas the agreement is about $\sim$ 80 KeV for ^{104}Sn. The same thing can be seen for the 4^+ state for the three isotopes, where the predicted states are a little bit above the experimental ones of about 100 KeV. What concerns the 6^+ and 8^+ the disagreement is clear and the differences with the experiment become more and more big arriving to $\sim$ 500 KeV. These results

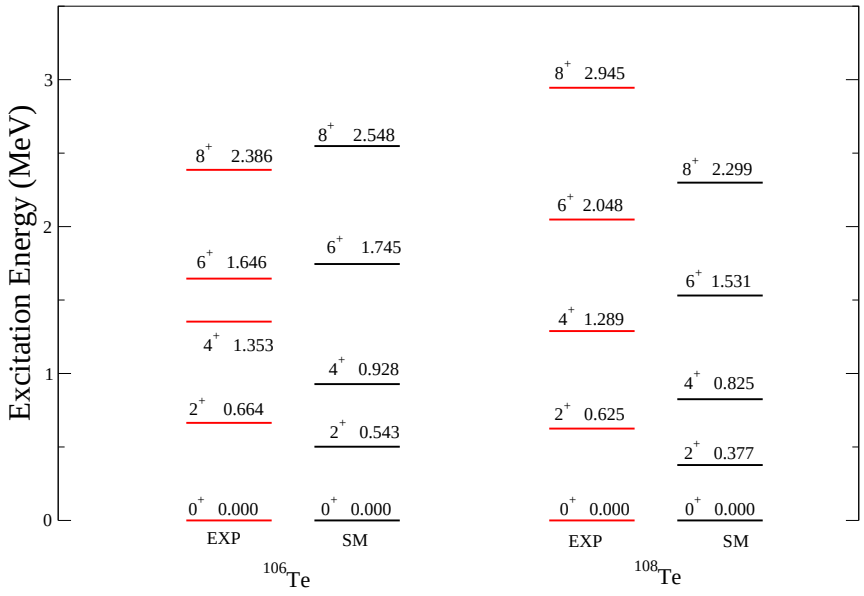

Figure 7.3: NuShell shell model calculations of ^{106,108}Te isotopes spectrums compared with the corresponding available experimental data.

need more perfections.

7.1.3 Te isotopes chain

For the Te isotopic chain, we present here shell model calculation results of even-even ^{106}Te and ^{108}Te isotopes. They consist of two proton outside the Z=50 proton shell closure, and four and six neutrons outside the N=50 neutron shell closure, respectively. The protons and neutrons numbers are just above the shell closure number and they verify $50 < Z, N < 82$. Thus, the model space consists of $1d_{5/2}, 0g_{7/2}, 1d_{3/2}, 2s_{1/2}$ and $0h_{11/2}$ for both type of nucleons.

The neutron single particle energies are defined as it is mentioned above in the previous section when we studied the Sn isotopes. They are established from the lightest existing odd isotope spectrum, ^{107}Sn, because of the lack of information on the ^{101}Sn spectrum and its nearest odd isotopes. The same problem we are encountered with when we look to establish the proton single

particle energies of the model space orbitals in this region. The best thing to do that is the existence of ($^{101}_{51}$Sb$_{50}$) spectrum. Unfortunately, neither the experimental spectrum of this nucleus nor its nearest neighbors spectra are yet obtained. ^{109}Sb is the lightest odd isotope which figures the orbitals of the model space: $1d_{5/2}$, $2s_{1/2}$, $1d_{3/2}$, $0g_{7/2}$, and $0h_{11/2}$, with excitation energies 0.0 MeV, 0.402 MeV, 0.752 MeV, 0.832 MeV and 1.501 MeV, respectively. Thus, the relative single particle energies adopted in this calculation are respectively : -2.062 MeV, -1.661 MeV, -1.310 MeV, -1.230 MeV and -0.561 MeV.

The results obtained for these two nuclei compared with the experimental data are represented on figure 7.3. It is clear that the sequence of the states 2^+, 4^+, 6^+ and 8^+ is well reproduced. Comparing the obtained shell model spectrum to the experimental one of ^{108}Te we can easily see that all theoretical states are lower than experimental ones. The differences are important and they are between 0.250 MeV and 0.650 MeV which are big.

For the second nucleus, ^{106}Te, the same comments could be made on the differences between the experimental data and shell model calculation results even it is a bit smaller than in the previous nucleus.

In summary, results obtained for the Sn isotopes are more or less, good compared with the experiment. For the other chain, Te isotopes, obvious discrepencies with the experimental data are obtained. The two isotopic chains have the same model space with additional two protons for Te isotopes. Therefore, one can conclude that the proton single particle energies adopted here are still far away the real ones. Also, this calculation need more perfections and experimental data are more than necessary.

7.2 Algebraic study of $^{102-108}$Mo

In parallel to the shell model calculation, we planned to achieve a relatively complete treatment of collective excitations in the A=100 mass region using different extensions of the interacting boson model (IBM). It is an algebraic

Table 7.1: Th experimental $E4^+/E2^+$ ratios in function of the neutron number in even-even molybdenum isotopes,$^{94-108}$Mo. The data are from [7]

isotope	$E4^+/E2^+$	N	
108Mo	563.8/192.9 = 2.92	66	
106Mo	522.29/ 171.548= 3.044	64	
104Mo	560.68/192.19 = 2.917	62	
102Mo	743.74/296.597 = 2.5075	60	Z= 42
100Mo	1136.11/535.57 = 2.12	58	
98Mo	1510.039/787.384 = 1.91779	56	
96Mo	1628.218/778.245 = 2.092	54	
94Mo	1573.72/871.087 = 1.8066	52	

description of collective states in the atomic nucleus. It is a truncation (plus a mapping) of the shell model. The pairs of nucleons are treated as bosons (s and d in its simplest version). In a first step, in the frame of the present work, the consistent Q formalism (CQF-IBM1) Hamiltonian is used to describe the structure of $^{102-108}$Mo isotopes.

The $^{102-108}$Mo (Z=42) isotopes show, at low energy, collective behaviour. This is clear from the experimental $E4^+/E2^+$ ratios given in the table 7.1.

It is clear that we can class the molybdenum isotopes into two classes on the basis of $E4^+/E2^+$: Isotopes which have this ratio amount higher than 2 and those which is for them lower than 2. The ^{100}Mo is a transition nucleus.

Table 7.2: CQF parameter values used in the calculations

isotope	a_1	a_2	$\sqrt{5}\chi$
102Mo	0.0175	-0.0400	-0.4
104Mo	0.0100	-0.0385	-0.6
106Mo	0.0125	-0.0300	-0.6
108Mo	0.0150	-0.0250	-0.5

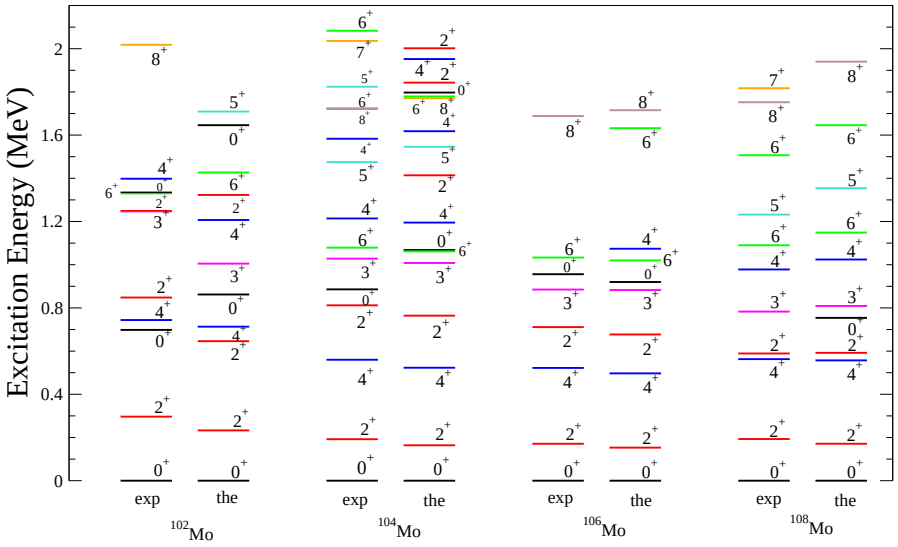

Figure 7.4: Algebraic model calculations in the interacting boson model framework of proton rich Mo isotopes chain spectrums compared with the available experimental corresponding data. Different colours are used for the different states: the colours black, red, magenta, blue, turquoise, green, orange and brown are associated for the states 0^+, 2^+, 3^+, 4^+, 5^+, 6^+, 7^+ and 8^+, respectively.

The latter, with lower ratios, can be studied in shell model basis. Whereas for the former, with higher ratios, it is expected they have a structure that can be described in IBM as an SU(3) to SO(6) transition. So the use of CQF technique is justified.

Results of calculation (Fig.7.4) uses the CQF parameters of table 7.2, show a fair agreement with experimental data. However, a beter parameter optimization is necessary.

Some significant discrepancies are noticed in ^{102}Mo probably to its different behaviour because of the relatively low $E4^+/E2^+$ ratio.

Similar tendency has been obtained recently [8] using a more complicated Hamiltonian. However a beter understanding of the ^{102}Mo needs more experimental data. Indeed, many low-lying states in the quasi-gamma and quasi-beta bands are still missing

Bibliography

[1] D.J. Deana, T. Engelandb, M. Hjorth-Jensenb, M.P. Kartamyshev and E. Osnes: Effective interactions and the nuclear shell-model, Prog. Part. Nucl. Phys. 53, 419 (2004)

[2] A. F. Lisetskiy , B. A. Brown , M. Horoi , H. and Grawe:New T=1 effective interactions for the $f_{5/2}p_{3/2}p_{1/2}g_{9/2}$ model space: Implications for valence-mirror symmetry and seniority isomers, Phys. Rev. C 70, 044314 (2004)

[3] N. Sandulescu , j. Blomqvist , R.J. Liotta : Microscopic description of light Sn isotopes, Nucl. Phys. A 582, 257(1995)

[4] M. Hjoth-Jensen, T. T.S. Kuob , E. Osnes : Realistic effective interactions for nuclear systems, Phys. Rep. 261, 125(1995)

[5] B.A. Brown , W.D.M. Rae : NUSHELL@MSU, MSU-NSCL Report, 2007 (unpublished)

[6] R. Machleidt, F. Sammarruca, and Y. Song, Nonlocal nature of the nuclear force and its impact on nuclear structure, Phys. Rev. C 53, 1483 (1996)

[7] www.nndc.bnl.org

[8] M. B*öyü*kta, P. Van Isacker and I. Uluer: Description of nuclei in the A 100 mass region with the interacting boson model, J. Phys. G37 (2010)105102

Chapter 8

Overview and Outlook

In this work we targted to study two regions of the nuclear chart which have a signeficant importance in nuclear structure and astrophysics: neutron rich light nuclei and proton rich nuclei in the vicinity of ^{100}Sn.

In the first region, the ^{18}C spectrum has been studied in a three body n+n+^{16}C model that includes deformation and the 2^+ excitation of the ^{16}C core as well as Pauli projection of forbidden states. The ^{16}C-n interaction, employed in this study, has been fitted to reproduce the experimental spectrum of ^{17}C. The calculations show that two neutron separation energy in ^{18}C in consistent with three-body structure of this nucleus and predict more states bound with respect to the three-body decay. The comparison of their position to known excited states in ^{18}C is discussed. These calculations suggest also that a few states may exist in astrophysically relevant region between the ^{17}C+n and ^{16}C+2n decay thresholds. The most important of them is 1^- as it can give a large E1 resonant contribution to the $^{17}\mathrm{C}(n,\gamma)^{18}\mathrm{C}$ neutron capture. The calculations also suggest that a virtual s-wave state may exist above the ^{17}C+n threshold that can give rise to non-negligible M1 contributions to the $^{17}\mathrm{C}(n,\gamma)^{18}\mathrm{C}$ reaction rate. The presence of these states in the ^{18}C spectrum can lead to an increased $^{17}\mathrm{C}(n,\gamma)^{18}\mathrm{C}$ reaction rate, which can signeficantly influence the abundances of uranium and thorium synthesized in the r-process in the supernovae explosions.

In the second region, we studied in nuclear shell model and interacting boson model the even-even $^{96-104}$Cd, $^{104-108}$Sn , ^{106,108}Te and $^{102-108}$Mo isotopes.

The calculations of $^{96-104}$Cd, $^{104-108}$Sn and ^{106,108}Te spectra have been carried out using the windows version of NuShell@MSU. To define the Hamiltonian, the two body matrix element of the effective interaction (TBME) and single particle energies(SPE) of the valence space orbitals are needed. The TBME are obtained from the renormalized two body effective interaction based on G matrix derived from the CD-Bonn free nucleon nucleon potential.

For Sn an Te isotopes we used ^{107}Sn and ^{109}Sb spectra to establish the single particle energies of the neutron and proton model space orbitals, respectively. Results are in good agreement with the experimental data, especially the reproduction of 2^+ and 4^+ in Sn isotopes. Some discrepancies, especially for the Te isotopes are obvious.

Calculations for the Cd isotopes are carried out using the same effective interactions of the NuShell@MSU library labled by jj44pna and jj45pna which are adjusted for nuclei in the vicinity of ^{132}Sn. Results need more perfection.

In order to study the $^{102-108}$Mo isotopes, which show collective behaviour at low energy, we used the consistent Q formalism (CQF-IBM1) Hamiltonian to describe their structure. Results of calculations show a fair agreement with experimental data. However, a better parameter optimization is necessary.

Results of this work open the door largely for more prospective studies. We can cite, in general, some of them:

- In the region of light neutron rich nuclei, some other nuclei show halo features (large rms radius, small separation energies of the last nucleons, narrow longitudinal momentum distributions...) like ^{19}C, ^{22}C , ^{15}B, ^{17}B and ^{19}B are waiting for more studies. Few body calculations for these nuclei may give us an idea whether it is worth to pay such high price in defining the core-n interaction in ^{17}C.

- More experimental data of the nearest neighbours of ^{100}Sn are indis-

pensable and invaluable. Shell model calculations using more appropriate single particle energies, for the orbitals of the model spaces in the region, obtained from nuclei spectra just near the doubly magic nucleus ^{100}Sn are more than necessary.

- Extending algebraic calculations to the broader region of nuclei close to ^{100}Sn (Ru, Pd, Zr,...) isotopes which show collective behaviour. In this context, different extensions of interacting boson model (IBM) will be used.

- More studies about the contribution of light neutron rich nuclei reactions in r-process nucleosynthesis, and proton rich nuclei in the vicinity of 100Sn in rp-process are needed.

In somehow, it is only the end of the beginning...

Appendix A

Pauli principle treatment

A.1 constructing the three body forbidden states

Let us specify how to construct the three body forbidden wavefunctions, given the two body occupied states. The $\mathbf{Y}$ coordinate system, $(\vec{x},\vec{y}) = (\vec{x_1},\vec{y_1})$ or $(\vec{x},\vec{y}) = (\vec{x_2},\vec{y_2})$ is the natural coordinate system to define two body forbidden states associated with the $(core+n)$ subsystem. We will represent these states as a sum over all two body channels identified by the quantum numbers $\{(l_k^p, s_k^p)j_k^p, I_k^p; J_2^p\}$ as in the following equation:

$$\phi^p = \sum_k \mathcal{U}_k^p(x_1)\phi_{I_k^p}(\hat{\xi})|(l_k^p, s_k^p)j_k^p, I_k^p; J_2^p\rangle \tag{A.1}$$

and each of these states is lablled by p corresponding to a particular total angular momentum and parity J_2^p. Here we have explicitly represented the radial part of the wavefunction as $\mathcal{U}_k^p(x_1)$ and is the intrinsic core's wavefunction as $\phi_{I_k^p}(\hat{\xi})$. To account for the necessary degrees of freedom of the three body system one needs a complete set in which to expand the three body forbidden state, accounting for the extra $(\vec{y_1})$ degrees of freedom of the three body system relative to the two body subsystem with an excited core. For this effect we use a spline expansion in the y_1 Jacobi coordinate, with the following quantum numbers: $\chi_n^p(y_1)|(l_n^p, s_n^p)j_n^p\rangle$, where $n = 1, ..., N_{splines}$.

One can then write down the two body forbidden wavefunctions $\Phi^{J_3^p}$ based on the two body ones ϕ^p as:

$$\Phi^{J_3^p} = \sum_{kn} \mathcal{U}_k^p(x_1)\chi_n^p(y_1)\phi_{I_k^p}(\hat{\xi})|\{(l_k^p, s_k^p)j_k^p, I_k^p\}J_2^p, (l_n^p, s_n^p)j_n^p; J_3^p\rangle \tag{A.2}$$

We now recouple the angular momentum such that the spins and orbital angular momenta of the valence neutrons are first coupled to a total spin of the nn subsystem and only then coupled to the spin of the core:

$$|\{(l_k^p, s_k^p)j_k^p, I_k^p\}J_2^p, (l_n^p, s_n^p)j_n^p; J_3^p\rangle \rightarrow |\{(l_k^p, l_n^p)L^p, (s_k^p, s_n^p)S^p\}J_{kn}^p, I_k^p; J_3^p\rangle \tag{A.3}$$

The three body wavefunction in this new coupling order is:

$$\Phi^{J_3^p} = \sum_{kn} \mathcal{U}_k^p(x_1)\chi_n^p(y_1)\phi_{I_k^p}(\hat{\xi})(-1)^{J_3^p+J_2^p-2I_k^p-j_k^p}\hat{J}_2^p\hat{J}_{kn}^p\hat{L}^p\hat{S}^p\hat{j}_k^p\hat{j}_n^p \times$$

$$W(I_k^p j_k^p, J_3^p j_n^p J_{kn}^p)\begin{Bmatrix} l_k^p & l_n^p & L^p \\ s_k^p & s_n^p & S^p \\ j_k^p & j_n^p & J_{kn}^p \end{Bmatrix}|\{(l_k^p, l_n^p)L^p, (s_k^p, s_n^p)S^p\}J_{kn}^p, I_k^p; J_3^p\rangle \tag{A.3}$$

The radial part of the wavefunction($\mathcal{U}_k^p(x_1)\chi_n^p(y_1)$) is expressed in the natural Jacobi coordinates for the problem. To proceed, one needs to represent it in the corresponding hyperspherical coordinates. For each component $\{p, k, n\}$specified by the quantum numbers $[\{(l_k^p, l_n^p)L^p, (s_k^p, s_n^p)S^p\}J_{kn}^p, I_k^p; J_3^p]$, one performs the hyperspherical decomposition:

$$\mathcal{U}_k^p(x_1)\chi_n^p(y_1) = \rho^{\frac{-5}{2}}\sum_K \chi_{Kl_k^p l_n^p}^{L^p S^p I_k^p}(\rho)\varphi_K^{l_k^p l_n^p}(\theta) \tag{A.4}$$

where $\chi_{Kl_k^p l_n^p}^{L^p S^p I_k^p}(\rho) = \int_{-1}^{1} d\cos(2\theta)\sqrt{1-\cos^2(2\theta)}\mathcal{U}_k^p(\rho\sin\theta)\chi_n^p(\rho\cos\theta)\varphi_K^{l_k^p l_n^p}(\theta)$. Remembering that $\varphi_K^{l_k^p l_n^p}$ is analytically defined in terms of the Jacobi polynomials, one can easily calculate the integrals defining $\chi_{Kl_k^p l_n^p}^{L^p S^p I_k^p}(\rho)$.

Finally, and because the wavefunction defined in equation (B.7) solution of the three body Hamiltonian, is represented in the **T** basis, it is necessary to perform a rotation from the **Y** basis to the **T** basis (see figA.1). Such a rotation can be performed by introducing the appropriate rotational coefficients associated with the hyperspherical method known by the Renal-Revai

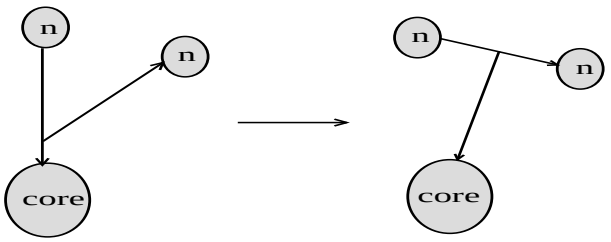

.

Figure A.1: Coordinate Transformation

coefficients [13]
Note that in general the set $\{(l_k^p, l_n^p)L^p, S^p, I_k^p, K\}$ is larger than $\{(\lambda_k, \lambda_n)L^p, S^p, I_k^p, K\}$ due to symmetry restrictions of the nn subsystem.

Summing up these results, one concludes that each component$\{(\lambda_k, \lambda_n)L^p, S^p, I_k^p, K\}$ of the three body forbidden state will be defined in the T basis as:

$$\Phi^{J_3^p}_{kn,(\lambda_k,\lambda_n)L^p,S^p,I_k^p,K}(\rho,\theta,\hat{x},\hat{y},\hat{\sigma}_1,\hat{\sigma}_2,\hat{\xi}) = \sum_{l_k^p,l_n^p}\langle\lambda_k,\lambda_n|l_k^p,l_n^p\rangle_{L^pS^pI_k^pK}$$

$$(-1)^{J_3^p+J_2^p-2I_k^p-j_k^p}\hat{J}_2^p\hat{J}_{kn}^p\hat{L}^p\hat{S}^p\hat{j}_k^p\hat{j}_n^p\begin{Bmatrix} l_k^p & l_n^p & L^p \\ s_k^p & s_n^p & S^p \\ j_k^p & j_n^p & J_{kn}^p \end{Bmatrix} W(I_k^p j_k^p, J_3^p j_n^p J_{kn}^p)$$

$$\chi^{L^pS^pI_k^p}_{Kl_k^pl_n^p}(\rho)\phi_{I_k^p}(\hat{\xi})|\{(l_k^p,s_k^p)j_k^p,I_k^p;J_2^p\},(l_n^p,s_n^p)j_n^p;J_3^p\rangle. \quad \text{(A.3)}$$

The total three body forbidden states are defined as a sum over all possible channels of the partial components:

$$\Phi^{J_3^p}(\rho,\theta,\hat{x},\hat{y},\hat{\sigma}_1,\hat{\sigma}_2,\hat{\xi}) = \sum_{\lambda_k,\lambda_n}\sum_{L^pS^pI_k^pK}\Phi^{J_3^p}_{kn,(\lambda_k,\lambda_n)L^p,S^p,I_k^p,K}(\rho,\theta,\hat{x},\hat{y},\hat{\sigma}_1,\hat{\sigma}_2,\hat{\xi}) \quad \text{(A.4)}$$

and should now be projected out from the three body Hamiltonian.

A.2 Projection into the allowed space

Having defined the three body forbidden states, we guarantee that the total wavefunction for the system is orthogonal to these by projecting them out of the Hamiltonian model space.

Let us first assume there is only one forbidden state Φ_0. The full three body wavefunctions should satisfy both equations:

$$\hat{H}|\Psi\rangle = E|\Psi\rangle \quad \text{and} \quad \langle\Phi_0|\Psi\rangle = 0, \tag{A.5}$$

and additionally to the necessary requirement for the bound states which should be square integrable.

If one defines a projection operator $\hat{P}_0 = |\Phi_0\rangle\langle\Phi_0|$ and $\hat{Q}_0 = 1 - \hat{P}_0$, the orthogonalisation condition can be expressed as:

$$\hat{Q}_0|\Psi\rangle = |\Psi\rangle \tag{A.6}$$

Then, from equation A.5 and equation A.6, the necessary condition to be satisfied is:

$$\hat{Q}_0\hat{H}\hat{Q}_0|\Psi\rangle = E|\Psi\rangle, \tag{A.7}$$

with the operator $\hat{Q}_0$ defining the allowed subspace into which the Hamiltonian is to be projected, and $\hat{P}_0$ defining the forbidden subspace. Notice that $\hat{P}_0|\Psi\rangle$ is a solution of equation A.7 if $E = 0$. Otherwise equation A.7 implies that $\hat{P}_0|\Psi\rangle \equiv 0$.

Let us now represent the wavefunction in terms of a non-orthogonal basis:

$$|\Phi_0\rangle = \sum_i f_i^0|\mathcal{S}_i\rangle$$
$$|\Psi\rangle = \sum_i c_i|\mathcal{S}_i\rangle, \tag{A.7}$$

where the subscript i stands for $\{l, j, I, J\}$. In this demonstration we are thinking of using the Sturmian basis for this expansion and, as was presented previously, the Schrödinger equation reduces to an algebraic generalized eigenvalue problem. The projection operator is then defined as:

$$\hat{Q}_0 = 1 - \sum_{ij} f_i^{0*} f_j^0 |\mathcal{S}_i\rangle\langle\mathcal{S}_j|. \tag{A.8}$$

One can now work out the explicit form of the matrix operator $\hat{Q}_0\hat{H}\hat{Q}_0$, in terms of the chosen basis set $\mathcal{S}_i$,

$$\hat{Q}_0\hat{H}\hat{Q}_0 = \hat{H} - \sum_{ij} f_i^{0*} f_j^0 \left(|\mathcal{S}_i\rangle\langle\mathcal{S}_j|\hat{H} + \hat{H}|\mathcal{S}_i\rangle\langle\mathcal{S}_j| \right) \sum_{ijmn} f_i^{0*} f_j^0 f_m^{0*} f_n^0 |\mathcal{S}_i\rangle\langle\mathcal{S}_j|\hat{H}|\mathcal{S}_m\rangle\langle\mathcal{S}_n|, \tag{A.8}$$

In order to obtain the explicit representation of the matrix elements $\langle\mathcal{S}_\mu|\hat{Q}_0\hat{H}\hat{Q}_0|\mathcal{S}_\nu\rangle$, it is useful to define the following matrices:

$$\mathbf{H}_{ij} = \langle\mathcal{S}_i|\hat{H}|\mathcal{S}_j\rangle \qquad \mathbf{M}_{ij} = \langle\mathcal{S}_i|\mathcal{S}_j\rangle. \tag{A.8}$$

Using these matrices, the representation of $\mathbf{H}^{proj}_{\mu\nu}$ is given by:

$$\begin{aligned} \mathbf{H}^{proj}_{\mu\nu} &= \langle\mathcal{S}_\mu|\hat{Q}_0\hat{H}\hat{Q}_0|\mathcal{S}_\nu\rangle \\ &= \mathbf{H}_{\mu\nu} - \sum_{ij} f_i^{0*} f_j^0 (\mathbf{M}_{\mu i}\mathbf{H}_{j\nu} + \mathbf{H}_{\mu i}\mathbf{M}_{j\nu}) \\ &\quad - \sum_{ijmn} f_i^{0*} f_j^0 f_m^{0*} f_n^0 \mathbf{M}_{\mu i}\mathbf{H}_{jm}\mathbf{M}_{n\nu} \end{aligned}$$

In order to simplify this expression, it is useful to introduce the following vector representation for partial sums:

$$\mathcal{H}^0_\mu = \sum_i f_i^0 \mathbf{H}_{i\mu} \quad \text{and} \quad \mathcal{H}^{0+}_\mu = \sum_i \mathbf{H}_{\mu i} f_i^{0*} \tag{A.8}$$

$$\mathcal{M}^0_\nu = \sum_j f_j^0 \mathbf{M}_{j\nu} \quad \text{and} \quad \mathcal{M}^{0+}_\nu = \sum_j \mathbf{M}_{\nu j} f_j^{0*} \tag{A.9}$$

By direct substitution in the expression of projector operator matrix elements we get:

$$\mathbf{H}^{proj}_{\mu\nu} = \mathbf{H}_{\mu\nu} - \left(\mathcal{M}^{0+}_\mu\mathcal{H}^0_\nu + \mathcal{H}^{0+}_\mu\mathcal{M}^0_\nu\right) + \left(\sum_j f_j^0 \mathcal{H}^{0+}_j\right) \mathcal{M}^{0+}_\mu \mathcal{M}^0_\nu. \tag{A.10}$$

Once the matrix $\mathbf{H}^{proj}_{\mu\nu}$ is calculated, one can perform a diagonalisation and solve the generalized eigenvalue problem in the restricted space $\Psi \perp \Phi_0$.

In fact this procedure will shift the energy of the forbidden state Φ_0 to zero. Naturally if one is interested in the region close to the threshold, as is the case for halo nuclei, it is preferable to shift the energy of this forbidden state away from the threshold, as much as possible, to avoid confusion with the physical solutions.

Instead of solving equation A.10, by taking into account the properties of the $\hat{P}_0$ operator, one should solve

$$\left(\hat{Q}_0\hat{H}\hat{Q}_0 + E_{shift}\hat{P}_0\right)\Psi = E\Psi \tag{A.11}$$

The matrix form of $\hat{P}_0$ can easily be deduced,

$$\begin{aligned}\hat{P}_{0\mu\nu} &= \sum_{ij} f_i^{0*} f_j^0 \mathbf{M}_{\mu i}\mathbf{M}_{j\nu} \\ &= \mathcal{M}_\mu^{0+}\mathcal{M}_\nu^0\end{aligned}$$

and therefore the algebraic equation to be solved is

$$\sum_\nu \left\{ \mathbf{H}_{\mu\nu} - \left(\mathcal{M}_\mu^{0+}\mathcal{H}_\nu^0 + \mathcal{H}_\mu^{0+}\mathcal{M}_\nu^0\right) + \left(\sum_j f_j^0 \mathcal{H}_j^{0+}\right)\mathcal{M}_\mu^{0+}\mathcal{M}_\nu^0 + E_{shift}\mathcal{M}_\mu^{0+}\mathcal{M}_\nu^0 \right\} C_\nu = E\sum_\nu \mathbf{M}_{\mu\nu}C_\nu \tag{A.10}$$

If instead of one forbidden state Φ_0, a set of n forbidden states $\{\Phi_i, \quad i = 1, ..., n\}$ is imposed, and assuming these are all orthogonal($\langle\Phi_i|\Phi_j\rangle = 0$, for $\quad i \neq j$) the full solution to the problem will satisfy

$$\hat{H}|\Psi\rangle = E|\Psi\rangle \quad \text{and} \quad \hat{Q}_i|\Psi\rangle = |\Psi\rangle, \quad \forall i = 1, n \tag{A.11}$$

Then, again, the method consists in solving:

$$\left(\hat{Q}\hat{H}\hat{Q} + E_{shift}\hat{P}\right)|\Psi\rangle = E|\Psi\rangle$$

$$\text{where} \quad \hat{Q} = \prod_{i=1}^{n}\hat{Q}_i \quad \text{and} \quad \hat{P} = \prod_{i=1}^{n}\hat{P}_i.$$

The orthogonality condition between forbidden states ϕ_i is necessary so that eq.(A.11) can be reduced to eq.(A.2). This equation, after appropriate algebraic manipulation can be reduced to the following matrix form, given

that the basis components for the forbidden states are previously defined, $\Phi_l = \sum_i f_i^l |\mathcal{S}_i\rangle, \quad l = \{1, ..., n\}$:

$$\sum_\nu \left\{ \mathbf{H}_{\mu\nu} - \sum_{l=1}^{n} \left(\mathcal{M}_\mu^{l+} \mathcal{H}_\nu^l + \mathcal{H}_\mu^{l+} \mathcal{M}_\nu^l \right) + \sum_{l,k} \left(\sum_j f_j^l \mathcal{H}_j^{k+} \right) \mathcal{M}_\mu^{l+} \mathcal{M}_\nu^k + E_{shift} \sum_{l,k} \mathcal{M}_\mu^{l+} \mathcal{M}_\nu^k \right\} C_\nu = E \sum_\nu \mathbf{M}_{\mu\nu} C_\nu \quad \text{(A.10)}$$

Appendix B

The Lanczos Diagonalization Method of the Hamiltonian Matrix

The LANCZOS algorithm appears as the most powerfull technique in diagonalizing the Hamiltonian matrix and in fact the standard method to do so.

The principle of the method is to build an orthogonal basis in which the Hamiltonian H matrix is tridiagonal. We start with a normalized vector ϕ_1 and apply the H operator on this vector. Then we get a parallel and orthogonal components to the initial vector ϕ_1:

$$H|\phi_1\rangle = E_{11}|\phi_1\rangle + E_{12}|\phi_2\rangle \tag{B.1}$$

with

$$E_{11} = \langle\phi_1|H|\phi_1\rangle \quad \text{and} \quad E_{12}|\phi_2\rangle = H|\phi_1\rangle - E_{11}|\phi_1\rangle \tag{B.2}$$

Acting again with H on ϕ_2, we generate a third vector ϕ_3 orthogonal to the first two

$$H|\phi_2\rangle = E_{21}|\phi_1\rangle + E_{22}|\phi_2\rangle + E_{23}|\phi_3\rangle \tag{B.3}$$

$E_{12} = E_{21}$ since in our basis H matrix is real symmetric.

Continuing this process, at iteration n, we obtain the diagonal energy of the vector $|\phi_n\rangle$, a new vector $|\phi_{n+1}\rangle$ and the non diagonal energy E_{nn+1}

$$H|\phi_n\rangle = E_{nn-1}|\phi_{n-1}\rangle + E_{nn}|\phi_n\rangle + E_{nn+1}|\phi_{n+1}\rangle \tag{B.4}$$

$$E_{nn-1} = E_{n-1n}, \quad E_{nn} = \langle\phi_n|H|\phi_n\rangle \tag{B.5}$$

$$\text{and} \quad E_{nn+1}|\phi_{n+1}\rangle = H|\phi_n\rangle - E_{nn}|\phi_n\rangle - E_{nn-1}|\phi_{n-1}\rangle \tag{B.6}$$

Due to the hermiticity of the Hamiltonian H, the construction of the Lanczos matrix ensures that the elements E_{ij} with $|i-j| > 1$ are zero. That's means $\langle\phi_i|H|\phi_j\rangle = \langle\phi_j|H|\phi_i\rangle$ if $|i-j| > 1$. Hence, tridiagonal matrix is constructed:

$$\mathbf{H} = \begin{pmatrix} E_{11} & E_{12} & 0 & 0 & 0 & \dots \\ E_{21} & E_{22} & E_{23} & 0 & 0 & \dots \\ 0 & E_{32} & E_{33} & E_{34} & 0 & \dots \\ 0 & 0 & E_{43} & E_{44} & E_{45} & \dots \\ \vdots & \vdots & \vdots & \vdots & \ddots & \end{pmatrix} \tag{B.7}$$

This iterative process will continue until all the eigenvalues that we need are converged. For this reason the choice of the pivot state is crucial. An other important point to notice concerning this method is that all the Lanzos vectors must be kept during the calculation in order to use them in calculating the eigenvectors and to avoid numerical problems. Mathematically the Lanczos vectors should be orthogonal, however numerically this is not strictly so. Hence, small numerical precision errors can, after some iterations, produce catastrophes. To avoid that it is necessary to reorthogonalized each new Lanczos vector to all the precedent.